SENSITIVITY ANALYSIS OF LAYERED WALL SYSTEMS UTILIZING SUSTAINABLE COMPOSITES INCORPORATING MICRO-ENCAPSULATED PCMS

A THESIS SUBMITTED TO
THE GRADUATE SCHOOL OF NATURAL AND APPLIED SCIENCES
OF
MIDDLE EAST TECHNICAL UNIVERSITY

BY

HATİCE DENİZ ÖZDEMİR

IN PARTIAL FULFILLMENT OF THE REQUIREMENTS
FOR
THE DEGREE OF MASTER OF SCIENCE
IN
MECHANICAL ENGINEERING

NOVEMBER 2023

Approval of the thesis:

SENSITIVITY ANALYSIS OF LAYERED WALL SYSTEMS UTILIZING SUSTAINABLE COMPOSITES INCORPORATING MICRO-ENCAPSULATED PCMS

submitted by **HATİCE DENİZ ÖZDEMİR** in partial fulfillment of the requirements for the degree of **Master of Science in Mechanical Engineering Department, Middle East Technical University** by,

Prof. Dr. Halil Kalıpçılar
Dean, Graduate School of **Natural and Applied Sciences** _____

Prof. Dr. M.A. Sahir Arıkan
Head of Department, **Mechanical Engineering** _____

Prof. Dr. Derek K. Baker
Supervisor, **Mechanical Engineering, METU** _____

Assoc. Prof. Dr. Çağla Meral Akgül
Co-supervisor, **Civil Engineering, METU** _____

Examining Committee Members:

Assoc. Prof. Dr. Hüsnü Dal
Mechanical Engineering, METU _____

Prof. Dr. Derek K. Baker
Mechanical Engineering, METU _____

Assoc. Prof. Dr. Çağla Meral Akgül
Civil Engineering, METU _____

Assoc. Prof. Dr. Ulaş Yaman
Mechanical Engineering, METU _____

Assist. Prof. Dr. Mehdi Mehrtash
Energy Systems Engineering, Atılım University _____

Date:24.11.2023

I hereby declare that all information in this document has been obtained and presented in accordance with academic rules and ethical conduct. I also declare that, as required by these rules and conduct, I have fully cited and referenced all material and results that are not original to this work.

Name, Surname: HATİCE DENİZ ÖZDEMİR

Signature :

ABSTRACT

SENSITIVITY ANALYSIS OF LAYERED WALL SYSTEMS UTILIZING SUSTAINABLE COMPOSITES INCORPORATING MICRO-ENCAPSULATED PCMS

ÖZDEMİR, HATİCE DENİZ
M.S., Department of Mechanical Engineering
Supervisor: Prof. Dr. Derek K. Baker
Co-Supervisor: Assoc. Prof. Dr. Çağla Meral Akgül

November 2023, 125 pages

It is crucial to reduce the energy demand in buildings in order to slow down the rate of global warming and become more resilient against energy crises. In order to accomplish this, both the composite development studies that lower energy demand by using phase change material (PCM) incorporated waste materials and the parameter research that have the biggest impact on energy demand in buildings are speeding up. In light of these demands, this research is intended to identify the most critical parameters for a wall with PCM with different orientations in Ankara, Türkiye, and develop microencapsulated phase change material (MPCM) incorporated fuel gas desulfurisation gypsum (FGDG) and commercial plaster composites for building applications. After the development of physical samples of the composites, the mechanical, thermal and microstructural properties are characterised. The sensitivity analysis results show that regardless of the orientation of the wall, the melting temperature of PCM is the most important parameter for both summer and winter seasons. In this context, adding PCM with a suitable melting temperature to mortar and/or plaster materials that can be applied to the interior of the wall might be an appropriate solution for

increasing wall performance. Considering the mechanical and thermal characteristics of the developed composites, it is concluded that they are technically suitable for use in wall applications.

Keywords: Microencapsulated phase change material (MPCM), Fuel gas desulfurization gypsum (FGDG), Gypsum, Finite difference method (FDM), Global sensitivity analysis (GSA)

ÖZ

MİKRO KAPSÜLLÜ PCMS İÇEREN SÜRDÜRÜLEBİLİR KOMPOZİTLERİN KULLANILDIĞI KATMANLI DUVAR SİSTEMLERİNİN DUYARLILIK ANALİZİ

ÖZDEMİR, HATİCE DENİZ
Yüksek Lisans, Makina Mühendisliği Bölümü
Tez Yöneticisi: Prof. Dr. Derek K. Baker
Ortak Tez Yöneticisi: Doç. Dr. Çağla Meral Akgül

Kasım 2023 , 125 sayfa

Küresel ısınmanın hızını yavaşlatmak ve enerji krizlerine karşı daha dirençli olabilmek için binalarda enerji talebinin azaltılması büyük önem taşıyor. Bunu başarmak için hem faz değiştiren malzeme (PCM) içeren atık malzemeleri kullanarak enerji talebini azaltan kompozit geliştirme çalışmaları hem de binalarda enerji talebini en fazla etkileyen parametre araştırmaları hızlanıyor. Bu talepler ışığında, bu araştırmanın Ankara, Türkiye'de farklı yönelimlere sahip PCM'li bir duvar için en kritik parametreleri belirlemesi ve mikrokapsüllenmiş faz değişim malzemesi (MPCM), yakıt gazı kükürt giderme alçısı (FGDG) ve ticari alçı kompozitleri geliştirmesi amaçlanmaktadır. Bina uygulamaları için. Kompozitlerin fiziksel numunelerinin geliştirilmesinden sonra mekanik, termal ve mikroyapısal özellikleri karakterize edilir. Duyarlılık analizi sonuçları, duvarın yönelimi ne olursa olsun, PCM erime sıcaklığının hem yaz hem de kış mevsimleri için en önemli parametreler olduğunu göstermektedir. Bu bağlamda duvar iç kısmına uygulanabilecek harç ve/veya sıva malzemelerine uygun erime sıcaklığına sahip PCM'nin eklenmesi duvar performansının arttırılması için uygun bir çözüm

olabilir. Geliştirilen kompozitlerin mekanik ve termal özellikleri dikkate alındığında teknik olarak duvar yapılarında kullanıma uygun olduğu sonucuna varılmıştır.

Anahtar Kelimeler: Mikroenkapsüle faz değiştiren malzeme (MPCM), Baca gazı kükürt giderme Alçısı, Alçı, Sonlu farklar yöntemi, Küresel duyarlılık analizi

To my beautiful grandmothers: Meliha Küçüker (1939-2014) and Hatice Özdemir (1942-2017)

ACKNOWLEDGMENTS

First of all, I would like to thank Prof. Dr. Derek Baker for his incredible support and guidance. I am so lucky to have had the opportunity to work with Prof. Baker. In this stressful process, let alone stressing me out, he always relaxed me and I was able to work much more efficiently thanks to him. He is always open to learning new things, his incredible adaptability and very balanced, open and sincere communication are his qualities that I will take as my compass throughout my life. I hope our communication with you will continue. I would also like to thank you for introducing me to Assoc. Prof. Dr. Çağla Meral Akgül and helping me to be involved in the TESBE project. Dr. Akgül, I would like to thank you for always guiding me in my thesis and for your incredible dedication to the development of both me and the thesis during this process. You have contributed a lot to me, both professionally and personally.

I would like to express my endless thanks to Tolga Tamer, who both guided and helped me in this thesis. He supported me so much both during the experiments and during the thesis process. Our long and tiring lab times have become much better thanks to you. I believe that you will be a very successful academician in the future, my dear friend.

I thank my dear family for being and being my family. I am very, very happy to be walking with you on the path of life. You have a great share in all the good work I do.

My dear father Ömer Özdemir, you show me how humility, joy and skill can come together to make life better not only for the environment but also for ourselves. You are living proof that professional achievements and depth are not by pretending, but by actually doing it and giving yourself to your craft.

I am grateful to my dear mother, Ruhsar Özdemir, for proving how important and perhaps the most important virtues in life are determination and stability. You taught us that in some situations we have to move forward despite our feelings and that's where improvement sometimes comes from.

I would like to thank my dear siblings Meliha Zeynep Özdemir and Ali Enes Özdemir for always adding joy, meaning, and beauty to my life. I am so happy to be your sister. There are no words to describe how much I love you.

I thank to my husband, Mertcan Bulut, for always being with me and believing in me. Everything is better with you. We will rock.

I would also like to thank my dear friends who made my life better in Ankara after the pandemic. Thank you to Elçin, Esra and Zeynep for making my life at LUK and METU enjoyable. I would like to thank Erkan, Zehra and Mehmet for their beautiful friendship and for adding joy and warmth to work life and beyond. I would like to thank to dear Aslı, Özge, Seden, Yasin, Cihan, Dilara and Simge for their beautiful friendship. Glad you are my friend.

This research was supported by TUBITAK-Royal Academy of Engineering TSP Programme Grant No. 220N292.

Scientia Dux Vitae Certissimus

TABLE OF CONTENTS

LIST OF TABLES

TABLES

LIST OF FIGURES

FIGURES

CHAPTER 1

INTRODUCTION

1.1 Motivation and Problem Definition

Global warming is now an imminent danger to the world, with several adverse ecological implications [11]. The primary source of this worldwide warming is greenhouse gas (GHG) emissions, primarily CO_2 emissions. According to the International Energy Agency (IEA), the building sector consumes 40% of produced energy globally [12]. According to the United Nations Environment Programme (UNEP), the building sector contributes up to 30% of the yearly emissions of greenhouse gases. [13]. For the past several years, the energy demand for the building sector has been rising at 1.8 % annually [14]. If not controlled, it will exceed 180 exajoules around 2050 [15]. The building sector in the EU is responsible for over 40% of all CO_2 emissions and around 40% of total final energy consumption. [16][17]. Also, note that only around 17.5% of residual building energy consumption is provided by renewable sources in EU-28. However, it is one of the regions that attaches the most importance to renewable energy in the world [15]. Consequentially, one of the main objectives of energy policy at the regional, national, and international levels is to increase the energy efficiency of buildings. [18].

Decreasing energy consumption and improving energy conservation in buildings significantly promotes energy efficiency and building sustainability [1]. By using Thermal Energy Storage (TES) technologies, buildings' dependency on fossil fuels can be reduced. Additionally, TES technologies can support the usage of ecologically friendly energy that is more efficient. Among other benefits, TES makes load shifting and uninterrupted thermal energy delivery possible, which can increase the potential

to integrate variable renewable energies. Renewable energy and TES system coupling will accelerate the scaling-up of renewable energy technologies to reduce greenhouse gas emissions.

The three main categories of TES technologies are latent heat storage, which stores thermal energy through a phase change; sensible heat storage, which stores energy proportionally to a medium's change in temperature; and thermochemical heat storage, which keeps heat through exothermic/endothermic chemical reactions, adsorption-desorption, and absorption-desorption. Latent heat storage alters the phase of the storage medium, enabling more energy to be stored with less material than latent heat storage. Hence, a building's energy usage for heating and cooling can be significantly decreased by adding. Phase Change Materials (PCM) into its Latent Heat Thermal Energy Storage (LHTES) systems. In the limited temperature range of 0-120°C [19] for low-temperature latent heat storage, PCMs maintain a large heat capacity, and PCMs can behave similarly to a nearly isothermal heat reservoir. PCMs change phase from solid to liquid with increasing temperature. PCMs absorb heat because the phase change is endothermic. Liquid-to-solid phase transitions occur in PCMs with decreasing temperature. The heat is released this time because the phase change is exothermic. Even though the principles of use of PCMs are relatively simple, it is difficult to assess how effectively latent heat loads contribute to improving the energy efficiency of the entire structure [1].

Research about PCMs has increased momentum in recent years due to their promising features [20]. Many studies focused on building implementation methods based on simulation and experimentation. Also, increasing the thermal conductivity of PCMs is a significant topic since low thermal conductivity is the most prominent drawback of PCMs. Also, many incorporation studies were performed to increase PCMs features such as thermal conductivity and prevent leakage. Much research demonstrates the usefulness of PCMs to reduce energy consumption in building applications. Marin et al. indicate PCMs significantly reduce energy consumption for heating and cooling in several weather conditions [21]. According to James et al., PCMs could reduce heating, ventilation, and air conditioning (HVAC) system energy usage by 10–30% in various weather conditions in the United States [22].

Different incorporation techniques for PCM are explained in detail in Chapter 2. One of the most promising and widely used methods for incorporation is microencapsulation. Microencapsulated PCMs (MPCMs) are much easier and more economical to incorporate into construction materials [3].

Plasters and mortars play a vital role in building applications, significantly influencing the thermal and acoustic performance of structures and, consequently, the comfort of occupants in terms of both thermal and acoustic aspects. Also, plasters and mortars are easy to apply to building structures and can be used after construction<. Due to its ease of application, incorporating PCM, especially in MPCM form, into gypsum mortars and plasters is a promising area.

There is growing interest in the integration of PCM with waste materials. This is an up-and-coming field of study since not only is LHTES achieved, but also reusage of waste material is performed. In this way, carbon emission can be reduced in two ways: by reducing energy consumption and peak load shifting of buildings and reusing already produced material, thereby preventing procurement of new material, which has positive environmental effects.

This thesis investigates whether using MPCMs and plaster will provide significant thermal performance gains and whether this material is suitable for building use. It was investigated whether FGDG mortar containing MPCM could be used instead of gypsum mortar with MPCM.

1.2 Research Questions and Approach

The literature review shows that the integration of FGDG and PCM was not previously studied.

This thesis focuses on developing a building material with lower environmental impacts. To achieve this goal, composites are developed with MPCM to decrease, peak shave, and/or peak shift thermal energy demand of a wall system by passively harvesting thermal energy. MPCMs are integrated with FGDG and commercial plaster, and their thermal, mechanical, and acoustic properties are investigated and compared.

This study is a step to fill the gap of studies of byproduct gypsum (FGDG) and MPCM composites in the literature. In addition, different performance comparisons of waste gypsum containing PCM and any commercial plaster containing PCM bring innovation to the field.

1.3 Structure of the Thesis

The content of this thesis is separated into two parts: 1) numerical investigation of annual heating and cooling loads using a wall model that includes researching the most influential parameters by a performing Global Sensitivity Analysis; 2) preparing and the experimental investigation of MPCM-FGDG and MPCM-Commercial Plaster samples.

Chapter 2 presents a comprehensive literature review on PCMs, thermal characterisation methods of PCM-added composites, waste material-added PCM composites, and gypsum-added PCM composites. Also, the type and importance of byproduct gypsum is explained.

Fundamentals of Finite Difference Method (FDM) and wall modelling are explained comprehensively in Chapter 3.

The aim and usage areas and methods for Sensitivity Analysis (SA) are presented in Chapter 4. Also, how the wall model was modified for SA and the parameters used are explained.

Raw materials, composite development methodology and the methods used to characterise these composites are explained in Chapter 5.

In Chapter 6, results obtained from FDM for the wall model, SA for the wall model and characterisation methods are presented and discussed.

In Chapter 7, composites and model results developed with a holistic perspective are explained. In addition, possible future works are defined.

CHAPTER 2

LITERATURE REVIEW

2.1 Introduction

This section provides a comprehensive overview of various aspects related to Phase Change Materials (PCMs). The content includes classifications of PCMs, an analysis of different thermal measurement techniques employed for characterising PCM-containing composites, the rationale behind integrating PCMs in building structures and the crucial criteria involved in PCM selection. Furthermore, the section summarises numerous studies investigating the integration of PCMs with waste materials. A detailed explanation of waste plaster types and their usage areas is also provided. Additionally, the section reviews relevant research on integrating plaster and PCMs in a separate subsection.

2.2 Overview of Phase Change Materials

There are different PCM classifications according to their chemical properties (organic PCMs, inorganic PCMs and Eutectic PCMs), their incorporation into construction materials and elements (direct, encapsulation, etc.), and their implementation to the building (passive, active).

2.2.1 Chemical Classification of PCMs

The four states of material phase change are gas-liquid (condensation/vaporisation), gas-solid (sublimation/deposition), solid-liquid melting/solidification and solid-solid.

Due to technical constraints in other types, the solid-liquid type is the only feasible option for heating or cooling buildings. [23] [24] .

Abhat [19] defined a useful PCMs classification for thermal energy storage applications. Based on the chemical composition, PCM can be inorganic, organic, and eutectic, as represented in Figure 2.1. Organic PCMs can be classified as either paraffins or non-paraffins. Alcohols, fatty acids, esters, and glycols, organic materials are among the non-paraffins [25]. Hydrated salts and metallics are two types of inorganic PCMs. Metal melting temperatures are too high for building applications [1]. A minimum-melting combination of two or more components is known as eutectic. During crystallisation, each of these components melts and freezes concurrently to produce a variety of component crystals. [26]. Organic-organic, organic-inorganic, and inorganic-inorganic PCMs are different eutectics PCMs. A comparison of the benefits and drawbacks of different types of PCMs [1] [27] [2] [28]. Table 2.1 compares and summarises each type's advantages and disadvantages. Figure 2.1 presents the classification of different PCM types.

Table 2.1: Comparison of organic, non-organic and eutectic PCMs.

Classification	**Advantages**	**Disadvantages**
Organic: Paraffin and non-paraffins	Availability throughout a wide temperature range (roughly ranging from 20 1C to 70 1C)	Low thermal conductivity (usually less than 0.2 W m-1 K-1)
	Reasonable latent heat of fusion (120 J/g up to 210 J/g)	Moderately flammable
	Freeze with little or no supercooling	Non-compatibility with plastic containers
	Slight volume change during phase transition (around relatively low temperature, i.e. room temperature) [28]	
	Recyclable	

Table 2.1 Continued:

	Non-toxic (except some non-paraffins which show some toxicity) Non-corrosive, (except fatty acids)	
Inorganic: Hydrated salt	Greater capability for latent heat storage in volume	Freeze with supercooling
	Higher latent heat of fusion	Segregation during phase change
	High thermal conductivity (0.5 W/m.K)	Corrosive to the majority of metals and slightly poisonous
	More affordable and accessible	High volume change
	Non-flammable	High vapor pressure
	Appropriate for plastic containers	Decomposition and phase separation
	Sharper phase-change	
	Low environmental effect (it is preferable to employ salt hydrates rather than paraffins to minimize the environmental impact during production and disposal).	
	Having recycling potential	
Eutectic	Generally sharp melting temperature	No test data on their thermophysical properties.
	Density of thermal storage per volume slightly above organic compounds	Certain fatty eutectics have a strong odour and should not be used as PCM wallboard.

Table 2.1 Continued:

	No segregation and congruent phase-change

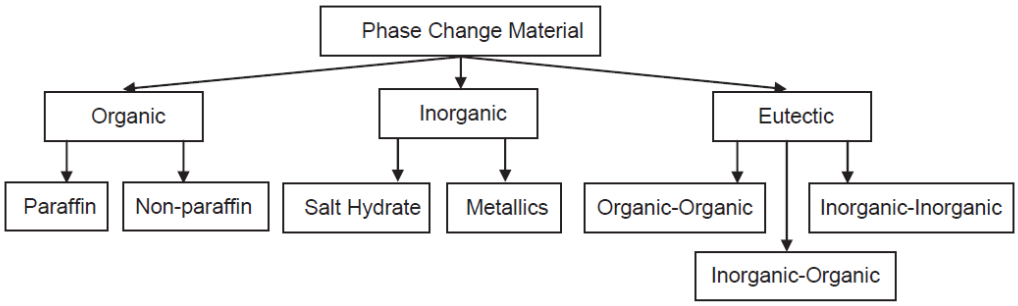

Figure 2.1: Classification Different types of PCMs[2]

2.2.2 Incorporation of PCM into construction materials and elements

There are several approaches to integrating PCMs into building materials and structures [29]. Note that although direct incorporation and immersion are represented and explained in this paper, these methods have a high risk of leaking while the PCM phase changes in liquid. Consequently, the direct incorporation and immersion of PCM in other building materials is not generally considered feasible [27].

2.2.2.1 Direct Incorporation

The direct incorporation approach is the most basic and cost-effective. During production, powdered or liquid PCM is combined directly with building materials such as cement paste, gypsum, concrete, or plaster [30], and no additional apparatus is needed. However, leakage and potential compatibility issues with some construction materials can occur. Consequently, the system's mechanical and durability attributes may be altered [1].

2.2.2.2 Immersion

The immersion method includes immersing the porous construction material (brick, gypsum board, wallboard, or concrete block) into the liquid PCM, absorbing the PCM by capillary action. A leakage problem might be problematic for long-term usage [3]. Additionally, the mechanical and durability characteristics of the building materials may be impacted[2].

2.2.2.3 Encapsulation

Before being incorporated into building elements, PCMs can be encapsulated. According to Regin et al., [31], the PCM containment should (i) ensure the requirements for flexibility, durability, thermal stability, and strength; (ii) serve as a barrier to protect the PCM from destructive interactions with the surrounding environment; (iii) provide an adequate heat transfer's surface; and (iv) be structurally stable and provide ease in handling. In general, there are two PCM encapsulation methods: microencapsulation and macroencapsulation.

Microencapsulation In microencapsulation technology, PCM particles are covered in a thin, sealed polymeric film with a high molecular weight, usually made from natural. Synthetic polymers preserve the form during the phase transition process and stop PCM from leaking [3]. PCM particles have sphere shapes ranging from 1 µm to 1000 µm (around 1 µm to 300 µm according to Hawlader et al. [32]). Polymers, both natural and synthetic, are typically used to make polymetric film [27]. This technique may produce phase change materials with temperatures between 10 and 80 °C [33]. The microencapsulated PCM (MPCM) model is presented in Figure 2.2. Also, SEM images of MPCM at different thermal cycles are given in Figure 2.3.

Macroencapsulation PCMs encapsulated in any container, like spheres, tubes, or panels, that can be used as heat exchangers or integrated into building materials are known as macroencapsulation. According to Cabeza et al., these containers' sizes are usually greater than 10 mm [34] and can go up to several litres [35]. A drawback of

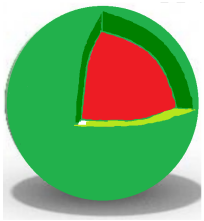

Figure 2.2: A wax core and polymeric shell microencapsulated PCM model [6]

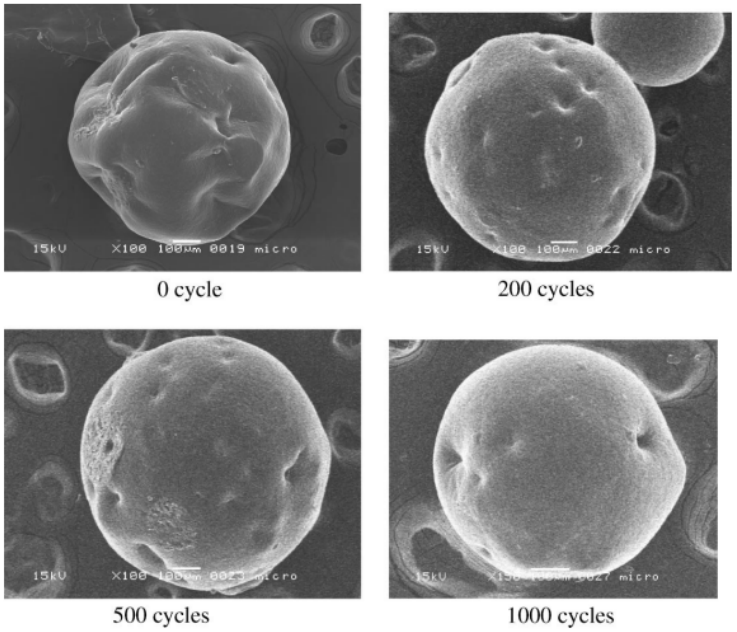

Figure 2.3: SEM evaluation of the microencapsulated paraffin profile at various thermal cycles.[7]

macroencapsulation is its propensity to solidify or melt at the edges, which causes a slower energy intake and release and may prevent the system from discharging completely overnight because the majority of PCMs have low thermal conductivity. The macrocapsules' size implies that they must be protected against destruction or perforation, which may make them more challenging to integrate into the building structure, potentially increasing the cost of these systems [36].

2.2.2.4 Shape-stabilized PCM

Shape-stabilized PCM is made using supports for shape stabilisation, such as high-density polyethylene (HDPE). An example of some shape stabilised PCM (SSPCM) is given in Figure 2.4, which is taken from [1]. When both the supporting material (or supporting materials) and the PCM are liquid, they are combined at a high temperature, and the supporting material is then cooled to a temperature below the glass transition temperature until it solidifies. They are gaining popularity due to their high apparent specific heat, good thermal conductivity, ability to keep the shape of PCM stable during the phase change process, and long-term performance and durability after multiple thermal cycles [37] [38]. On the other hand, according to Zhang et al. [39], products with low rigidity or shape-stabilized products with large-volume PCM will deform due to the inability to support their weight.

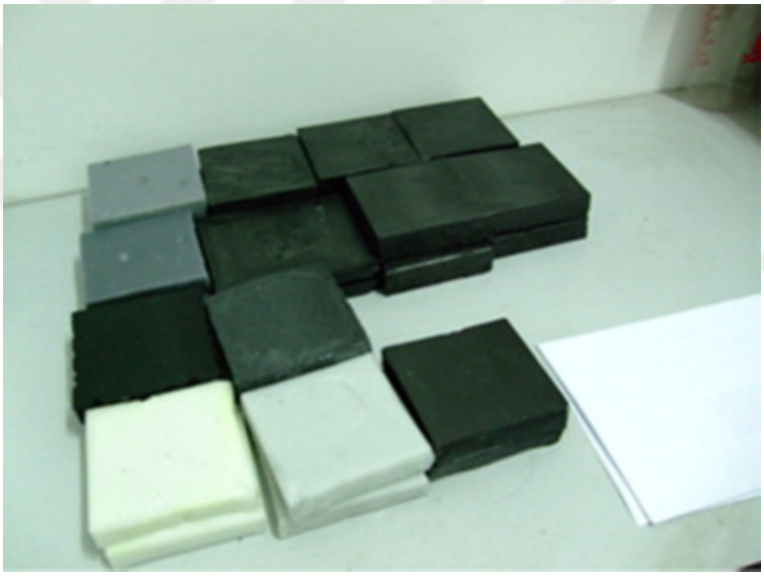

Figure 2.4: An illustration of SSPCMs that resemble a homogeneous material [1]

2.2.3 PCM Implementation & Methods

There are many different implementations of PCMs, such as Solar Water Heating, Waste Heat Recovery and Space Heating. There is much detailed research about all different PCM implementations. Since the scope of this literature survey focuses on space heating and cooling, this topic is explained in detail.

2.2.3.1 Space Heating and Cooling

The concept of thermal mass focuses on using PCM to regulate the temperature conditions within a structure. Thermal mass refers to a building construction approach that introduces resistance to fluctuations in temperature by incorporating inertia. The building's structure functions as a thermal energy storage source and is crucial for heat buffering to reduce indoor temperature swings and mitigate external heat flows. As a result, during hot weather, the structure acts as a heat sink [40]. By incorporating PCM into the building structure, the thermal mass is enhanced, effectively obstructing heat transfer into the occupied space [41]. For heating and cooling purposes in buildings, it is suggested to utilise PCMs that have a melting point ranging from 20 °C to 32 °C. These PCMs are recommended for thermal storage, whether combined with passive or active solar storage methods[26].

Passive Systems Passive building systems used for thermal energy management consider the thermal mass that may help reduce the need for cooling and/or heating equipment. [42]. A form of thermal energy storage known as LHTES can be encased in building materials or structures. Since no conventional energy is required, the system is described as passive. Integrating PCMs into building materials during free cooling enables the PCM to absorb cold temperatures overnight, triggering the solidification process. During the daytime, the PCM releases the stored cold through the melting process, reducing heat transfer from the outdoor environment to the indoors. [43]. The system can heat the building during the winter by capturing solar energy during the day. Passive methods instantly release any heat or cold held when interior or outdoor temperatures rise or fall over PCM's melting point. The benefit of using PCM in building constructions is that it eliminates the need for a separate plant and space. Consequently, several investigations on PCMs included in building materials (such as glass, brick, or concrete) or components like wallboards, floors, ceilings, underfloors, shutters, and roofs have been carried out [43].

Active Systems Forced convection is the primary mechanism for heat transfer between storage and indoor air in active applications where specific auxiliary electrical

or mechanical equipment is required [44]. Active systems are divided into two subclasses: free active cooling and space heating active method. The reason for this classification is that heating systems generally require an auxiliary heating source, whereas active cooling systems are more likely to be used without an auxiliary heating source. It should be noted that this classification is an initiative generalisation and that contrary cases are possible [43].

Free Active Cooling The coolness of a source for cooling buildings, such as outside air, is referred to as free refreshment. For example, suppose night-time coldness is kept and used during the day to reach comfortable temperatures indoors. In that case, mechanical ventilation may either be eliminated entirely or limited throughout the day to specific times. This process is called free cooling because the cold source does not require energy. LHTES systems are also able to deliver free cooling by improving mechanical ventilation systems' cooling potential or even contributing to mechanical ventilation system size reduction. This leads to higher temperatures and, as a result, better thermal comfort conditions. Free cooling has some main advantages: cooling while reducing emissions of greenhouse gases and maintaining good indoor air quality within the facility. The PCMs used in free cooling systems must be selected such that the cooled air temperature falls within an acceptable range that is comfortable for people. In the summer, for example, the human comfort zone ranges from 23 to 27 ° C [43]. The temperature differential between the air temperature and the PCM's melting point should be between 3-5 °C to accomplish effective heat transfer. An active free cooling system is defined as such because it uses electric devices [43]. An active system ensures the storage of this coolness by using a free source of cooling (such as night coolness). Active storage involves actively moving heat transfer fluid, known as forced convection, and lowering the internal temperature. It has the potential to not only significantly reduce energy consumption but also reduce it to a fraction of what it is now. Only a fan's energy consumption remains. This type of system also allows for complete control of the process during PCM charging and discharging, which improves overall system performance.

Active methods for space heating (using an auxiliary source) For space heating, a comparable approach of active free cooling was developed. Yet, the PCM-TES is typically connected to auxiliary heat sources like heat pumps or solar thermal collectors during the winter since the desired warm air temperature is not always available at that time of year. This will once again allow for a reduction in heating system capacity and annual operating costs. Building many PCM layers with various phase change temperatures to accommodate various auxiliary heat sources allows for space heating. Air conditioning systems, solar thermal collector panels, and heat pumps are the primary sources. Free heating sources (such as solar radiation) are stored by an active system. Space heating is beneficial for reducing thermal heating demand by increasing space temperature [43].

2.2.4 PCM Selection Criteria

Choosing the appropriate PCM for a particular thermal energy storage application in buildings necessitates a meticulous evaluation of the thermal, kinetic, physical, chemical, environmental, and economic characteristics of the different available options; this involves comparing their strengths and weaknesses and, in certain instances, finding a suitable compromise. [2]. An assessment of the benefits and drawbacks of various types of PCMs has been presented by several authors [1] [2] [3] [4]. In Table 2.2, each type's primary benefits and drawbacks are contrasted and outlined.

Table 2.2: Main criteria that govern the selection of PCMs [1] [2] [3] [4].

Thermal properties	Proper phase-transition temperature for building applications.
	High latent heat of fusion per unit volume
	High specific heat
	High thermal conductivity
	Thermal reliability (i.e. cycling stability)
Physical properties	Small volume change during phase change
	High density
	Small vapour pressure

Table 2.2 Continued:

	Complete melting process (i.e. congruent melting)
Kinetic properties	High rate of nucleation to avoid supercooling
	High rate of crystal growth
Chemical properties	Chemical stability
	Compatibility with materials of construction
	Non-toxic, non-flammable and non-explosive
	Non-corrosiveness
Economic properties	Effective cost
	Commercially available
Environmental properties	Low impact on the environment and non-polluting throughout the service life
	Having potential for recycling

2.3 Thermal Property Measurement Methods

2.3.1 Thermal Conductivity

Thermal conductivity is a transport property and a characteristic of the material. The heat transfer rate through a material's unit cross-sectional area under conditions of a temperature gradient is referred to as its thermal conductivity, resulting in heat transfer by conduction. [5].

Temperature, chemical structure, particle size, porosity, and the direction of heat flow are only a few examples of the factors that affect a material's thermal conductivity. Temperature and density are the most critical factors in thermal conductivity. The following are some of the influencing factors [20] [45]:

1. Temperature: Thermal conductivity increases with increasing temperature until

it reaches a maximum value, which remains constant over a small temperature range. After that, as the temperature rises, it drops rapidly until it approaches its lowest value, near the material's melting point.

Thermal conductivity increases with increasing temperature: At lower temperatures, the thermal conductivity of a material generally increases as the temperature rises. This is because the thermal energy excites more phonons, increasing the number of heat carriers available for heat transfer. As a result, the thermal conductivity tends to rise.

Maximum value and plateau: As the temperature continues to increase, there is a point where the thermal conductivity reaches a maximum value. This maximum can occur due to the interplay between different mechanisms affecting thermal conductivity, such as changes in phonon-phonon interactions, phonon scattering, and lattice vibrations. Once the maximum value is reached, the thermal conductivity remains relatively constant over a small temperature range. This plateau occurs because the increase in phonon population is offset by the increased scattering events, resulting in a steady state thermal conductivity.

Sharp decrease towards the melting point: As the temperature continues to rise beyond the plateau, the material's thermal conductivity often decreases sharply as it approaches the melting point. This decrease occurs because the material undergoes a phase transition, such as melting or a structural transformation. During these transitions, the crystal structure becomes less ordered, and the phonon-phonon interactions and phonon mean free paths are disrupted, reducing thermal conductivity.

Minimum near the melting point: The thermal conductivity reaches a minimum value near the material's melting point. The minimum occurs when the material is in its liquid state, which typically has a lower thermal conductivity than the solid state. The lack of long-range order and increased molecular vibrations in the liquid phase contribute to reduced thermal conductivity.

2. Density: The density of a material, or changes in density, has a significant impact on thermal conductivity, particularly when phase change and reactions occur.

3. Grain size: As the grain size increases, the thermal conductivity also increases. This is because grain boundaries serve as obstacles to heat conduction. Therefore, materials with larger grain sizes consistently exhibit higher thermal conductivity, while materials with smaller grain sizes demonstrate lower thermal conductivity.

4. Porosity: Compared to solid materials, greater porosity corresponds to lower thermal conductivity. The thermal conductivity is influenced by porosity and factors such as pore size, distribution, shape, and connectivity.

5. Crystal structure: The crystal orientation does not impact the heat conductivity of cubic-system materials, whereas the thermal conductivity of other crystal systems is affected by anisotropy.

6. Chemical composition: Impurities significantly impact thermal conductivity. Materials having a simple chemical and molecular structure have higher thermal conductivity than materials with more complex structure

7. Direction of Heat Current: The measurement direction is vital for heat conduction in anisotropic materials.

2.3.1.1 Thermal Conductivity Measurement Methods

There are many different thermal property measurement methods based on different principles, which can be divided into two: steady state methods and Transient Methods. Classification of these methods is given in Figure 2.5.

steady state Measurement Methods steady state methods rely on applying a constant heat flux from one side of the sample and measuring temperatures along the sample length when the temperature distribution in the sample reaches a steady state. Thermal properties are calculated using the steady state temperature difference in the sample [20]. There are two steady state techniques that work well with low-thermal conductivity materials: Guarded hot plate, which is an absolute technique, and Heat flow meter, which is a comparative technique [46].

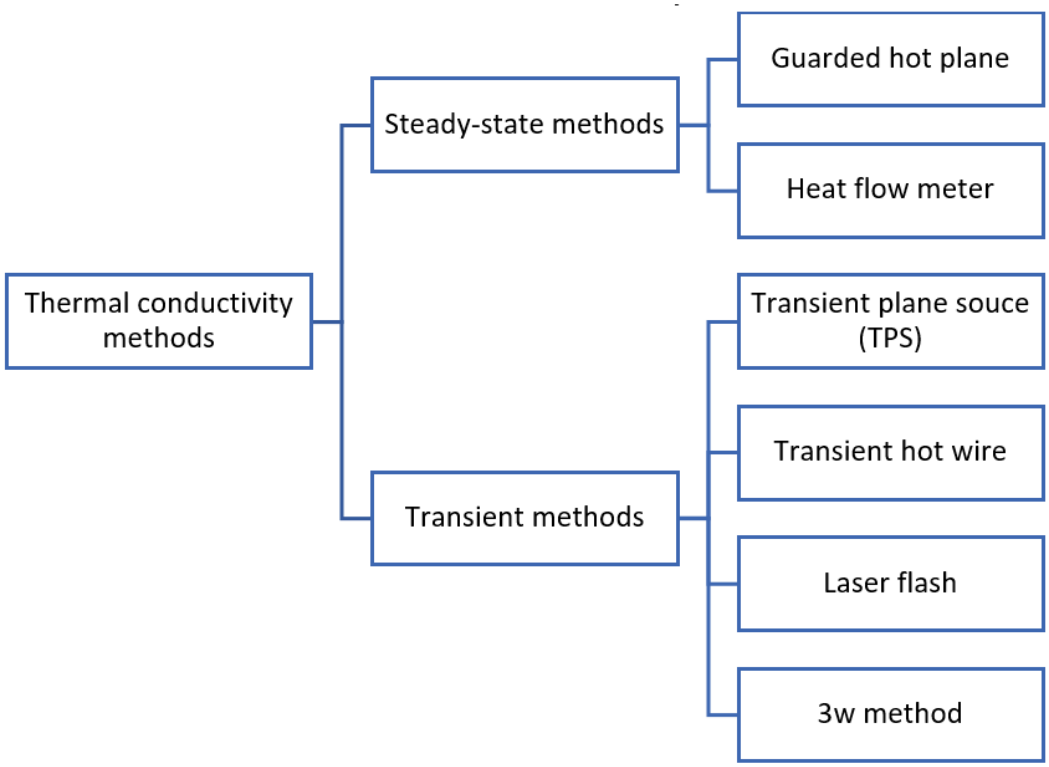

Figure 2.5: Thermal conductivity methods classification.

Guarded Hot Plate The most widely utilised and dependable method for measuring the thermal conductivity of insulating materials is the Guarded Hot Plate (GHP) method [47]. Among the methods employed under steady state conditions, the GHP technique stands out as the most precise and accurate[48] and is traditionally acknowledged as the sole, absolute method for measuring thermal conductivity in steady state conditions for homogeneous materials; it is possible to obtain a global measurement uncertainty of less than 2% using the GHP technique [49]. For the measurement, a solid sample is positioned between two temperature-controlled plates that are parallel to each other. An inner heater heats the hot plate, ensuring a targeted temperature gradient; the sample acts as a channel for the energy, which then heats the cold plate. Heat losses should be prevented, and backward heat flows should be eliminated to achieve uniaxial heat transfer. This is provided by using a guarded heater and thermal insulation and lateral and backward heat flow eliminated [50]. The surface-to-thickness ratio should be sufficient to reduce heat losses during the process. Once the system reaches a state of equilibrium, the thermal conductivity can be determined by applying Fourier's conduction equation, which involves analysing the heat flow,

temperature gradient, and thickness of the sample. The main disadvantages of that method are the required specimen thickness and time-consuming [51].

Heat Flow Meter The Heat Flow Meter is a commonly employed and precise method used to assess the thermal conductivity of low-conductivity materials. [51]. Firstly, calibration of the heat flux transducer is performed by a specimen with known thermal conductivity. Then, by using Fourier's law of heat conduction and the measured heat flux, it is straightforward to determine the sample's thermal conductivity. This method is commonly employed to evaluate materials with low thermal conductivity, including building insulation materials. It is important to note that the heat-flow meter method typically has a maximum temperature limit of around 200°C [52] and in practical application, limit is about 100°C [20]. Like the guarded hot plate technique, this method applies solely to solid samples and is effective for measuring thermal conductivity values up to 2 W m^{-1} K^{-1} [20].

Transient Measurement Methods In transient methods, a heat source generates a transient heatwave. This heatwave causes a transient change in the temperature of the sample, and thermal properties are calculated using the time-dependent temperature increase. Transient methods are advantageous because they do not necessitate waiting for a steady state; measurements can be completed in a short period of time [46]. This section discusses four frequently used transient techniques: the pulsed power technique, Transient Hot Wire, Transient Plane Source, Laser Flash, and 3ω Method.

Transient Hot Wire The transient hot wire method is an invasive technique that measures the temperature increase at a predetermined distance from a linear heat source, typically a hot wire, embedded within the test sample [51]. Using this method, the thermal conductivity of non-conductive materials may be determined [20]. Unlike steady state measurements, this technique is considerably faster and applicable over a broader temperature range [20]. It can be used to measure the thermal conductivity of liquids, solids, gases, and powders [20]. The transient hot wire method has found wide application in measuring the thermal conductivity of liquids. In this method, the heated wire is viewed as the ideal linear heat source, producing heat uniformly

throughout the length of the sample. The technique builds its assumptions on an idealised "one-dimensional radial heat flow" model within the isotropic and homogeneous test sample[51]. This assumption relies on the idea that the linear heat source has an infinite diameter and infinite length [51]. By monitoring the temperature variation that takes place at a predetermined distance from the hot wire over a predetermined amount of time while a constant electric current flows through it, it is possible to calculate the test sample's thermal conductivity under these conditions[51].

Transient Plane Source (TPS) The transient plane source technique (also known as the hot disk method) is a recent improvement of the hot-strip method [20]. The method was designed to measure thermal diffusivity as well as conductivity. Sensor probes of the TPS contain long wires in the shape of a thin spiral disk. Thus, it can be obtained reasonably high resistance of the wire in a compact form is convenient to work with smaller samples [46]. The experimental setup involves enclosing a metal disk with electrical insulation and enclosing it between two identical, thin testing samples in the form of slabs. Thermal insulation is used on the remaining surfaces of the testing samples. In the experiment, only a small electrical current is used to heat the metal disk. The two attached testing samples significantly influence the temperature increase of the metal disk, allowing for the determination of their thermal properties by monitoring the temperature rise over a short duration. This usually only takes a few seconds, but it makes sure that the metal disk stays in touch with infinitely large samples all the way through the transient signal recording process. It is possible to measure the temperature rise at the sensor surface (ΔT) as a function of time. Generally, the measurement's 2-5 K total temperature increase is suitable for accurate results. A temperature increase of less than 2 K is insufficient for accurate results. On the other hand, a high-temperature increase can damage the sensor [46]. Temperature sensor (temperature resistance thermometer) measurement accuracy is typically -+0.01 [53]. The equipment suggested in the literature provides for a temperature range of 30 to 1200 K[20], thermal conductivities from 0.001 to 1800 W/m K and thermal diffusivity from 0.1 to 1200 mm^2/s [46]. The main advantages of the transient plane source measurement are that it is able to provide quick results (typically in less than 10 minutes), and various sensor sizes can be employed to ac-

commodate different types of specimens. TPS can measure the thermal properties of various materials, including bulk solids, sheet metals, slabs, anisotropic materials, porous structures, one-dimensional materials, liquids, pastes and powders at a wide temperature range [46]. Also, this technique is widely used for measuring the thermal conductivity of PCM composites, pure PCMs and encapsulated PCMs. PCM leakage above the melting point can cause sensor damage due to chemical incompatibility. Furthermore, the composite's mechanical stability at temperatures over the phase change point in the case of PCM or the reaction temperature in the case of PCM can influence the measurement conditions and, as a result, the results obtained [20].

Laser Flash Laser flash analysis (LFA) is regarded as one of the most versatile and successful methods for determining thermal characteristics [20]. Thermal diffusivity is measured, ideally for solid materials such as glasses, metals and ceramics; however, by employing suitable sample holders and adjusting measurement conditions accordingly, liquids and composites can be measured at a variety of temperatures [52]. The temperature is sensed non-destructively and in a non-contact way using the laser flash technique, allowing for high levels of accuracy. It is capable of measuring temperatures within a range of approximately -125°C [54] to 3000°C [20].

The laser flash method applies a laser pulse from a laser beam source that strikes the bottom of the sample. An infrared sensor measures the temperature variations occurring on the sample's opposite side. It is possible to measure the thermal diffusivity along the sample's thickness (usually in disk shape) by analysing the temperature rise on the sample's surface [20] [55]. Even at elevated temperatures, it is possible to achieve relative measurement uncertainties in the range of 3-5% [55]. In this method, one-dimensional heat conduction is assumed[51].

3ω Method The 3ω method, introduced by Cahill et al. in 1990, is a widely employed technique for determining a material's bulk and thin-film thermal conductivity [56]. Many different values of thermal conductivity are reported in the literature, ranging from 0.20 to 20 W/m K, with temperature ranges extended up to 77-900 K [55]. Likewise to the hot wire method, the 3ω technique also involves a radial heat flow generated by a thin metallic strip that serves as both the heater and temperature

sensor. However, in the 3ω technique, a heat wave with a frequency of 2ω is produced when a sinusoidal current with a frequency of ω is run through the metal wire. This heat wave can be deduced by analysing the voltage component at the frequency of 3ω. That means instead of a time-domain response, the temperature oscillations have a frequency dependence [20] [55]. The setup comprises a metal strip positioned above the thin film sample, featuring four contact pads for measurement purposes. The metallic strip (such as gold, platinum, or aluminium) is typically deposited onto either a substrate or a film-on-substrate stack. The dimensions of the metallic strip commonly range from a half-width of 10-50 μm to a length of 1000-10,000 μm [51]. The presence of alternating current in the system causes resistance oscillations along the metallic strip, occurring at a frequency of 3. In this experimental configuration, it is assumed that the heater is in direct thermal contact with the sample, disregarding its heat capacity while assuming its mass to possess infinitely conductive properties [20].

2.3.2 Phase Change Temperature and Latent Heat of Fusion

2.3.2.1 Differential Scanning Calorimetry (DSC)

DSC is a thermodynamic instrument that determines how much heat is needed to keep a substance at a certain temperature. The tests change the temperature linearly with time, and the measurement temperature range should be arranged according to cover melting and freezing temperatures. PCM specimens are compared to a control sample with known thermal characteristics. DSC test is conducted, which generates a curve representing heat flow in relation to temperature or time. The resulting DSC curve provides information on crystallisation and melting temperatures and the magnitude of latent heat. However, DSC has certain limitations, including reported supercooling effects caused by small sample sizes and their consequent weak nucleation effects [57]. This method uses waste-added PCM composite research in order to determine melting/freezing temperature and latent heat of fusion [57]. In DSC measurements, the heating rate is an important parameter [1]. To minimise modelling and measuring errors, Mehling and Cabeza [58] suggests utilising heating rates ranging from 0.5 K min^{-1} for small masses to 2 K min^{-1} for larger masses.

2.3.2.2 Differential Thermal Analysis (DTA)

DTA and DSC differ in that DTA measures temperature variation between the reference pans and reference pans, whereas DSC measures the differences in energy [59] . In DTA method, heat flux to the sample and reference is constant, and the temperature difference is measured. The temperature differences are then used to calculate thermal properties [60]. The heat transfer rate at different temperatures is visually shown by time versus temperature graphs created by DTA [61]. When operating in bulk units, testing with tiny sample sizes might distort the thermo-physical performance evaluation of a given material [60]. Another limitation of DSC and DTA is their high cost and inability to measure multiple samples at the same time [60].

2.4 PCM and Waste Material Added Composites For Building Applications

Waste material and PCM incorporation from literature are selected, and 21 papers are presented. This selection is made based on different waste material types in a wide range from coffee waste to medical waste, also different incorporation techniques are included, such as MPCM to direct incorporation. All 21 papers are detailed investigated, and innovative/important aspects of these studies are tabulated in Table 2.3. Also, essential results from these studies are presented. Different matrix and PCM combinations are used. Therefore, it is hard to generalise findings. However, few generalisations might be made for investigated papers. Compressive strength tends to reduce with the inclusion of PCMs; however, for different matrices and different PCM materials, the volumetric fraction of PCM changes correlates with compressive strength. Latent heat increases with PCM inclusion, as expected. Thermal conductivity generally decreases with PCM inclusion; however, it is not always the case [62].

Thermal characterisation methods performed in these 21 papers are presented in Figure 2.6.

Table 2.3: Evaluation of waste-added PCM papers.

Title	Innovative Aspects	Important Findings

Table 2.3 Continued:

[62]	Innovative waste material and acoustic evaluation	The thermal conductivity measurements verified that an increase in the quantity of MPCM resulted in a corresponding increase in thermal conductivity. The frequency that was discovered was within the mid-frequency region, and a shift in the pattern suggested that the coffee waste was degreased using MPCM (DCWB) at 3, 5, and 10 wt% demonstrating a higher sound absorption coefficient.
[63]	Very comprehensive material characterisation, thermal behaviour test	The impregnated graphene PCM cement mortar's capacity to absorb heat rose as the concentration of SCW and LGW percentage load increased. At melting of the PCM, the SCW and LGW exhibited superior convective heat absorption compared to pure cement mortar. This improvement can be attributed to the conductive properties of the latex waste.

Table 2.3 Continued:

[64]	Showing the applicability of non-capsulated PCM and cement and fly ash mortars composite	In terms of the mechanical properties, including flexural and compressive strengths, of the mortars, it can be concluded that the addition of 5% and 10% of PCM did not result in significant changes, 4% and 5% strength decrease. Nevertheless, increasing the PCM content leads to a greater reduction in mechanical strengths, with a decrease of 19%. Thermal evaluation was performed for a specific climate for the summer and spring seasons. It found that including a higher PCM content results in improved thermal properties and thermal performance in terms of decreasing climatisation energy needs.
[65]	Paraffin wax impregnated expanded graphite used. Thermal and mechanical properties are	No leakage was observed due to calcium silicate forming a capsule-like wall barrier. Encapsulated PCM expanded graphite is mechanically and chemically stable. The compressive strength of the geopolymer composite is 10.3 MPa. The expanded graphite encapsulated PCM thermal conductivity value is 0.9425 W/mK, and the inclusion of paraffin into expanded graphite demonstrated a substantial improvement in thermal conductivity, with an increase of 90%.

Table 2.3 Continued:

[66]	Suggesting MPCM's particle size is correlated to the workability of concrete; Effect of curing temperature and how it changes with time;	The slump of GPC was lower than PCC due to the high viscosity of the alkaline solution when MPCM was added. Also, PMC's phase state does not significantly affect GPC but affects PCC. As a result, for concrete that has MPCM included, GPC is a better choice when these construction materials are subjected to temperature fluctuations.
[67]	Detailed explanation of the numerical method and numerical analysis based on the orientation of the wall	The power reduction with the addition of 5.2 wt% MPCM was about 25–27%, and the highest annual power reduction is obtained when the wall is facing the southern and western walls in both Madrid and Oslo. In addition, the incorporation of MPCM resulted in increased concrete porosity, consequently lowering thermal conductivities. As a result, the power consumption was reduced by up to 15%, even under extreme temperature conditions.
[68]	Comparison of MPCM added PCC and GPC regarding mechanical and thermal performance. It also suggested that MPCM-added building materials can satisfy mechanical demands.	For GPC(2.7 wt.% MPCM and decreased around 51%), the compressive strength decrease is more pronounced than that of PCC. (3.2 wt.% MPCM and decreased around 42%) due to a higher porosity rate increase of GPC compared to PCC. Possible energy reduction is calculated to stabilise indoor temp at 23 C . (11% for PCC and 15% for GPC)

Table 2.3 Continued:

[69]	A comprehensive study about the effect of MPCM on cement, says possible ways to increase cement mPCM added composite quality	The inclusion of MPCM led to a reduction in compressive strength and subjecting the samples to temperatures above the melting point of the MPCM core had a more significant impact on PCC compared to GPC.
[70]	Effect of core/shell ratio on the interface bond and mixture uniformity	The compressive strength at 5.2% MPCM varies for different shell core compositions. Some MPCMs satisfy the mechanical European regulation; however, thermally, the most promising one does not satisfy due to larger air pockets and a higher core-to-shell ratio.
[71]	Comparison of effect of different types of bricks on thermal conductivity; bending test	It was observed that those mixtures produced with High porosity Poroton® fired-clay blocks RBAs had a slightly lower thermal conductivity compared to the Standard recycled bricks RBA mixtures due to a higher air content. Also, an increasing filling degree of PCM leads to a declining compressive strength for both the SB and PB PCM-RBA mortars (23% and 27% for SB mixture and between 13% and 19% for PB mixture)

Table 2.3 Continued:

[72]	Annual modelling for three different cities using three different specimens	In warmer regions, the benefit of utilising wool-PCM-based insulation was spectacular. Still, it was significantly diminished in regions with a longer and harsher winter season. Compared to polyurethane foam insulation, wool-based insulation, which accounts for 41 per cent of the weight of PCM, uses 31.6 per cent less energy annually for cooling and 26 per cent less annually for air conditioning climate locations like Palermo.
[73]	Novel incorporation materials	PEG1000 added to PCM-stone composite with different mixing times and the longest time,60 minutes, is most desirable due to longer impregnation time can ensure a deeper penetration of PEG and, in turn, a further increased stability.
[57]	Novel incorporation materials and detailed assessment of end product	The maximum indoor centre temperature differs by 3 °C between the control and n-octadecane-GP room models. The composite PCM cement paste disk containing n-octadecane-GP demonstrated a significant reduction of 31.1% in thermal conductivity value.

Table 2.3 Continued:

[74]	Comprehensive bending test result of composite	The composite's strength is mostly increases with an increase in the mixture's thickness. In contrast, the influence of the aerogel mat's thickness in this regard is relatively less significant.t. Depending on aerogel thickness, thermal resistance takes values from 0.41 m2 K/W to approx. 2.44 m2 K/W .
[75]	Novel incorporation materials	Incorporating expand perlite/paraffin encapsulated by calcium silicate and expand perlite/paraffin into clay geopolymer mortar causes the compressive strength to rise compared to clay geopolymer mortar with impregnated expand perlite. Using calcium silicate and glass water as the capsules, the PCM building materials can effectively avoid paraffin leakage. Thermal conductivity decreases with PCM (paraffin) addition. PCM and Calcium silicate addition has increased thermal inertia and maximum temperature
[76]	Yearly energy demand change based on months	The optimal PCM content in the mortar was found to be 15%, which allowed for maintaining the compressive strength above 31 MPa. Thermal storage capacity is 240% more than regular mortar, and PCM addition caused a 1.2°C temperature difference of internal space in the control experiment

Table 2.3 Continued:

[77]	Sustainability assessment of the process; evaluation of silica fume to improve the mechanical properties of PCM-incorporated concrete two different PCM with different matrix compositions	Silica fume improves the compressive strength of concrete containing PCM by roughly 20 to 45 per cent while having no negative effects on the PCM's thermal performance. As a result, it was discovered that adding silica fume to concrete was a promising way to increase the concrete's compressive strength.
[78]	Very comprehensive material characterisation	The addition of PCM at 15% and 30% into GFC (Geopolymer Foam Concrete) reduced indoor temperature in simulated test rooms by 1.85 °C and 3.76 °C, respectively. Although geopolymer concrete decreased compressive strength, the GFC has demonstrated increased compressive strength qualities as a consequence of a drop in foam content and a corresponding increase in the amount of gel particles (as a consequence of PCM addition).

Table 2.3 Continued:

[79]	Very comprehensive material characterisation	The thermal conductivity of the capric-stearic acid eutectic mixture (CSEM) increased by 79% after being combined with sugar beet pulp (CSBP). The phase transition temperatures of Composite with CSEM (70%) and CSBP remained the same, but the latent heat values decreased by roughly 33% when compared to pure CSEM. Due to the composite PCM's melting temperature remaining nearly constant after 1000 thermal cycles, its latent heat was lowered by less than 3%.
[80]	Novel incorporation materials	No chemical reaction is observed between the supporting material of calcium carbide furnace dust (CCFD) and paraffin. The melting and crystallisation temperature of CCFD PCMs was imperceptibly changed compared with pure paraffin wax, which is 59.1°C and 53.7°C due to the physical interaction between paraffin and CCFD. The Paraffin/ACCFD exhibited outstanding phase change properties, with high melting/freezing enthalpy reaching 76% and 73% higher than that of Paraffin/CCFD.
[81]	Development of ceramic tiles with a PCM that was directly included	Decreases temperature fluctuations inside a room by up to 22% The best content was discovered to be 5.4 wt% PCM.

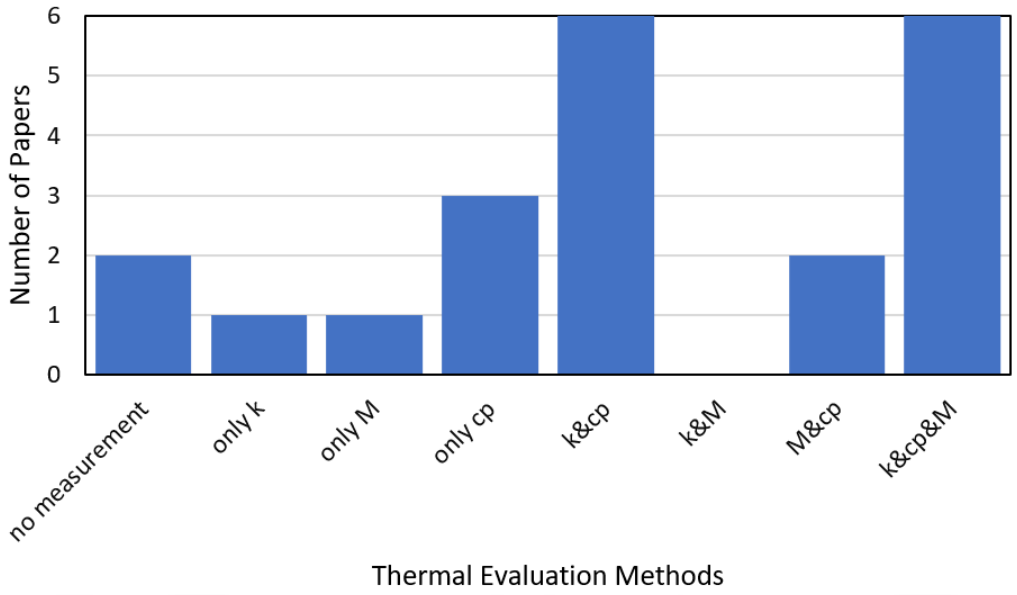

Figure 2.6: Thermal evaluation methods of investigation papers. Note that no measurement=there is no thermal investigation for thermal aspects; only k= only thermal conductivity is measured; only M = only thermal modelling and experiment is performed; only cp= only specific heat is measured; k&cp= thermal conductivity and specific heat are measured; k&M= thermal conductivity is measured and thermal experiment/modelling is performed; M&cp= specific is measured and thermal experiment/modelling is performed; k&cp&M= thermal conductivity, specific heat is measured and thermal modelling/experimentation is performed.

2.5 Byproduct Gypsum

Byproduct gypsum is produced as a byproduct during several industrial processes. This particular variety of gypsum results from unintended manufacturing or industrial processes. Gypsum byproducts can come in various compositions and qualities depending on the processes from which they are produced. The three main types of byproduct gypsum are phosphogypsum (PG), flue gas desulfurisation gypsum (FGDG), and red gypsum (RG). [82]. Phosphogypsum is a byproduct of the phosphate fertiliser industry. It is generated during the production of phosphoric acid from phosphate rock. Phosphogypsum production varies depending on the global demand for phosphate fertilisers and the scale of phosphate mining and processing. Global PG production is estimated at around 100–280 Mt per year [83]. FGDG is a byproduct of

the flue gas scrubbing process used to remove sulfur dioxide (SO2) emissions from power plant flue gases. It is a form of synthetic gypsum produced from the reaction of lime or limestone with the sulfur dioxide in the flue gas [84]. An estimated 255 million tons of FGDG were produced worldwide in 2020, mainly in Asia (55%) and then in Europe (22%), North America (18%), and the rest of the globe (5%) [85]. RD is a by-product of titanium(IV) oxide extraction from the ilmenite ores.

2.5.1 Flue Gas Desulfurization Gypsum (FGDG)

FGDG has gained significant attention as a sustainable and environmentally friendly building material. It offers several advantages, including fire resistance, sound insulation, and excellent thermal properties [86]. FGDG is commonly used in the construction industry for applications such as gypsum boards, plaster, and cementitious materials. Its use helps reduce the demand for natural gypsum and mitigates the environmental impact of mining and extraction. Additionally, incorporating FGDG in construction materials provides an opportunity for recycling and reusing industrial byproducts, promoting a circular economy approach in the building sector [87].

More research is needed about developing composites containing both FGDG and PCM. During this literature review, no study was found in which a composite was developed with MPCM and FGDG, where FGDG is the primary matrix, not an addition to cement, etc.

2.6 Gypsum and PCM Compositions

Given the widespread usage of gypsum, plasterboards, and wallboards in constructing interior walls and ceilings, enhancing the thermal performance of these materials, MPCM-review is necessary. There are several studies about composite development with gypsum and PCM. As represented by Table 2.4, direct and microencapsulated PCM incorporation is used. PCM percentage varies a lot depending on the impregnation method and additives to mixtures. For example, one study used PCM weight more than plaster weight because fibre was added to the mix [88]. In some studies, commercial PCM was used, especially in MPCM incantations. In these studies,

generally, organic PCMs were used. In Table 2.5, which characterisation methods were used in the same studies in Table 2.4 and whether experiments and modelling were carried out are presented. While all studies performed different levels/types of thermal characterisation, less than half performed mechanical characterisation. SEM is widely used for micro-structural investigations in these studies, and the density of produced specimens is measured widely. Hot Box was The most common experiment setup; in only two studies, some modelling was presented. Generally, with the addition of PCM, mechanical strength decreased at some level, and the heat capacity of specimens was increased.

Table 2.4: PCM types, PCM incorporation methods, and PCM ratios of gypsum-containing PCM studies.

Paper	**PCM material**	**Incorporation method**	**PCM percentage**
[89]	commercial grade butyl stearate	direct incorporation	21-22% (weight to dry product)
[88]	n-octadecane as core material; melamine–formaldehyde copolymers as shell material	MPCM	micro-PCMs/gypsum weight ratios: 30/70, 50/49
[90]	eutectic mixture (63% capric acid +37% palmitic acid)as core material; melamine formaldehyde (MF) as shell material	MPCM	5% and 10%
[91]	n-octadecane	direct impregnation (under vacuum)	(18, 22, 21, and 36)% (weight ratio to specimen before impregnation)

Table 2.4 Continued:

[92]	heptadecane, octadecane and nonadecane as core material; poly-methil-metacrilate as shell material	MPCM	5.7%-26.3% (final wt)
[93]	paraffin as core material; polymer as shell material	MPCM	23%, 30% and 40% (wt)
[94]	Four different kinds of MPCM, namely mSP-(PSt-RT27), mSD-(LDPE·EVA-RT27) with and without CNFs, and Micronal®DS 5001X	MPCM	7.5%-15% (wt)
[95]	capric acid–palmitic acid	direct impregnation (under vacuum)	0%-10%-20%-30%-40% (Volume fraction)
[96]	paraffin	direct impregnation (under vacuum)	0%-10%-20% (wt)

Table 2.5: Characterisation methods of specimens and experimental setup and modelling methods used in studies

Paper	**Measured Mechanical Characteristics**	**Measured Thermal Characteristics**	**Other Characterization Methods**	**Experiment**	**Model**
[89]	N/A	latent heat (DSC) and thermal conductivity (TPS)	Water absorption; fire resistance; thermal ageing	N/A	N/A

Table 2.5 Continued:

[88]	N/A	latent heat (DSC) and thermal conductivity (TPS)	thermal ageing; SEM	N/A	N/A
[90]	Compressive and flexural strength	latent heat (DSC)	FESEM; FTIR;Thermogravimetric analysis ;apparent density	Hot Box	N/A
[91]	N/A	thermal conductivity (TPS)	CUP test (water vapour resistance); density	N\A	wall Heat transfer and moist transfer model by WUFI Pro 5.3

Table 2.5 Continued:

[92]	N/A	thermal conductivity (TPS) and latent heat (TPS)	density	slab test using thermocouples	thermal conductivity, latent heat and density model using exp data
[93]	N/A	specific heat (DSC)	density	test cell experiment (one side hot and one side cold)	N\A
[94]	Compression test	thermal conductivity and latent heat (measured by homemade equipment)	SEM; density; Thermo gravimetric analysis (TGA)	N\A	N\A
[95]	Compressive and flexural strength	latent heat (DSC) and thermal conductivity (TPS)	SEM; FTIR	Hot Box	N\A

Table 2.5 Continued:

[96]	Compressive and flexural strength	thermal conductivity (hot wire method) and latent heat (DSC)	thermal ageing test; XRD; SEM	Hot Box	N\A

CHAPTER 3

FUNDAMENTAL OF FINITE DIFFERENCE METHOD

The finite difference method is a method with high accuracy and quick computing. The explicit scheme, the fully implicit scheme, and the Crank-Nicolson scheme (semi-implicit scheme) are the three different finite difference schemes [97]. The fully implicit scheme which is first order in time and Crank-Nicolson scheme which is second order in time function well and provide high accuracy for big-time steps, whereas the explicit scheme requires tiny time steps to produce stable data [97]. This study uses the explicit method due to its various advantages, such as ease of implementation and computational efficiency. The explicit solution method evaluates these temperatures at the previous time [98]. Reducing values for space step (Δx) and time step (Δt) can increase the accuracy of the finite-difference solution. As Δx decreases, more internal nodal points must be taken into account, and as Δt decreases, more time intervals are needed to carry the solution to a specified final time [98]. Thus, as Δx and Δt decrease, computing time also increases. A trade-off between accuracy and computing needs typically determines the choice of Δx [98]. In order to choose proper Δx dependence from node number and time step, it should be obtained. Note that the value of t cannot be selected independently after this decision. Stability needs are what control it instead [98]. Since the stability of the explicit method is not unconditional, there is a stability check criterion. The stability criterion is:

$$Fo \leq \frac{1}{2} \tag{3.1}$$

Where Fourier number (*Fo*) is:

$$Fo = \frac{\alpha \Delta t}{(\Delta x)^2} \tag{3.2}$$

Thermal diffusivity (α) is defined as:

$$\alpha = \frac{k}{\rho c_p} \tag{3.3}$$

Where *k* is thermal conductivity, ρ is density, and c_p is specific heat capacity.

3.1 MPCM Integrated Wall Model

The focus of the model is obtaining both heating and cooling needs. Computational properties and multilayering are explained in the following pages. Also, details of outside boundary and inside boundary conditions are presented in this section. Wall orientation is also considered by modelling sun-earth geometries are modelled as defined later in this section. Several assumptions are made for the wall model:

- Heat transfer occurs in only one dimension since the thickness is significantly smaller than the other two dimensions.
- The MPCM-added layers are homogeneous and isotropic.
- The convection effect in the melted MPCM is neglected.
- Density change between liquid and solid phases is neglected.
- The specific heat changes linearly during the phase change. i.e., specific heat is the function of liquid-solid ratio (ϵ).
- Latent heat is the constant in the melting/freezing range.
- Constant convection coefficients are assumed for both the indoor and outdoor environments.
- The heat generation from people and devices is omitted.
- Inside room temperature is assumed constant.
- Reflection of solar radiation from the Earth's surface is neglected.

3.2 Fundamental Equations of One-Dimensional Transient Heat Transfer

In this part, the one-dimensional heat transfer equation is discussed. Since one wall dimension is smaller than the other two dimensions, it is customary to assume one dimension (1D) heat transfer throughout the border. No heat is generated within the wall. Therefore, the overall heat transfer equation throughout the wall becomes:

$$\frac{\partial^2 T}{\partial x^2} = \frac{\rho c_p}{k} \frac{\partial T}{\partial t} \tag{3.4}$$

Since PCM's thermal and mechanical properties change with phase transition, it is practical to define a liquid fraction. The fraction of liquid during the phase change can change from 0 (solid) to 1 (liquid), and this fraction (*f(T)*) is temperature-dependent. This function is defined as *f(T)* [99]:

$$f(T) = \begin{cases} 0, & T < T_s \text{ (solid)} \\ \frac{T-T_s}{T_l-T_s}, & T_s < T < T_l \text{ (mushy)} \\ 1, & T \geq T_l \text{ (liquid)} \end{cases} \tag{3.5}$$

Graph for temperature vs *f(T)* is shown in Figure 3.1. Since most PCM, especially paraffin, lacks an easily determined phase change temperature and the transition between the liquid and solid phases occurs over an extensive temperature range, it is necessary to define a nominal melting temperature (T_m). Transition temperature range ($\Delta\ T$) can be characterised as the variance in temperature between which PCM is perfectly solid (T_s), i.e. *f(T)*=0, and the temperature at PCM is fully liquid (T_l), i.e. *f(T)*=1.

Latent heat (LH) is the enthalpy difference between solid and liquid states of matter ΔH and can be defined as:

$$\triangle H = LH \tag{3.6}$$

LH is implemented into specific heat $c_p(T)$ equation:

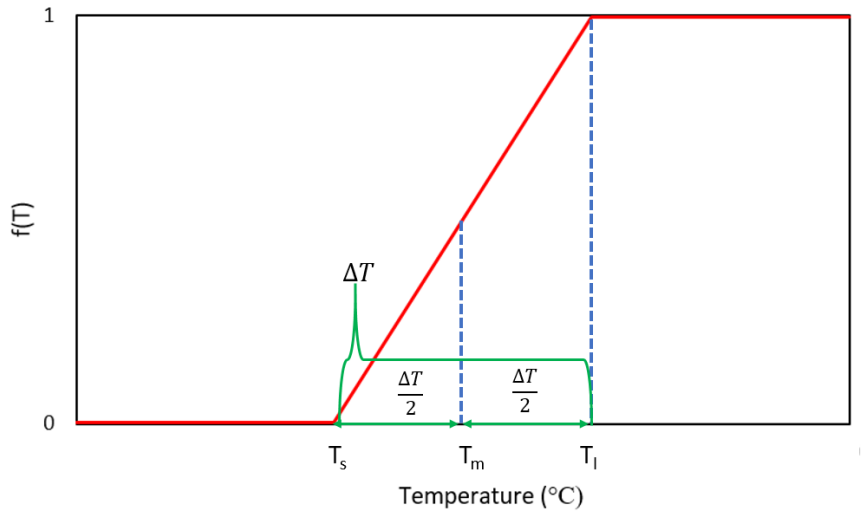

Figure 3.1: T vs $f(T)$ graph.

$$c_p(T) = \begin{cases} c_{p,s}, & T < T_s \text{ ,solid state (sensible region)} \\ \frac{c_{p,s}+c_{p,l}}{2} + \frac{L}{\Delta T}, & T_s < T < T_l \text{,phase change range} \\ c_{p,l}, & T \geq T_l \text{ liquid state (sensible region)} \end{cases} \tag{3.7}$$

Where $c_{p,s}$ is the specific heat at the solid state and assumed constant at the whole solid state and $c_{p,l}$ is the specific heat at the liquid state and assumed constant at the entire liquid state.

3.3 Configurations

As presented in Figure 3.2, four different wall configurations are analysed during this study.

- Config. 1: Only concrete
- Config. 2: Outermost layer insulation + concrete
- Config. 3: 5 cm insulation (outermost layer) + concrete + 80 vol% PCM incorporated concrete (innermost layer)

- Config. 4: concrete + 80 vol% PCM (T_m= 24°C) incorporated concrete (innermost layer)

Thermophysical properties of concrete, insulation materials and PCM are presented in Table 3.1. Properties of concrete and insulation material are taken from literature [98]; properties of PCM are founded from both literature and experimental methods used in this thesis, explained in Section 6.4.

Table 3.1: Thermophysical Properties of Concrete, Insulatıon Material and PCM used in Configuration. Sources: * = Incropera [5]; ** = data sheet; *** = Empirical data obtained from DSC measurement (Section 6.8)

Thermophysical Properties	**Material**		
	Concrete	**Insulatıon Material**	**PCM**
ρ (kg/m^3)	2300 (*)	145 (*)	900(**)
k (W/mK)	1.4 (*)	0.058 (*)	0.08 [10]
c$_p(J/g)$	880 m(*)	1000 (*)	DSC Curve (***)
T$_m(\deg C)$	-	-	24 (**)
Latent Heat (J/g)	-	-	73.5 (***)

(a) Representation of Config. 1.

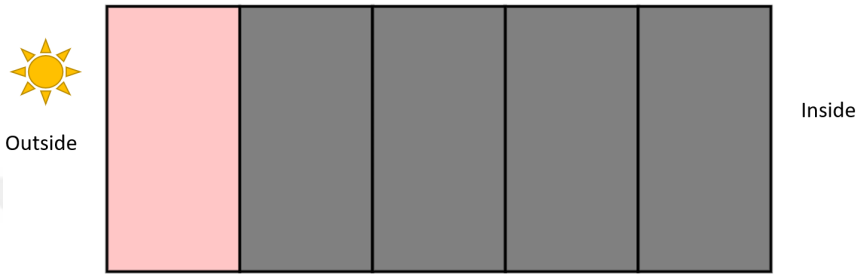

(b) Representation of Config. 2.

(c) Representation of Config 3.

(d) Representation of Config 4.

Figure 3.2: Four different combinations of three building materials. Note that grey colour= **concrete**; pink colour= **insulation material**; blue colour= **PCM included concrete matrix**

3.4 Computational Properties

Various combinations of Δt and Δx were tested to examined values for the simulation where the simulated data is stable, and there is no difference when the values of Δt and Δx are changed to accomplish stability and accuracy. The accuracy of the model is investigated for four different configurations explained in Section 3.3 by changing Δt and Δx for both summer and winter seasons. Temperature distributions of various times are compared for different Δx. After selecting the appropriate Δx, Δt is determined by checking the stability criterion. Note that if the model does not have sufficient time and spatial steps, results can be misleading. Δt and Δx for different configurations are presented in Table 3.2.

Table 3.2: Values of time (Δt) and spatial (Δx) step for different configurations.

Wall Model Description	**Δx [m]**	**Δt [s]**
Config. 1	0.0125	20
Config. 2	0.0025	1
Config. 3	0.0025	1
Config. 4	0.0031	5
Generic Wall	0.0025	1

3.5 Multilayer PCM integration

There are some studies that investigated the effect of PCM location on walls [100] [101] [102] [103] [104]. However, in all scanned articles, it was observed that PCMs were approached as a separate layer; in other words, they were modelled as macro-encapsulated PCM layers.

To investigate the effect of the location of the PCM integrated layer, the wall is divided into five layers. There are some reasons behind the wall layer number chosen. Firstly, this study aims to understand the position effect of PCM in the wall. To have a clear understanding, at least three layers should be integrated (left-side, middle, and right-side). On the other end, the more layering we have, the more computational effort

is needed, so it is not meaningful to choose a large number of layers, e.g. 20 layers. Also, integrating too many layers might not be practical in terms of some possible future work that will mimic this system. Due to these reasons, five is considered a meaningful and practical number for layering. The multilayer wall schematic can be seen in Figure 3.3.

3.6 Initial and Boundary Conditions

Initial conditions and inner and outer boundary conditions are explained for the FDM wall model.

3.6.1 Initial Condition

The initial condition is assumed as 15 °C for the temperature profile presented in Section 6.2. The initial condition of the model used at Section 4 is also set as 15 °C; however, the initial condition is updated until reaching the highest wall temperature change ratio of 1 %, determining final values as explained in Section 6.2. The initial condition of the model used at Section 4 is also set as 15 °C; however, the initial condition is updated two times by taking a run for the same day to minimise the effect of the initial condition for determining the final values as explained in Section 4.4.1.

3.6.2 Boundary conditions

The following sub-sections explain the outside and inside boundary conditions in detail.

3.6.2.1 Outside Boundary Condition

Both radiation and convection heat transfer modes are considered outside the wall, i.e. the outermost node. Outside temperature data are taken from TYM3 data, and dry bulb temperature is used. Hourly irradiation is calculated by using Direct normal

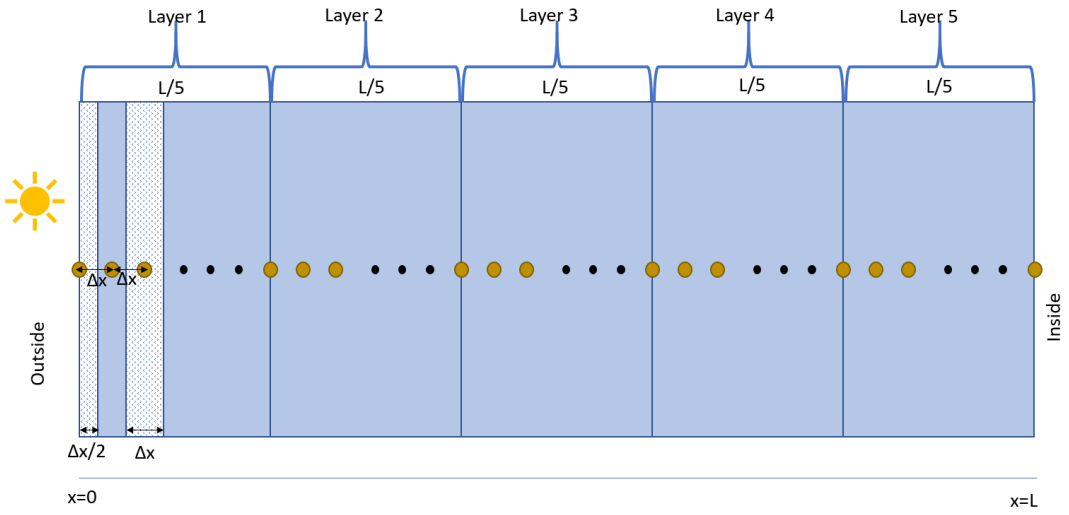

Figure 3.3: The energy balance approach and boundary conditions are employed in the finite differences method, illustrated schematically for the entire multilayered PCM wall.

irradiance (DNI), and Diffuse horizontal irradiance (DHI) was combined using standard sun-earth geometry relations to estimate the total irradiation (direct + diffuse) on each surface at all points in time. Figure 3.4 shows outer boundary conditions and heat transfer schematic of the outermost node.

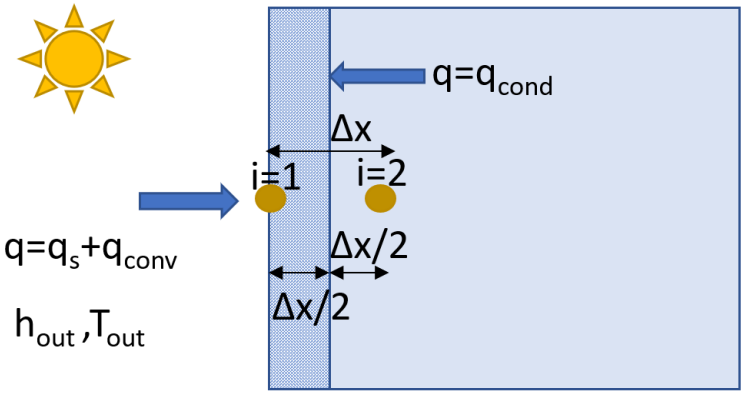

Figure 3.4: The energy balance approach and outer boundary conditions are employed in the finite differences method, illustrated schematically for the entire multilayered MPCM wall.

The difference between inlet energy (E_{in}) and outlet energy (E_{out}) on control volume

gives stored energy ($E_{storage}$) with the assumption of no heat generation inside the volume. Therefore, the energy equation becomes:

$$E_{storage} = E_{in} - E_{out} \tag{3.8}$$

$$\dot{E}_{storage} = \dot{E}_{in} - \dot{E}_{out} \tag{3.9}$$

$$\rho c_p(T)(\Delta x A)\frac{\partial T}{\partial t} = k(T)A\frac{\partial T}{\partial x} + h_{out}A(T_{out} - T) + q_s^{"}A \tag{3.10}$$

If all expressions are divided into area (*A*):

$$\rho c_p(T)(\Delta x)\frac{\partial T}{\partial t} = k(T)\frac{\partial T}{\partial x} + h_{out}(T_{out} - T) + q_s^{"} \tag{3.11}$$

If the explicit finite difference method is introduced to the energy balance equation, the equation becomes:

$$k(T_{1,2}^{t-1}) = \frac{k_1(T_1^{t-1}) + k_2(T_2^{t-1})}{2} \tag{3.12}$$

$$\rho c_p(T_1^{t-1})\frac{\Delta x}{2}\frac{T_1^t - T_1^{t-1}}{\Delta t} = k(T_{1,2}^{t-1})\frac{T_2^{t-1} - T_1^{t-1}}{\Delta x} + h_{out}(T_{out}^{t-1} - T^{t-1}) + q_s^{"(t-1)} \tag{3.13}$$

By arranging both sides:

$$T_1^t - T_1^{t-1} = \frac{2k(T_{1,2}^{t-1})\Delta t}{\rho\, c_p(T_1^{t-1})(\Delta x)^2}(T_2^{t-1} - T_1^{t-1}) + \frac{2h_{out}\Delta t}{\rho c_p(T_1^{t-1})\Delta x}(T_{out}^{t-1} - T^{t-1}) + \frac{2\Delta t}{\rho c_p(T_1^{t-1})\Delta x}q_s^{"(t-1)} \tag{3.14}$$

By introducing numerical Fourier number (Fo_{num}):

$$Fo_{num,out} = \frac{k(T_{1,2}^{t-1})}{\rho c_p(T_1^{t-1})} \frac{\Delta t}{(\Delta x)^2} \tag{3.15}$$

And Biot Number:

$$Bi_{num,out} = \frac{h_{out}\Delta x}{k(T_{1,2}^{t-1})} \tag{3.16}$$

If $Fo_{num,out}$ and $Bi_{num,out}$ are implemented to 3.14:

$$T_1^t = T_1^{t-1} + 2Fo_{num,out}(T_2^{t-1} - T_1^{t-1}) + 2Fo_{num,out}Bi_{num,out}(T_{out}^{t-1} - T_1^{t-1}) + 2\frac{\Delta x}{k(T_{1,2}^{t-1})}Fo_{num,out}q_s^{"(t-1)} \tag{3.17}$$

If terms which are containing T_1^{t-1} are collected on the same side:

$$T_1^t = (1 - 2Fo_{num,out} - 2Fo_{num,out}Bi_{num,out})T_1^{t-1} + 2Fo_{num,out}T_2^{t-1} + 2Fo_{num,out}Bi_{num,out}T_{out}^{t-1} + 2\frac{\Delta x}{k(T_{1,2}^{t-1})}Fo_{num,out}q_s^{"(t-1)} \tag{3.18}$$

Wall Orientation DNI data are used to calculate direct solar irradiance on four orientations. To calculate direct solar irradiance on four orientations DNI data are used using the method in Duffie & Beckman [105], where the equation numbers refer to those in Duffie & Beckman. Firstly, declination is calculated using equation 1.6.1a, and solar time is estimated using equations 1.5.2 and 1.5.3. Following the calculation of the hour angle, the solar azimuth angle and zenith angle of the sun, which are the exact locations of the sun at a given time for specific latitudes and longitudes, are calculated using equation 1.6.6 and equation 1.6.5. The angle of incidence, defined as the angle between the radiation beam on a surface and the normal to that surface, is computed for four orientations using equation 1.6.3. As a result of all these calculations, direct irradiation on the walls in the north, south, east, and west directions at Ankara location was obtained. DNI values for every hour of the year are presented in Figure 3.5, and direct irradiance on north, south, east, and west surfaces are given

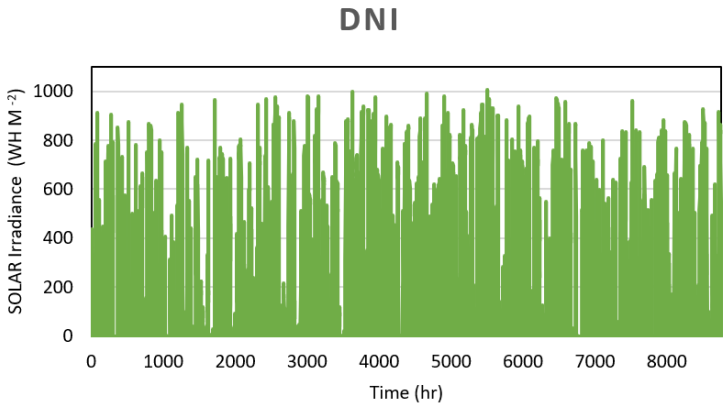

Figure 3.5: DNI data for Ankara,Türkiye.

in Figure 3.6. Diffuse radiation is modelled as an isotropic diffuse model and is re-calculated in Equation 3.19.

$$F_{wall} = \frac{1 + cos\beta}{2} \tag{3.19}$$

Where β is the slope of the surface, which is 90 °for vertical surfaces.

The results presented in Figure 3.6 are consistent with expectations for seasonal variations in direct radiation for a building at 40°N as follows: The direct radiation on the South and North walls are complementary with direct radiation on the south wall peaking in the winter when the sun is relatively low in the southern sky at noon and peaking on the north wall in the summer when the sun rises/sets north of due east-/west. Also, the east and west walls demonstrate similar trends with differences due to differences in cloud cover in the mornings and evenings.

Total irradiance is obtained by summing the direct and diffuse irradiation (DHI data). In Figure 3.7 total irradiance for four orientations is shown.

3.6.2.2 Innermost Boundary Condition

The inside of the wall (room side) is fixed to 23 °C for the whole year. The reason for this selection is according to ASHRAE Standard 55, the human comfort zone for

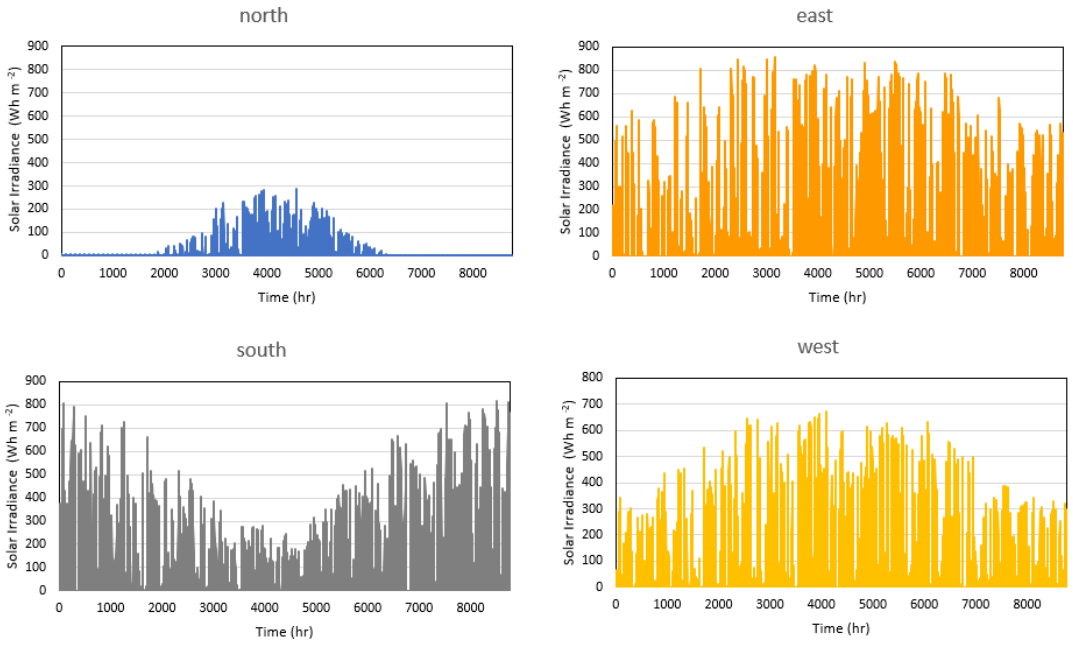

Figure 3.6: Direct Solar Radiation for North, South, East, and West oriented walls.

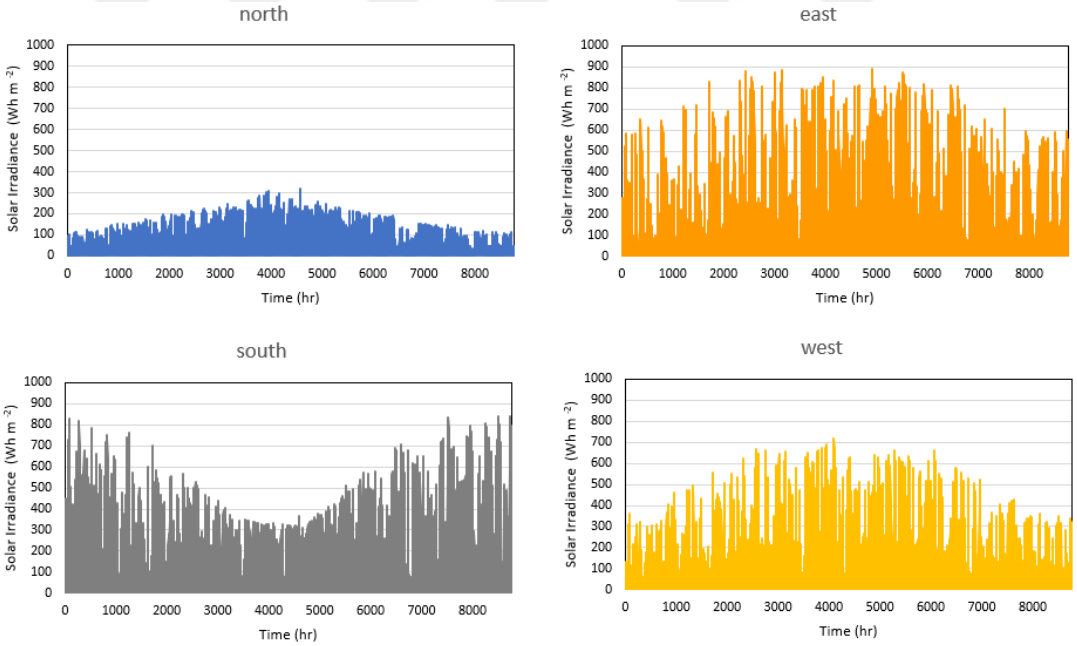

Figure 3.7: Total Solar Radiation (Direct+Diffuse) for North, South, East, and West oriented walls.

indoor temperatures is between 68.5 °F (20 °C) to 80.5 °F (27 °C) [106]. The average of these values is selected. Also, the same value was chosen in a similar study [107]. Note that indoor temperature comfort zones may vary depending on the season of the year, hour of the day, location, age, sex, and body mass of humans. A widely accepted temperature, 23 °C, is selected for simplicity. The only heat transfer mode from the inside surface of the wall to the inside room air is convection; i.e., radiation is neglected due to the relatively low temperatures and temperature difference. Figure 3.8 shows innermost boundary conditions and heat transfer schematic of innermost node.

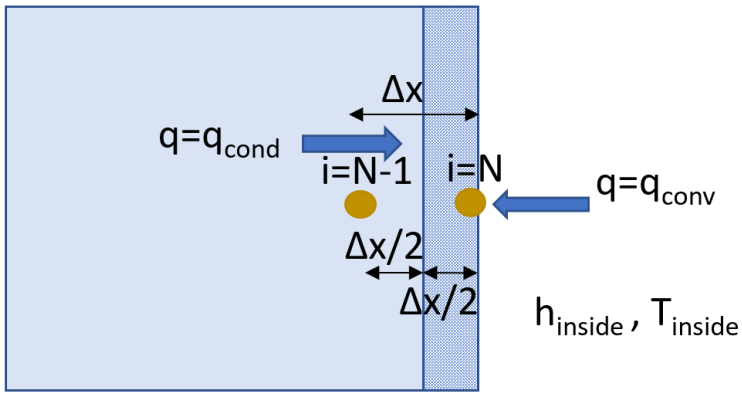

Figure 3.8: The finite differences method using the energy balance approach and inner boundary condition, represented schematically for the multilayered MPCM wall.

$$E_{storage} = E_{in} - E_{out} \tag{3.20}$$

$$\dot{E}_{storage} = \dot{E}_{in} - \dot{E}_{out} \tag{3.21}$$

$$\rho c_p(T)(\Delta x A)\frac{\partial T}{\partial t} = k(T)A\frac{\partial T}{\partial x} + h_{in}A(T_{in} - T) \tag{3.22}$$

If all expressions are divided into A:

$$\rho c_p(T)(\Delta x)\frac{\partial T}{\partial t} = k(T)\frac{\partial T}{\partial x} + h_{in}(T_{in} - T) \tag{3.23}$$

If the explicit finite difference method is introduced to the energy balance equation, the equation becomes:

$$k(T_{N-1,N}^{t-1}) = \frac{k_{N-1}(T_{N-1}^{t-1}) + k_N(T_N^{t-1})}{2} \tag{3.24}$$

$$\rho c_p(T_N^{t-1})\frac{\Delta x}{2}\frac{T_N^t - T_N^{t-1}}{\Delta t} = k(T_{N-1,N}^{t-1})\frac{T_{N-1}^{t-1} - T_N^{t-1}}{\Delta x} + h_{out}(T_{in}^{t-1} - T_N^{t-1}) \tag{3.25}$$

By arranging both sides:

$$T_N^t - T_N^{t-1} = \frac{2k(T_{N-1,N}^{t-1})\Delta t}{\rho\, c_p(T_N^{t-1})(\Delta x)^2}(T_{N-1}^{t-1} - T_N^{t-1}) + \frac{2h_{in}\Delta t}{\rho c_p(T_N^{t-1})\Delta x}(T_{in}^{t-1} - T_N^{t-1}) \tag{3.26}$$

By introducing numerical Fourier number (Fo_{num}):

$$Fo_{num,in} = \frac{k(T_{N-1,N}^{t-1})}{\rho c_p(T_2^{t-1})}\frac{\Delta t}{(\Delta x)^2} \tag{3.27}$$

and Biot Number:

$$Bi_{num,in} = \frac{h_{in}\Delta x}{k(T_{N-1,N}^{t-1})} \tag{3.28}$$

If $Fo_{num,in}$ and $Bi_{num,in}$ are implemented to 3.39:

$$T_N^t = T_N^{t-1} + 2Fo_{num,in}(T_{N-1}^{t-1} - T_N^{t-1}) + 2Fo_{num,in}Bi_{num,in}(T_{in}^{t-1} - T_N^{t-1}) \tag{3.29}$$

If terms which are containing T_N^{t-1} are collected on the same side:

$$T_N^t = (1 - 2Fo_{num,in} - 2Fo_{num,in}Bi_{num,in})T_N t - 1 + 2Fo_{num,in}T_{N-1}^{t-1} + 2Fo_{num,in}Bi_{num,in}T_{in}^{t-1} \tag{3.30}$$

3.6.3 Middle Nodes

In Figure 3.9, heat transfer schematic for middle nodes is presented.

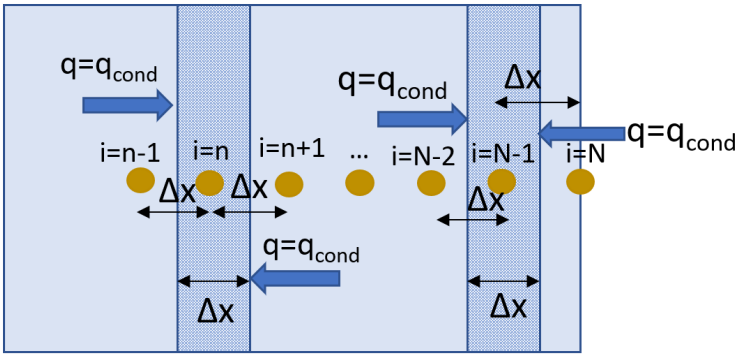

Figure 3.9: The finite differences method using the energy balance approach for middle nodes, represented schematically for the multilayered MPCM wall.

Heat transfer equation for all middle nodes is:

$$T_i^t = -Fo_{Left}(T_i^{t-1} - T_{i-1}^{t-1}) + Fo_{Right}(T_{i+1}^{t-1} - T_i^{t-1}) + T_i^{t-1} \tag{3.31}$$

$$E_{storage} = E_{in} - E_{out} \tag{3.32}$$

$$\dot{E}_{storage} = \dot{E}_{in} - \dot{E}_{out} \tag{3.33}$$

$$\rho c_p(T)(\Delta x A)\frac{\partial T}{\partial t} = k(T)A\frac{\partial T}{\partial x} \tag{3.34}$$

If all expressions are divided into A:

$$\rho c_p(T)(\Delta x)\frac{\partial T}{\partial t} = k(T)\frac{\partial T}{\partial x} \tag{3.35}$$

If the explicit finite difference method is introduced to the energy balance equation, the thermal conductivity equations for the right and left sides become:

$$k_{left} = \frac{k_{n-1}(T_{n-1}^{t-1}) + k_N(T_n^{t-1})}{2} \tag{3.36}$$

$$k_{right} = \frac{k_{n+1}(T_{n+1}^{t-1}) + k_N(T_n^{t-1})}{2} \tag{3.37}$$

$$\rho c_p(T_n^{t-1})\Delta x \frac{T_n^t - T_n^{t-1}}{\Delta t} = k_{left}\frac{T_{n-1}^{t-1} - T_n^{t-1}}{\Delta x} + k_{right}\frac{T_{n+1}^{t-1} - T_n^{t-1}}{\Delta x} \tag{3.38}$$

By arranging both sides:

$$T_n^t - T_n^{t-1} = \frac{k_{left}\Delta t}{\rho\, c_p(T_n^{t-1})(\Delta x)^2}(T_{n-1}^{t-1} - T_n^{t-1}) + \frac{k_{right}\Delta t}{\rho\, c_p(T_n^{t-1})(\Delta x)^2}(T_{n+1}^{t-1} - T_n^{t-1}) \tag{3.39}$$

By introducing numerical Fourier number for left ($Fo_{num,left}$):

$$Fo_{num,left} = \frac{k_{left}}{\rho c_p(T_2^{t-1})}\frac{\Delta t}{(\Delta x)^2} \tag{3.40}$$

and numerical Fourier number for right ($Fo_{num,right}$):

$$Fo_{num,right} = \frac{k_{right}}{\rho c_p(T_2^{t-1})}\frac{\Delta t}{(\Delta x)^2} \tag{3.41}$$

If $Fo_{num,left}$ and $Fo_{num,right}$ are implemented to 3.42:

$$T_n^t = T_n^{t-1} + Fo_{num,left}(T_{n-1}^{t-1} - T_n^{t-1}) + Fo_{num,right}(T_{n+1}^{t-1} - T_n^{t-1}) \tag{3.42}$$

If terms which are containing T_n^{t-1} are collected on the same side:

$$T_n^t = (1 - Fo_{num,left} - Fo_{num,right})T_n t - 1 + Fo_{num,left}T_{n-1}^{t-1} + Fo_{num,right}T_{n+1}^{t-1} \tag{3.43}$$

CHAPTER 4

SENSITIVITY ANALYSIS

Sensitivity Analysis (SA) methods are crucial in developing and utilising numerical simulation models. They offer insightful information about how various sources of uncertainty in the model's input parameters might be linked to uncertainty in the model's output [108]. SA can help identify the most influential input variables, distinguish non-influential inputs, and reveal interactions inside the model. The objectives of SA encompass model verification and understanding, model simplification, and factor prioritisation. Furthermore, SA directs research, supports computer code validation, and provides justification for system design safety. There are many application areas of SA, from economy [109] to biology [110].

The sensitivity analysis methods can be categorised into global and local approaches. Local sensitivity analysis concentrates on how modest input perturbations affect model output. These minor alterations occur close to nominal values, like the mean of a random variable. This deterministic approach entails computing or estimating the model's partial derivatives at a specified location. Models having a lot of input variables can be processed using adjoint-based methods. Also, local methods have limitations, such as linearity and normality assumptions [111]. Therefore, local sensitivity analysis is unsuitable for non-additive, non-linear, and non-monotonic models. Contrary to local sensitivity analysis, global sensitivity analysis (GSA), a statistical method, considers the whole variation range of the inputs [108]. Global sensitivity analysis requires much more computational power than local sensitivity analysis, but this method can be used for more complex models such as non-linear ones. It considers multiple input variables' interactions and combined effects on the model output.

Sensitivity analysis can also be categorised according to its purpose. They are clas-

sified as (1) Ranking, (2) Screening, or (3) Mapping [8]. The objective of ranking or factor prioritisation is to establish the relative contribution of input factors (x_1, x_2, ..., x_M) to the variability of the output, and it involves generating a ranked list that indicates the importance or influence of each input factor on the overall variability of the output [8]. The purpose of screening or factor fixing is to identify the input factors that have minimal impact on output variability. The goal is to determine if input factors can be considered insignificant or negligible in their influence on the output variability [8]. Mapping identifies the specific region within the input variability space that results in significant or extreme output values. The objective is to determine the range or area of the input variables that lead to notable outcomes, such as severe or critical values in the output.

Another way to categorise SA is the sampling approach. The sampling approach can be divided into One At a Time (OAT) and All At a Time (AAT)[112]. One at a time is a method where each input is varied while fixing the others [111]. Local sensitivity analysis and Morris methods (aka Elementary Effect Test (EET)) are examples of the OAT method. Regression models and variance-based models are examples of AAT methods. This thesis uses Sobol's sensitivity analysis and an AAT model, and the AAT method is explained in detail.

4.1 Classification According to Type of SA

4.1.1 Global Sensitivity Analysis (GSA)

GSA can be divided into four main groups: Multiple starts perturbation, Regional Sensitivity Analysis, Correlation & Regression Analysis, and Variance-based and density-based methods. Since the variance-based Method is used in this thesis, it is explained in detail.

4.1.1.1 Variance-based GSA Methods

The variance-based method produces a distribution in the output space using stochastic variables as input elements. The sampling approach for these input elements is

discussed in Section 4.2. Variance-based SA quantifies how each input individually affects output and how the interaction of these inputs affects output. In variance-based SA, it is possible to define several variance-based indices, such as first-order indices, which refer to the direct contribution of individual input factors to output variance.

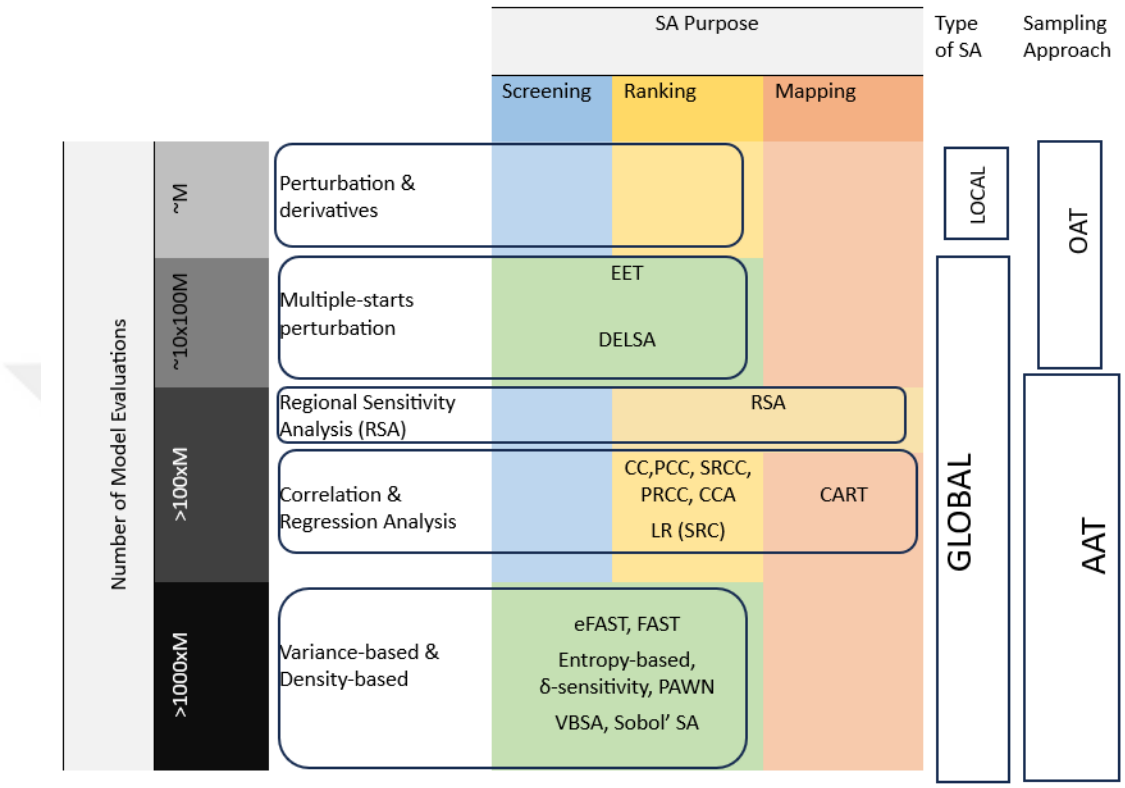

Figure 4.1: Categorization framework for SA method utilising computational intricacy (represented on the vertical axis, where M signifies the count of input factors under SA) and the intended objectives of the analysis. This Figure is adopted from [8].

4.2 Sampling Approach

4.2.1 All-At-a-Time (AAT)

In principle, any random or quasi-random sampling technique can be used for AAT methods like Correlation and Regression Analysis, Regional Sensitivity Analysis, and density-based methods. Among these, Latin-Hypercube and Sobol' quasi-random

sampling are most commonly used in the GSA literature. The reason for the popularity of these methods is the accuracy obtained in the sensitivity analysis results [113].

4.2.1.1 Random Sampling

The random method generates all samples independently. Therefore, it is more likely to have cluster regions, which leads to overemphasised calculations in random method, especially for small sample sizes [108]. Samples for the sampling of the quasi-random number generator are given in Figure 4.2, which is adopted from [9]. Figure 4.2: sampling shows some gaps and clusters are in line a. However, distribution is more balanced in line b. Monte Carlo sampling is a well-known random sampling method.

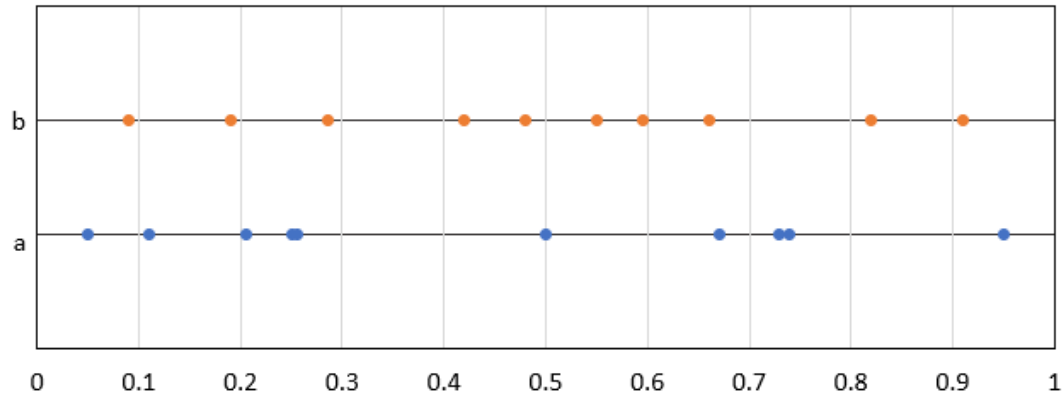

Figure 4.2: Sampling methods for 1D sampling. Note that lines a and b represent results of the same pseudo-random number generator [9].

4.2.1.2 Quasi-Random Sampling

Quasi-random sequences are created to achieve a nearly uniform distribution of samples for multiple parameters across the multi-dimensional parameter space. In quasi-random sequences, the sample values are chosen while considering the previously sampled locations, successfully preventing the creation of clusters and gaps. This is the significant difference between quasi-random sequences and pseudo-random numbers. Sobol' sequence is an example of the quasi-random sampling.

4.2.1.3 Stratified Sampling

In a stratified sampling scheme, the domain of x_i is partitioned into subintervals of equal size. An equal number of sample points are present inside each subinterval. Using a pseudo-random number generator, these spots are chosen at random. Latin hypercube sampling is a well-known stratified sampling method.

4.3 Sobol' Sensitivity Analysis

Sobol' sensitivity analysis is named after famous Russian mathematician Ilya M. Sobol, and it is a GSA method. Sobol' sensitivity analysis (Sobol' SA) is a variance-based method, and the sampling method is quasi-random sampling which is an AAT approach. As shown in Figure 4.1, Sobol' SA has a high number of model evolutions, and it is a computationally expensive model, which is the main drawback of this method.

In this thesis, Sobol' SA is used due to its ability to work with non-linear and non-monotonic models and with higher-order interactions of parameters [114]. Sobol' SA offers valuable insights into the influence of individual input parameters and their interactions on the variability of the model's output.

4.3.1 Sobol' Decomposition

Sobol' decomposition, also called Sobol sensitivity indices or Sobol indices, is used in sensitivity analysis to decompose the total variance of a model's output into contributions from individual input parameters and their interactions.

Let $f(x)$ be a square-integrable and deterministic function defined on the unit hypercube $[0,1]^d$.

Consider a random model with d input parameters, represented as:

$$x = (x_1, x_2, ..., x_d) \tag{4.1}$$

The model output, which is denoted as Y, is a function of these input parameters, which are independent of one another:

$$Y = f(X) \tag{4.2}$$

This function can be represented as the Hoeffding-Sobol decomposition [111]:

$$Y = f(\mathbf{x}) = f_0 + \sum_{i=1}^{d} f_i(x_i) + \sum_{i<j}^{d} f_i(x_i, x_j) + ... + f_{12..d}(\mathbf{x}) \tag{4.3}$$

Where:

$$f_0 = E[Y], f_i(x_i) = E[Y|x_i] - f_0, f_i(x_i, x_j) = E[Y|x_i, x_j] - f_0 - f_i - f_j, ... \tag{4.4}$$

f_0 is the mean value. Higher order terms are recursively created conditional expectations that define a distinct orthogonal decomposition of the model response [115]. Consequently, a functional decomposition of the variance—often referred to as functional ANOVA—is provided:

$$Var(Y) = \sum_{i=1}^{d} D_i(Y) + \sum_{i<j}^{d} D_{i,j}(Y) + ... + D_{12..d}(Y) + \tag{4.5}$$

Where:

$$\begin{aligned} D_i(Y) &= Var[E[Y|x_i]], \\ D_{i,j}(Y) &= Var[E[Y|x_i, x_j]] - D_i(Y) - D_j(Y) \end{aligned} \tag{4.6}$$

According to Sobol [116], the so-called "Sobol' indices" or "Sobol' sensitivity indices" are calculated as follows :

$$S_i = \frac{D_i(Y)}{Var(Y)}, S_i = \frac{D_{i,j}(Y)}{Var(Y)}.... \tag{4.7}$$

These indices express the proportion of Y's variance caused by a specific input or input combination. The amount of indices increases exponentially with the dimension d: there are 2^d-1 indices. Therefore, one should not estimate indices of order more than two for computational and interpretive concerns.

4.4 Specific Features of the Method and Parameters

In this thesis, a code developed by Flavio Cannavò is used [117]. This tool allows users to implement up to 50 parameters. Using this code, the first/ total Sobol' indices are calculated. The objective of GSA is to determine the most critical parameters of the generic wall model described in Chapter 3 for variation in heating and cooling at summer and winter seasons separately, for Ankara, Türkiye.

4.4.1 FDM Implementation and Modifications for SA

Several modifications were implemented on the FDM to enhance its suitability for sensitivity analysis. Firstly, the specific heat and thermal conductivity of PCM for the solid and liquid phases assumed the same since their range overlaps, and reducing these parameters reduces computational efforts. Secondly, the outside boundary condition is updated. Instead of running the simulation for a whole year, the hourly average for both dry bulb temperature and solar irradiance for the summer and winter seasons was calculated. The simulation was run separately over these days. The reason for performing the season is to reduce computational effort. Thanks to the seasonal average of summer and winter, the required computational power and time are reduced to 1 in 180. The last modification is updating the initial condition. Since the prominence of the initial condition increases with the decrease in the time period covered by the simulation (e.g. instead of 365 days, one day for summer and one day for winter), it is essential to adjust the initial condition. A wall with parameters set to average values was modelled to accomplish this. A uniform temperature distribution (15 °C) was assigned as the initial condition in the initial step. Following the execution of the code, an updated temperature distribution was calculated that would act as the starting point for the following iteration. The number of iterations was increased

until the highest ratio of temperature change through the wall, compared to the prior iteration, was 1%. Temperature values along the wall were established from the final loop findings.

As mentioned in Chapter 3, the FDM model's stability and accuracy are vital to have meaningful results. If stability reaches a critical value of 0.5, the simulation is terminated, and stability is assured. Sensitivity analysis on generic wall models. The accuracy of the FDM model is controlled for the generic wall sensitivity analysis model by checking extreme values. To achieve accuracy, the independence of FDM models from the time step and spatial step are checked for extreme values, such as very low/high thermal diffusivity and extreme PCM inclusion, such as 0% to 80%, which are the lowest and highest possible volumetric PCM rate in the models. Time step and spatial steps for the generic wall model are presented in Chapter 3 Table 3.2.

4.4.2 Sample Size Selection and Parameters

The selection of sample size for GSA is a widely investigated area. Studies are showing that different sample sizes are sufficient for different models, and the results converge. For instance, for a complex environmental model with 13 parameters, a 1050 sample size was needed for accurate results for first and total Sobol indices [118]. On the other hand, $2(k+1)N$ model evaluations with a sample size of N = 500 are suggested for a building energy model where k is the number of parameters [119]. As can be seen from this situation, different sample sizes can be indicated for different models. In this thesis, a relatively large sample size was chosen for a more conservative approach. Since Sobol' decomposition was used for 21 parameters, as shown in Table 4.1, the sample size for convergence is selected as 5,000 for first-order indices. Note that this sample size was selected based on the analysis of different sample sizes. There was no meaningful improvement when the sample size was 10,000 and 20,000.

It is essential that the density of the binder was taken as a function of conductivity and implemented into the model. There are two main reasons for this implementation. Firstly, there is a strong relation between density and thermal conductivity of building materials, in general, [120] and defining these two parameters separately can lead to unrealistic binder compositions such as extremely high thermal conductivity

with very low density. Therefore, these unrealistic cases during Sobol' simulation can affect the sensitivity of indices. Secondly, reducing parameter numbers can be beneficial to lower computational expenses, especially computationally heavy models like Sobol'. Density as a function of thermal conductivity is defined as [120] :

$$\rho_{binder,layer_i} = 625 * log(\frac{k_{binder,layer_i}}{0.04}) \tag{4.8}$$

Table 4.1: SA Parameters used in Wall Model

Input parameters	Unit	Min	Max	COV Distribution	Ref
Volumetric ratio of PCM to other building materials at layer 1	-	0	0.8	Uniform	-
Volumetric ratio of PCM to other building materials at layer 2	-	0	0.8	Uniform	-
Volumetric ratio of PCM to other building materials at layer 3	-	0	0.8	Uniform	-
Volumetric ratio of PCM to other building materials at layer 4	-	0	0.8	Uniform	-
Volumetric ratio of PCM to other building materials at layer 5	-	0	0.8	Uniform	-

Table 4.1 Continued

Melting Temperature of PCM	°C	15	30	Sobol	-
Melting Temperature Range of PCM	°C	4	7	Sobol	-
Specific heat of PCM	J/kg K	1800	2200	Sobol	[121]
Latent heat of PCM	kJ/K	1,300	2,600	Sobol	[122]
Thermal conductivity of PCM (s)	W/m K	0.15	0.34	Sobol	[10]
Density of PCM	J/kg K	760	1200	Sobol	[10]
Specific heat of martix at layer 1	J/kg K	800	2100	Sobol	[120]
Specific heat of matrix at layer 2	J/kg K	800	2100	Sobol	[120]
Specific heat of matrix at layer 3	J/kg K	800	2100	Sobol	[120]
Specific heat of building material at layer 4	J/kg K	800	2100	Sobol	[120]
Specific heat of building material at layer 5	J/kg K	800	2100	Sobol	[120]
Thermal Conductivity of building material at layer 1	W /m K	0.07	2.30	Sobol	[120]
Thermal Conductivity of matrix at layer 2	W/m K	0.07	2.30	Sobol	[120]

Table 4.1 Continued

Thermal Conductivity of matrix at layer 3	W/m K	0.07	2.30	Sobol	[120]
Thermal Conductivity of matrix at layer 4	W/m K	0.07	2.30	Sobol	[120]
Thermal Conductivity of matrix at layer 5	W/m K	0.07	2.30	Sobol	[120]

CHAPTER 5

EXPERIMENTAL METHODS

5.1 Raw Materials

This section discusses the characteristics of the materials used to prepare composites and their properties.

5.1.1 FGDG

FGDG is a byproduct of the flue gas scrubbing process used to remove sulfur dioxide (SO_2) emissions from power plant flue gases. It is a form of synthetic gypsum produced from the reaction of lime or limestone with the sulfur dioxide in the flue gas [84]. FGDG has gained significant attention as a sustainable and environmentally friendly building material. It offers several advantages, including fire resistance, sound insulation, and excellent thermal properties [86]. FGDG is commonly used in the construction industry for applications such as gypsum boards, plaster, and cementitious materials. Its use helps reduce the demand for natural gypsum and mitigates the environmental impact of mining and extraction. Additionally, incorporating FGDG in construction materials provides an opportunity for recycling and reusing industrial byproducts, promoting a circular economy approach in the building sector [87].

The material used in half of the mixes is the hemihydrate from the calcination of FGDG. The hemihydrate is produced by heating FGDG to about 175 °C:

$$CaSO_4 \cdot 2H_2O \rightarrow CaSO_4 \cdot \frac{1}{2}H_2O + \frac{3}{2}H_2O \tag{5.1}$$

The conversion of gypsum dihydrate to hemihydrate is monitored by three different methods: physical property examination, weight loss, and X-ray diffraction (XRD). Changing physical properties during the conversion of FGDG to hemihydrate are colour and texture. As shown in Figure 5.1, the colour becomes lighter and texture smoother; i.e., a chunk of FGDG becomes much softer and easier to break up. Weight change is also observed, and the weight loss increases with the time the component is in the oven. The expected weight loss for pure gypsum is 15.67% [123]. However, since FGDG contains not only gypsum but also other compounds, the actual weight loss is less. XRD is the third and the most accurate method among all these three methods. XRD measurements are taken at different times, i.e., t=0, t=6 hours, and t=8.5 hours and XRD results for these times can be seen in Table 5.1. Figure 5.2 shows dihydrate peaks vanish over time. SEM image of raw FGDG, which is in hemihydrate form, can be seen in Figure 5.3.

FGDG was obtained from the Afşin Elbistan Thermal Power Plant located in Kahramanmaraş, Türkiye.

Table 5.1: Mineral ratio of FGDG during calcination process at different hours.

Mineral	**t=0 (%)**	**t=6 (%)**	**t=8.5 (%)**
Gypsum	68.1	26.9	1.6
Bassanite	0	32.7	47.4
Anhydrate	0	0	0
Calcite	31.4	39.8	49.8
Quartz	0.6	0.6	1.2

5.1.2 Commercial Plaster

Commercial plaster was obtained from ABS Alçı Corporation in Türkiye. According to the corporate catalogue, its physical properties include a minimum compressive strength of 1.96 MPa and minimum flexural strength of 0.8 MPa for plaster form, i.e.

Figure 5.1: FGDG in dihydrate (left) and hemihydrate (right) forms.

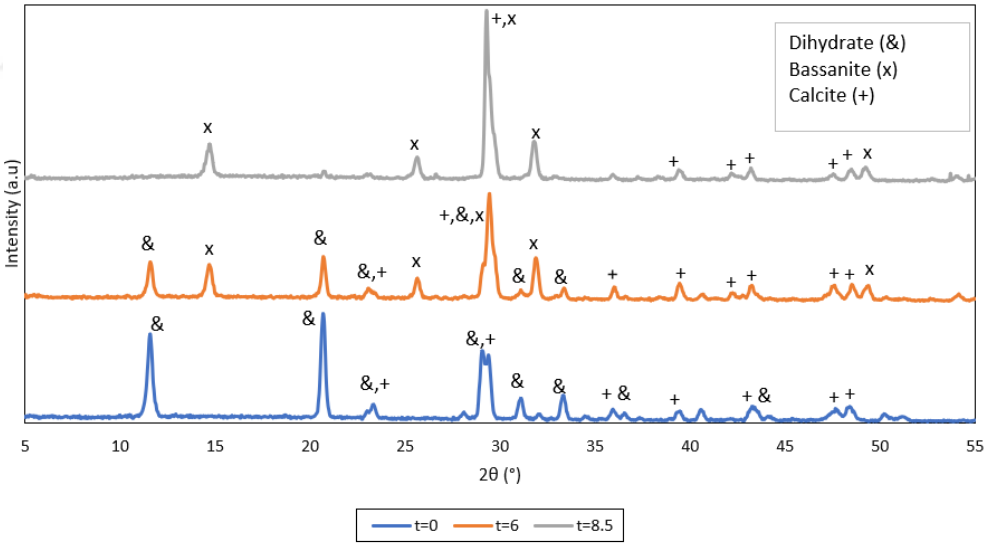

Figure 5.2: XRD result of FGDG before (t=0) and after dehydration process for 6 hours (t=6) and 8.5 hours (t=8.5).

no additives such as aggregates. Also, all particles are smaller than 160 micrometres. As shown in Figure 5.4, commercial plaster is white. SEM image of commercial

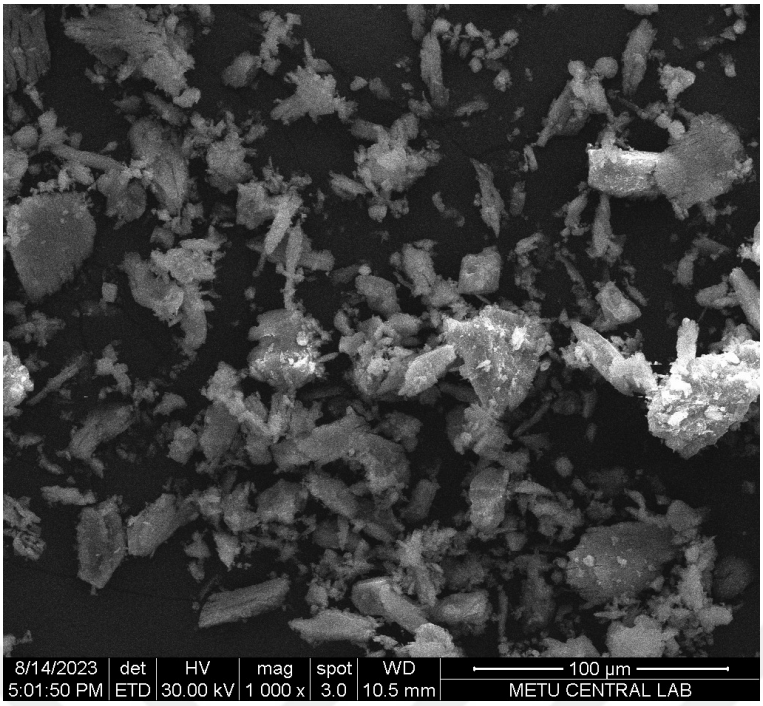

Figure 5.3: SEM image of raw FGDG.

plaster can be seen in Figure 5.5.

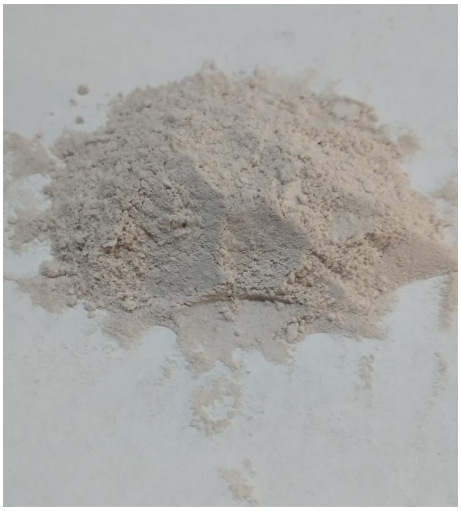

Figure 5.4: Commercial plaster in powder form.

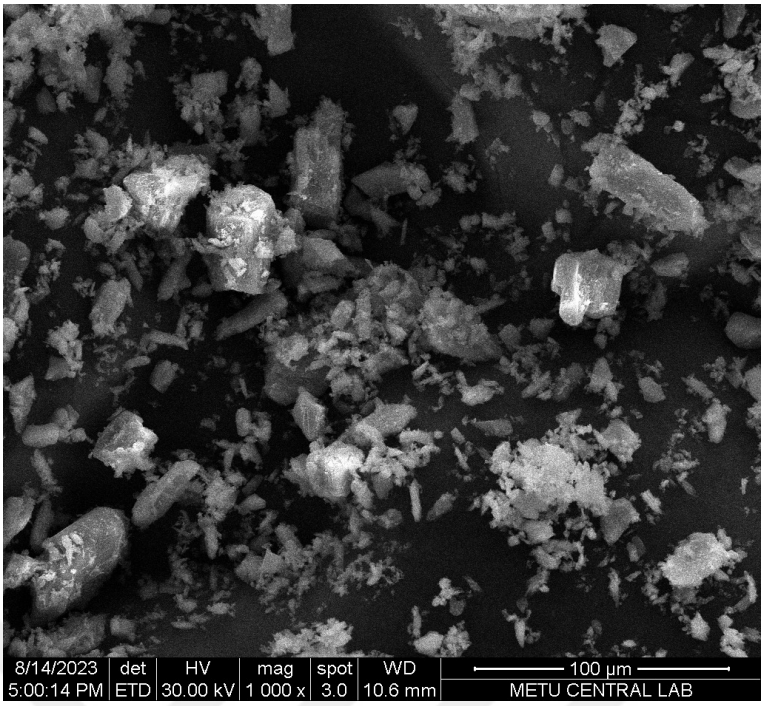

Figure 5.5: SEM image of commercial plaster.

5.1.3 Chemical Composition

The chemical composition of Thermal Power Plant gypsum can vary depending on factors such as the specific power plant, fuel used, and the efficiency of flue gas desulfurisation (FGD) processes, and the chemical composition cannot determined without measurement. Therefore, the X-ray fluorescence (XRF) analysis was performed to determine the elemental composition of FGDG. Also, the chemical composition of commercial plaster is investigated. METU Central Laboratory performed XRF analyses. Results are presented in Table 5.2.

5.1.4 Particle Size

All FGDG were sieved with an automatic sieving device to obtain a finer plaster. ASTM E11 no. 200 was used as a sieve to obtain 75 microns and below particle size before the mixtures were prepared. Particle size investigation of FGDG and commercial plaster is performed in this thesis. Particle properties might differ according to size, such as setting time, strength development, consistency, surface area, water

Table 5.2: Chemical compositions of FGDG and Commercial Plaster

Oxide Composition	**FGDG (wt%)**	**Commercial Plaster (wt%)**
CaO	57.4	53.6
SO_3	38.5	43.2
SiO_2	1.48	1.38
Fe_2O_3	0.972	0.268
Al_2O_3	0.794	0.318
MgO	0.509	0.477
P_2O_5	0.229	0.046
TiO_2	0.067	0.000
SrO	0.046	0.665
K_2O	0.041	0.067

demand, and rheological properties [124].

BAŞTAŞ ÇİMENTO performed particle size distribution analysis. The Malvern Mastersizer 2000 device was used to determine particle size using the laser diffraction method by dry analysis. The average particle size of the FGDG is 19.3 μm with a specific surface area of 0.59 m^2/g. d10, d50 and d90 were obtained as 1.53 μm, 9.79 μm, and 52.8 μm, respectively. Commercial has an average particle size of 13.9 μm and a specific surface area of 2.12 m^2/g. d10, d50 and d90 were obtained as 1.11 μm, 6.97 μm, and 37.69 μm, respectively. Particle size distribution results can be seen in Figure 5.6 and Figure 5.7.

5.1.5 Aggregate

Quartz sand with particles between 0.1 mm and 3 mm in size was employed as an aggregated. The ASTM C33 standard's maximum and minimum passing limitations were considered when grading the standard sand. The gradation of the sand used in this study is presented in Figure 5.8. The sand had a specific gravity of 2.75.

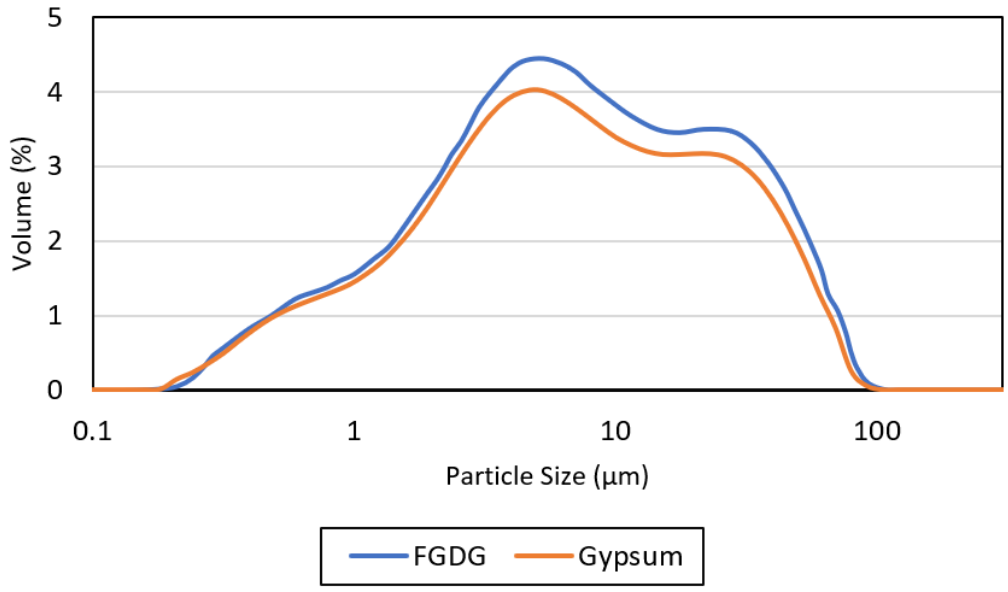

Figure 5.6: Particle size distribution of FGDG and commercial plaster.

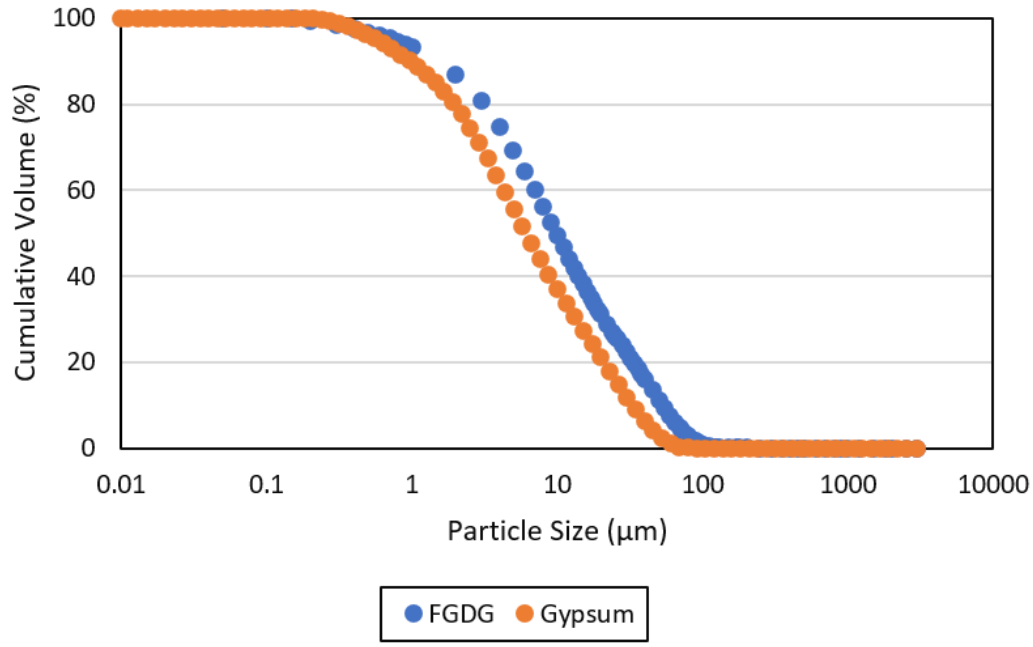

Figure 5.7: Particle size distribution of FGDG and commercial plaster.

5.1.6 MPCM

The present study used commercially available microencapsulated PCMs. Considering Türkiye's climate and occupant thermal comfort limitations, Micronal 24D® was

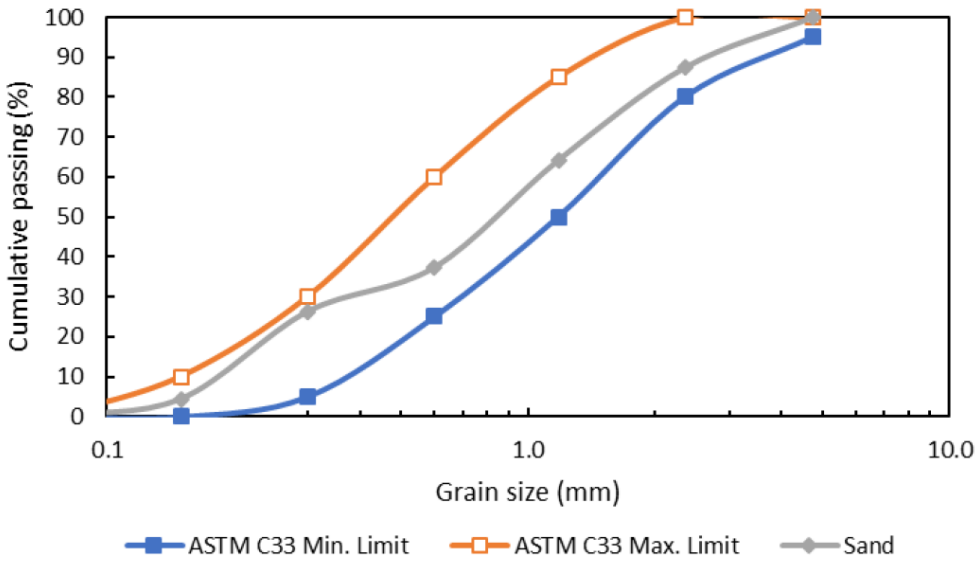

Figure 5.8: The grain size of the sand used in the study. This figure was directly adopted from [10].

selected and purchased from Microtek Laboratories in Dayton, Ohio, USA. The general properties of the MPCMs are given in Table 5.3. The MPCM particles comprise a core substance and a shell or capsule wall. The capsule wall is a polymer or plastic that is inert and stable. The core of MPCM melts at 24 °C. The polymer shell of PCM holds the melted paraffin together. The SEM images are in Figures 5.9 and 5.10. The EDS analysis reveals the composition of MPCM's robust hard shell, primarily composed of acrylic polymer, with the possibility of silicone inclusion in the acrylic matrix.EDS analysis of the PCMs is given in Figure 5.11. EDS analysis result of the tough shell of MPCM.

5.2 Mixture Design

In this section, the water ratio, sand ratio, and MPCM ratio in the mixture are explained.

Table 5.3: General properties of Micronal 24D®.

Properties	Micronal 24D ®
Melting point (°C)	24
Latent heat of fusion (J/g)	105
Mean particle size (µm)	50-300
Form	Dry Powder
Colour	White to slightly off-white
Density	0.9

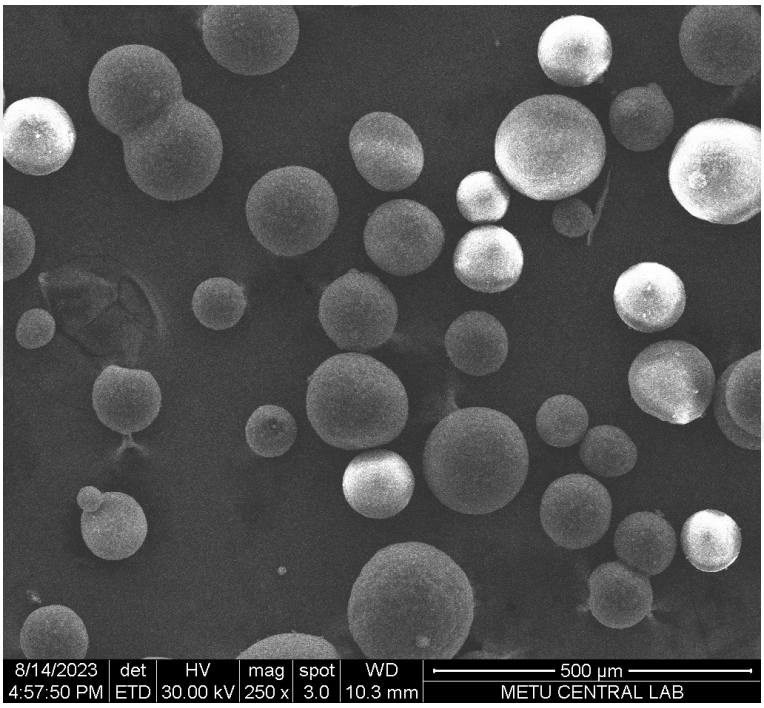

Figure 5.9: SEM image of MPCM with 250 magnification rate.

5.2.1 Water Ratio

To determine the appropriate amount of water for FGDG mixtures, FGDG blocks were synthesised using a specific proportion of FGDG, water, and sand, as indicated in Table 5.4. The sample preparation process involved mixing and stirring gypsum powder and sand for one minute before gradually adding water to the mixture under continuous vigorous agitation for at least 1 minute. The mixture was then stirred

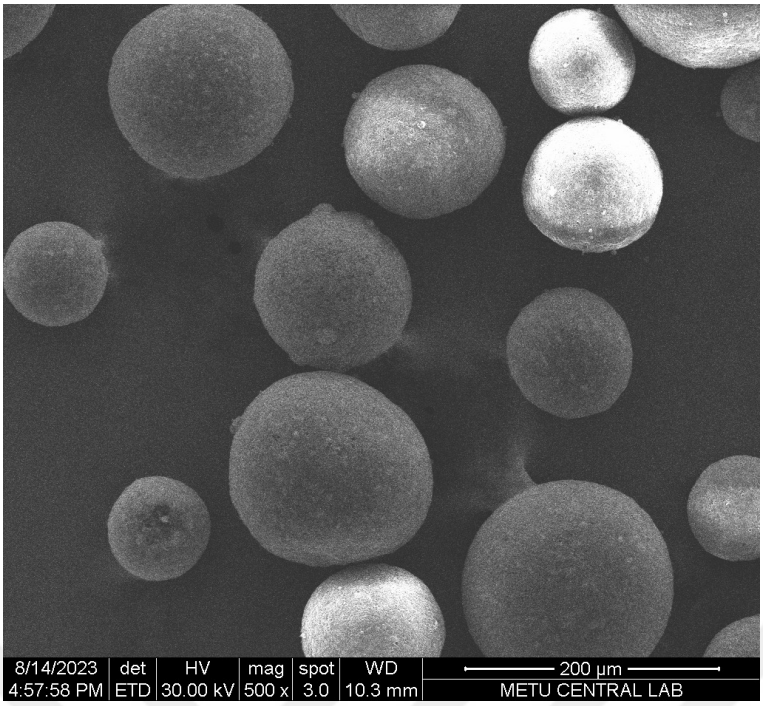

Figure 5.10: SEM image of MPCM with 500 magnification rate.

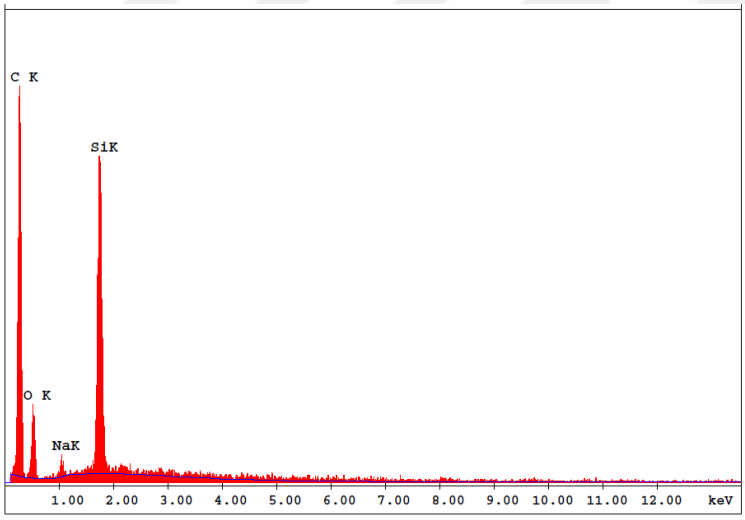

Figure 5.11: EDS analysis of MPCM.

for 2 minutes at low speed and another 2 minutes at high speed. Once thoroughly mixed, the FGDG was poured into one of three steel moulds, each measuring 40 mm × 40 mm × 160 mm, for testing mechanical strength. The moulds were left to set under atmospheric conditions for seven days before testing. Flexural and compressive strengths are measured after seven days according to ASTM C348 standard [125] and

ASTM C349 standard [126]. Flexure and compressive tests are presented in Figure 5.12. Based on the investigation results, a decision has been made in favour of the viability of using a water-to-FGDG ratio of 0.65. It should be noted that the commercial plaster variety used in this study has an ideal water-to-binder ratio ranging from 0.63 to 0.78. To achieve consistency in water proportions for both FGFG and commercial plaster mortar formulations, a water-to-binder ratio of 0.65 was prudently chosen.

Table 5.4: The mix proportions of Sand, FGDG, and water composite materials.

No.	Sand (g)	FGDG (g)	Water (g)	Water/Binder ratio (wt%)
FGDG-55%W	1068	534	300	55
FGDG-60%W	1046	523	314	60
FGDG-65%W	1104	552	359	65

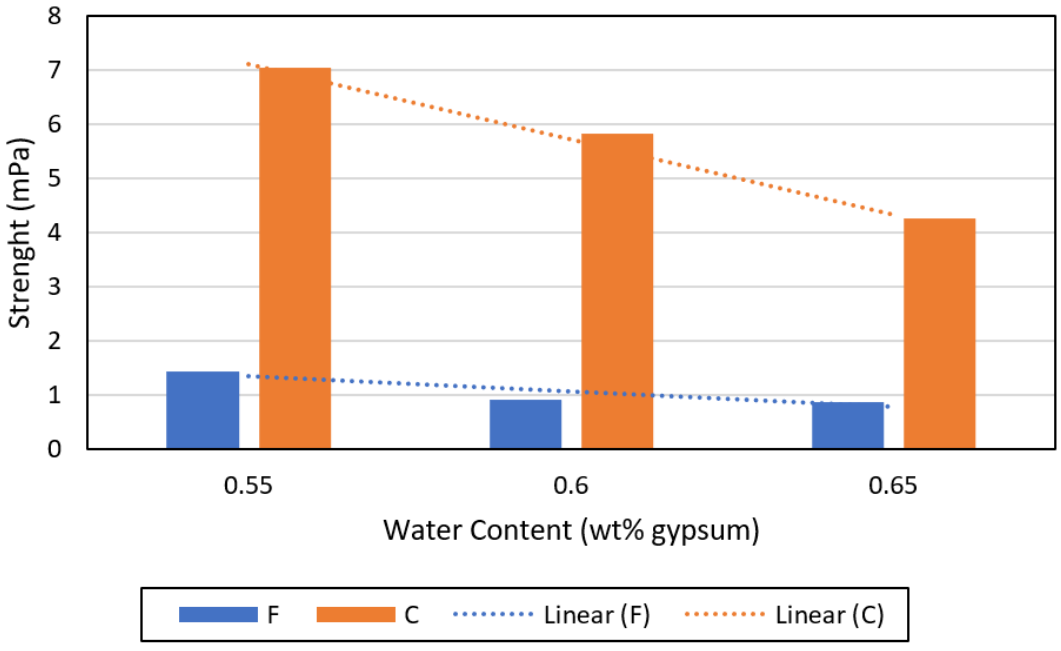

Figure 5.12: Flextural and compressive strength results of the composites, which have different water content, at seven days.

5.2.2 Sand Ratio for FGDG and Commercial Plaster Samples

Sand ratio in mortars affects workability, strength, setting time, and surface quality. The default sand-to-binder ratio is taken as 2:1. Note that with the replacement of PCM with sand, this ratio changes during mixtures.

5.2.3 PCM Ratio for FGDG and Commercial Plaster Samples

PCM can be incorporated into the mixture as an additive, or PCM can be substituted for sand. Since both aggregate and PCM are inert, the replacement approach is chosen in this study [10][127]. Therefore, the required volume percentage of PCM replaces the same volume percentage of sand. The weight of PCM was calculated based on the ratio of sand-to-PCM unit weight. In Table 5.5, the weights of the materials employed in the formulation of the mixtures are provided.

Table 5.5: The mix properties of investigated composites.

Code	**Binder (g)**		**Fine Aggregate (g)**		**Water (g)**	**Volume Ratio of Fine Aggregates**	
	FGDG	**CP**	**Sand**	**MPCM**		**Sand**	**MPCM**
FGDG-PCM0	700	0	1400	0	455	100	0
G-PCM0	0	700	1400	0	455	100	0
FGDG-PCM20	700	0	1260	45.8	455	80	20
G-PCM20	0	700	1260	45.8	455	80	20
FGDG-PCM40	700	0	1120	91.6	455	60	40
G-PCM40	0	700	1120	91.6	455	60	40

5.3 Material Characterization Experiments

5.3.1 Physical Properties

The specific weight of both FGDG and commercial plaster samples is calculated by dividing the weight of samples by their volume [90] [92]. The weight of samples is

measured with cylindrical samples DIA 70 mm x 40 mm at 56 days and is determined using the equation 5.2 as mentioned below:

$$\gamma = \frac{mg}{V} \tag{5.2}$$

Where *m* is the mass of the cylindrical sample, *g* is gravity and *V* is the volume.

5.3.2 Mechanical Properties

The newly developed composites' flexural and compressive strength is measured using a universal test machine (UTM) by UTEST with product code UTCM-3742.FPR. Flexural strength is measured in triplicates with 40 mm x 40 mm x 160 mm blocks at 14 days according to [125]. Flexure tests on prism specimens were performed using the centre point loading method at a loading rate of 0.04 kN/s. The uni-axial compressive strength of the samples was evaluated using the relevant standard [126], which utilised broken prism parts during the flexural test. Before testing, the specimens' end faces were polished to be flat and parallel, and the compression test was performed at a loading rate of 1.5 kN/s. Figure 5.13 resented the UTS machine during the flexural test.

5.3.3 Thermal Properties

In this section, the investigated thermal properties of mixes are presented.

5.3.3.1 Thermal Conductivity

Thermal conductivity of mixes was measured with the transient plane source (TPS) method, and Hot Disk TPS 2500 S thermal constants analyser, manufactured by Thermtest Europe AB in Sweden, was employed in strict adherence to the guidelines outlined in ISO 22007-2.[128]. Thermal conductivity of samples is measured with cylindrical samples DIA 70 mm x 40 mm at 14 days and 56 days. The sensor

Figure 5.13: Universal test machine used for measuring flexural and compressive strength.

was placed inside the measurement chamber with one of the samples, and the second sample was placed on top of the sensor. The Hot Disk Kapton sensor with a diameter of 6.403 mm (Sensor code: 5501) was used. A bulk measurement mode with a 40 mm probing depth is selected. Measurement time and heating power are adjusted to obtain a recommended temperature rise of 2 K- 5 K. Also, residual curves were checked to determine whether the scatter pattern was random in the vicinity of a horizontal line, which is the desired pattern, or if there were some abnormalities like clustering or increasing/decreasing trends in scatters. Also, the transient curve was controlled whether it showed a steady increase in temperature with no sharp jumps, discontinuities, or negative temperature development or there were some abnormalities. All specimens are measured three times by rotating the upper sample 120°to reduce the effect of regional properties such as voids, surface irregularities and so on. Thermal conductivity is obtained by averaging these measurements. Each sample's thermal conductivity was measured at 26°C, which is two °C above the nominal melting temperature of MPCM. Also, samples were at 26 °C for days, which means samples were at a steady state and had uniform temperature distribution. Given these data, it is safe to suggest that PCMs were liquid during measurement. In Figure 5.14, the replacement of the sensor during measurements is shown.

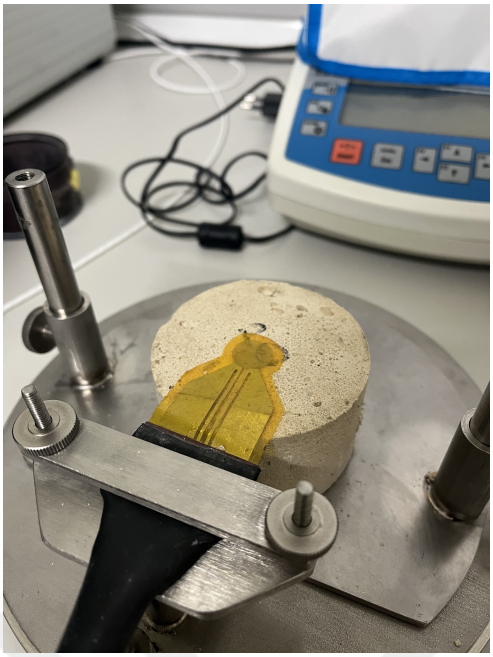

(a) The sensor was placed in the middle of the sample.

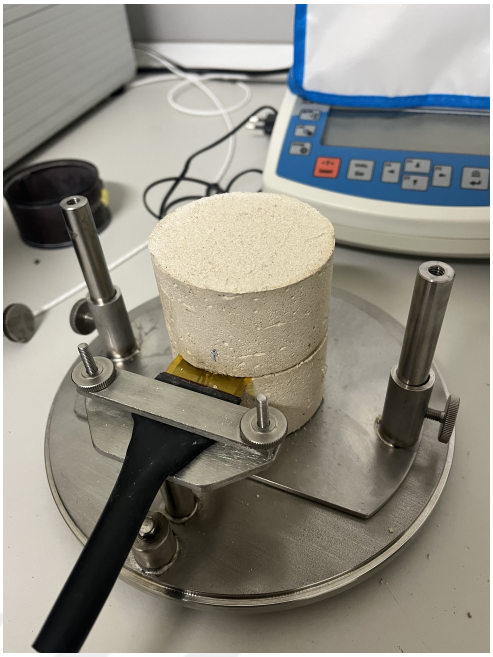

(b) The sensor was sandwiched between specimens.

Figure 5.14: Replacement step of the sensor for thermal conductivity measurements.

Sensor probes of the hot disk contain a long wire in the shape of a thin spiral disk, and these probes act as both a heat source and a heat sensor while measuring. Proper one of these sensors is selected, and this sensor is placed into two identical samples. Then, the sensor generates a thermal wave that penetrates the samples. The sensor's temperature and resistance increase when electrical pulses are given to the sensor. Resistance increases depending on time:

$$R(t) = R_0(1 + p(\Delta T_i + \Delta T_{samp}(\tau))) \tag{5.3}$$

In equation 5.3, R_0 represents the resistance of the disk before heating by an electrical pulse, P is the temperature coefficient of resistivity, ΔT_i is the temperature difference between the sensor and sample, ΔT_{samp} is the temperature difference of the contact surface of the sample to the sensor with time and, τ is dimensionless time.

In the light of TPS theory, the heat conduction equation is solved under the assumption that the hot disk consists of an infinite number of concentric ring heat sources

and dimensionless time-dependent temperature change in the sample becomes:

$$\Delta T_{samp}(\tau) = \frac{P}{\pi^{3/2} * r * k} * F(\tau) \tag{5.4}$$

In the equation 5.4, *P* represents the power given by the sensor, *r* is the radius of the disk, *k* is the thermal conductivity of the sample, and (τ) is the dimensionless time-dependent function.

Dimensionless time (τ) is expressed as:

$$\tau = \sqrt{\frac{t}{\theta}} \tag{5.5}$$

where t is measurement time and θ is characteristic time which is defined as:

$$\tau = \frac{r^2}{\alpha} \tag{5.6}$$

is the thermal diffusivity of the sample:

$$\alpha = \frac{k}{\rho * C_p} \tag{5.7}$$

Both α and θ are unknown before the experiment. Therefore, the final straight line from which thermal conductivity is calculated is obtained by iteration.

5.3.3.2 Specific and Latent Heat

DSC is used to determine the latent heat of mortar samples that contain different amounts of MPCM. Latent heat, along with melting and freezing points of Micronal 24D, was obtained. Specific heat of samples was not obtained due to the limitations of the operator in using the equipment. Therefore, enthalpy values obtained and mentioned in this part of the study are only latent heat. Before the experiment, mortar samples were crushed to obtain powder form. A sample of 10 mg of weighted powder was sufficient for the experiment. The heating/cooling rate is selected as 5 °C min $^{-1}$, as in similar studies [90] [95]. One and a half thermal cycles are applied to

the samples. DSC was performed using A PerkinElmer 8000 DSC with a thermal cycle from 10 °C to 50 °C with a 5 °C/min heating and cooling rate at METU Central Laboratory.

5.3.4 Microstructure

The morphology of the raw materials (FGFG, commercial plaster, MPCM) and the microstructure of all composites (FGDG-PCM0, FGDG-PCM20, FGDG-PCM40, G-PCM0, G-PCM20, G-PCM40) were both investigated by SEM. Before the investigation, all samples are placed into the oven to remove excessive moisture. This procedure aims to obtain a better vacuum during both sputter and SEM procedures. To improve surface conductivity, gold-palladium nanoalloy sputtering is performed on samples. After excessive moisture was extracted, small portions of each mixture were mounted on metal stubs using a carbon band and sputter-coated using gold before being examined under the electron microscope. All samples are magnified 100, 250, 500, 1000, 2500. SEM investigation is performed at METU Central Laboratory.

CHAPTER 6

RESULTS AND DISCUSSIONS

6.1 FDM Result Verification

Commercial software was used to verify the FDM model result. The length of the wall was selected as 0.025 m. The initial condition of the wall was chosen as 50 °C. The outer and inner boundary conditions (BC) were selected as convection BC, i.e., the third kind. The sink temperature of the outside BC was 5 °C, and the convection coefficient was 20 W/m K, while the sink temperature of the inner BC was 23 °C, and the convection coefficient was 8 W/m K. Temperature distribution results at t=900 s are compared with the result of commercial software, which is mentioned as "exact", and the result of the code developed by the author, which is referred to as "model" in Figures 6.1 and 6.2. In Table 6.1, the exact and model temperature on different x locations of the wall is shown. Normalised exact temperature and model temperature is calculated in such way:

$$T_{exact} = \frac{(T_{max} - T_{exact})}{(T_{exact} - T_{min})} \tag{6.1}$$

Where T_{max} is the initial condition, which is 50 °C, and T_{min} is the temperature outside, which is 5 °C.

Table 6.1: Temperature value of exact and model at different x positions(t=900 s). Normalised exact and model temperatures, as well as normalised errors, are presented.

x (m)	$T_{exact}(°C)$	$T_{model}(°C)$	$T_{exact,n}$	$T_{model,n}$	**Normalised Error**
0	32.24	32.21	0.61	0.60	0.11 %
0.005	33.96	33.93	0.64	0.64	0.11 %
0.01	35.24	35.21	0.67	0.67	0.11 %
0.015	36.05	36.02	0.69	0.69	0.11 %
0.02	36.39	36.36	0.70	0.70	0.11 %
0.025	36.25	36.21	0.69	0.69	0.11 %

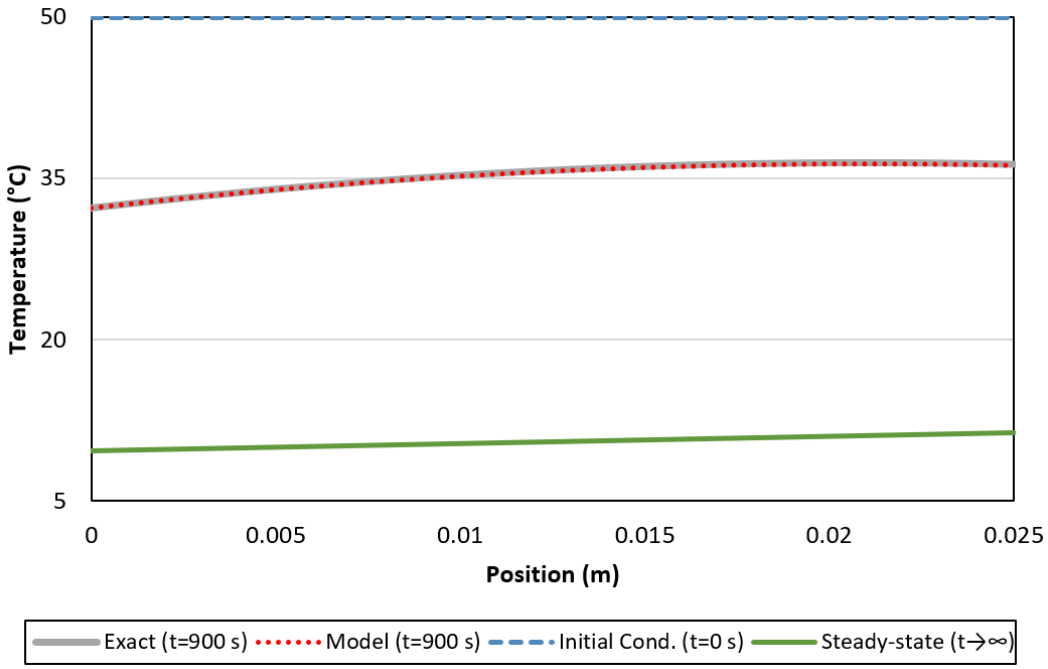

Figure 6.1: Temperature distribution of Wall at different times.

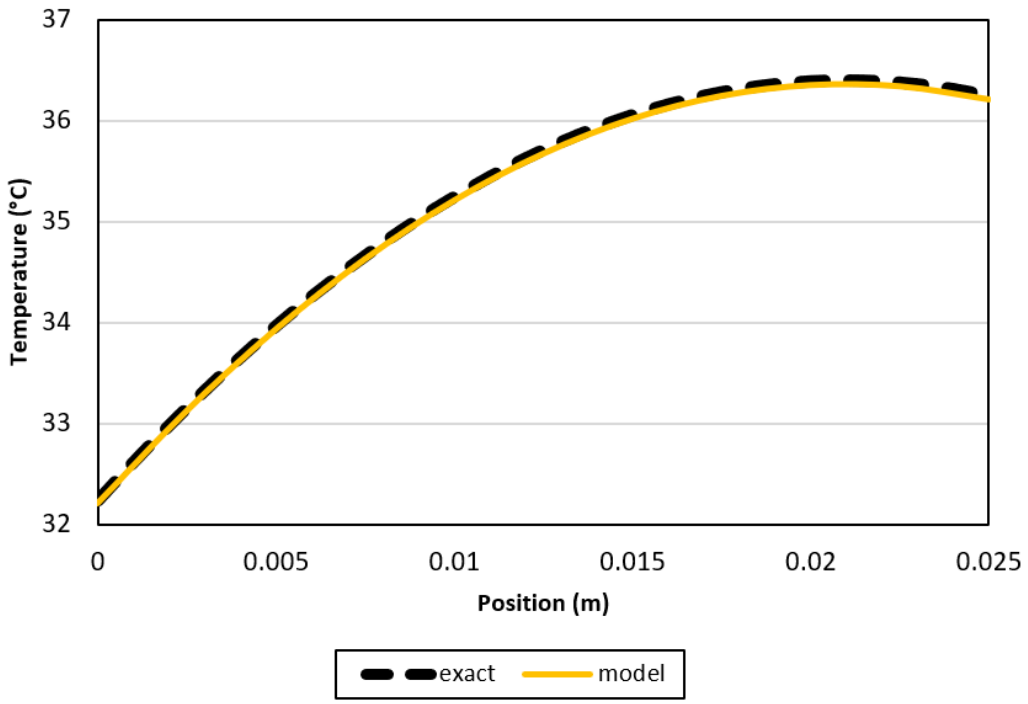

Figure 6.2: Exact temperature distribution and temperature distribution obtained by the model at t=900s.

6.2 Temperature Profiles

Temperature profiles for Config 1, Config 2, Config 3, and Config 4 were obtained for one week in winter and one week in summer. Temperature profiles for the outermost, middle and innermost nodes for the south-oriented wall are presented.

Summer and winter seasons are discussed separately in this paragraph.

In the summer season, Config. 1 has the most alteration at the innermost node, as seen in Figure 6.3. The reason for this is that concrete has higher α and k than both insulation material and PCM, which means concrete is more sensitive to outside temperature change, and it is easier to conduct heat flow to the inner layers. In contrast, the outermost node of the wall has the least alteration for Config 1 as well as Config 4. The reason for that is higher α and k, heat flux can be conducted in the inner layers, and temperature does not rise as in Config 2 and Config 3, which have insulation at the outermost layer. Config 3 has the most stable innermost temperature, also Config 2 also has very stable innermost temperature with small fluctuations. Config 4 tends

to have a stable temperature profile at the innermost node when the temperature at that layer is in the melting range. However, when the temperature at the innermost layer exceeds the melting temperature range, the temperature at the innermost node tends to rise.

In the winter season, Config. 1 has the most alteration at the innermost node, as seen in Figure 6.3, similar to the summer season. Config 2 and Config 3 have almost identical temperature profiles for the innermost node. While Config 3 is more stable in summer, the reason why Config 2 and Config 3 have the same stabilisation in the innermost node in winter is that the temperature of the inner layer in summer is closer to the nominal melting temperature of the PCM. Therefore, it is within the melting range, creating a latent heat region. It is entered and, therefore, has a higher specific heat. However, in winter, the temperature of the inner layer tends to be lower, and PCMs do not enter the melting range. Therefore, the innermost nodes of Config 2 and Config 3 have a more similar temperature profile in winter than in summer.

Config 2 and Config 3 also have very similar outermost node temperature profiles. The temperature profile of the middle nodes of Config2 and Config 3 differs slightly due to the different thermal conductivity values of the inner layers. In Config 2, since the inner layer is concrete, the middle node has a temperature profile closer to the innermost node.

Config 1 and Config 4 have similar temperature profiles. Temperature fluctuations are less in the innermost node because there is PCM only in the innermost layer of Config 4, and although PCM is in the sensible region due to its temperature, it has lower thermal conductivity than concrete.

6.3 Sensitivity Analysis

Sensitivity analysis is performed for the modified FDM model with the modifications described in Section 4.4.1.

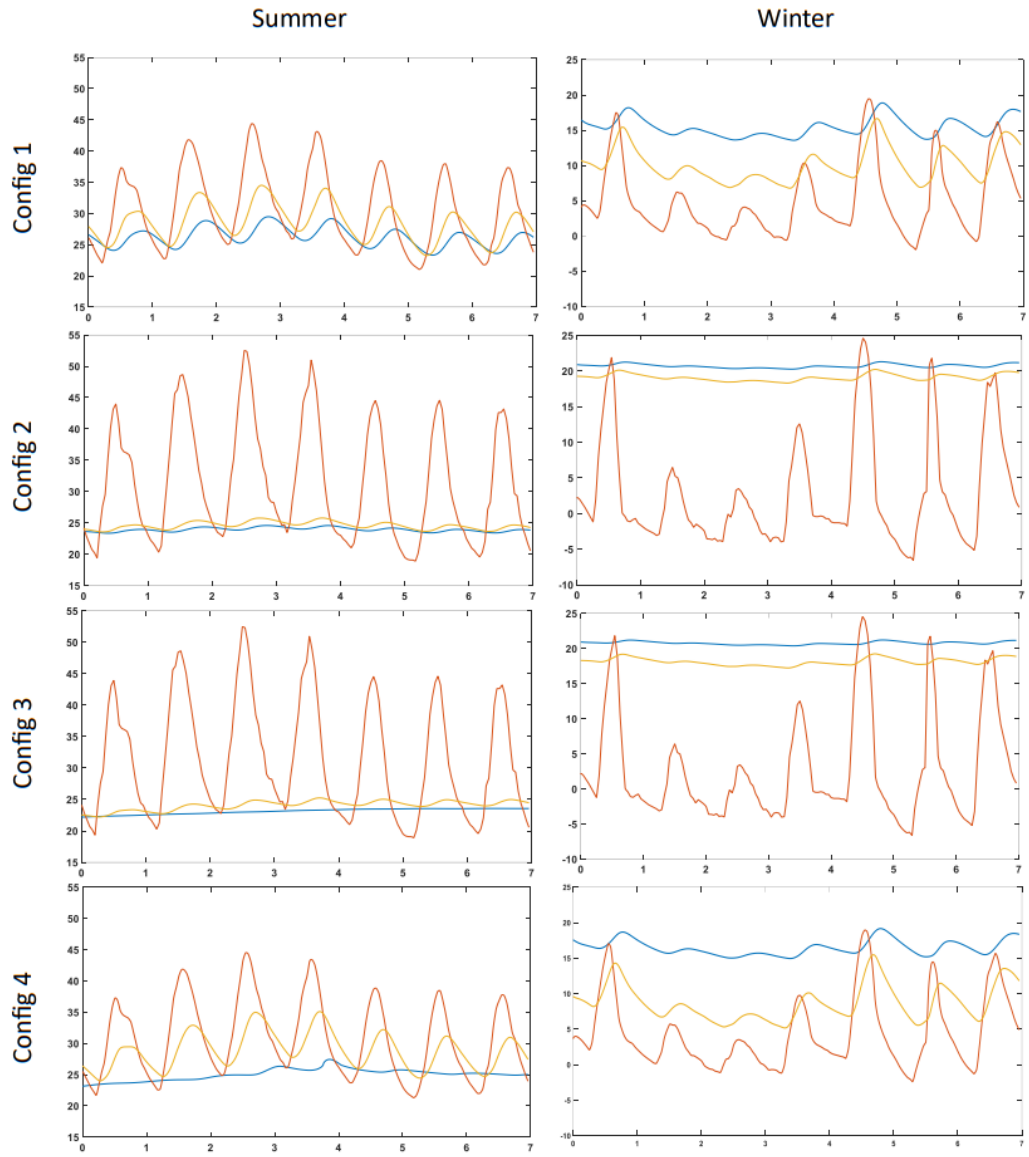

Figure 6.3: Temperature Profiles of four configurations of south-oriented wall for one representative week in summer and one representative week in winter. Note that the blue line = temperature profile of the innermost node, the orange line= temperature profile of the outermost node, and the yellow line= temperature profile of the middle node.

6.3.1 Generic Wall Model

Sobol' indices are obtained from the code, which is Section 4.4. Sensitivity analyses are performed for four different wall orientations. All 21 parameters and their

sensitivity indices for north-oriented walls, east-oriented walls, south-oriented walls, and west-oriented walls for summer are presented in Figure 6.4. Sensitivity indices for north-oriented walls, east-oriented walls, south-oriented walls, and west-oriented walls for winter are presented in Figure 6.5. As seen in Figures6.4 and 6.5, the nominal melting temperature of PCM (T_m) is the most influential parameter for four orientations. However, the sensitivity of T_m is greater for the winter season compared to the summer. For the summer season, the sensitivity of thermal conductivity increases progressively towards the innermost layer. Similarly, the sensitivity of volumetric PCM inclusion rises gradually towards the innermost layer. For the winter season, the model has no sensitivity to the thermal conductivity of any of the layers.

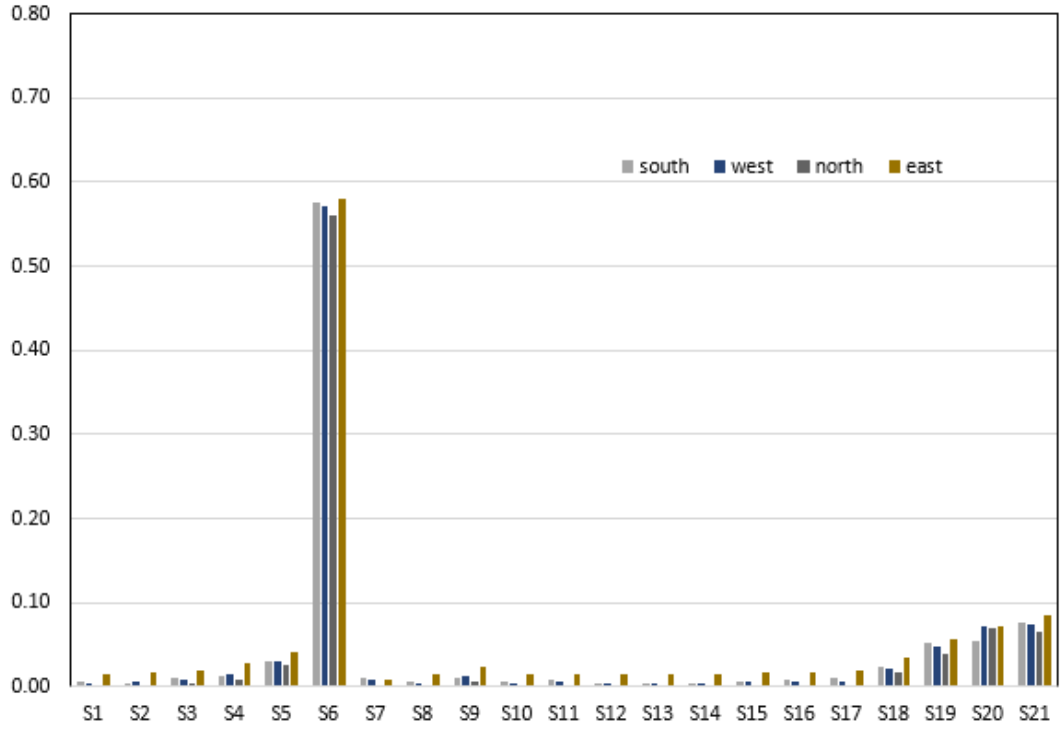

Figure 6.4: Sensitivity indices of 21 parameters for summer for four wall orientation.

6.4 Quantitative Phase Analysis

The focus of presenting quantitative phase analysis results from X-ray diffraction (XRD) is to learn the crystalline composition of a material. The analysis of XRD patterns distinguishes information regarding the presence and abundance of different

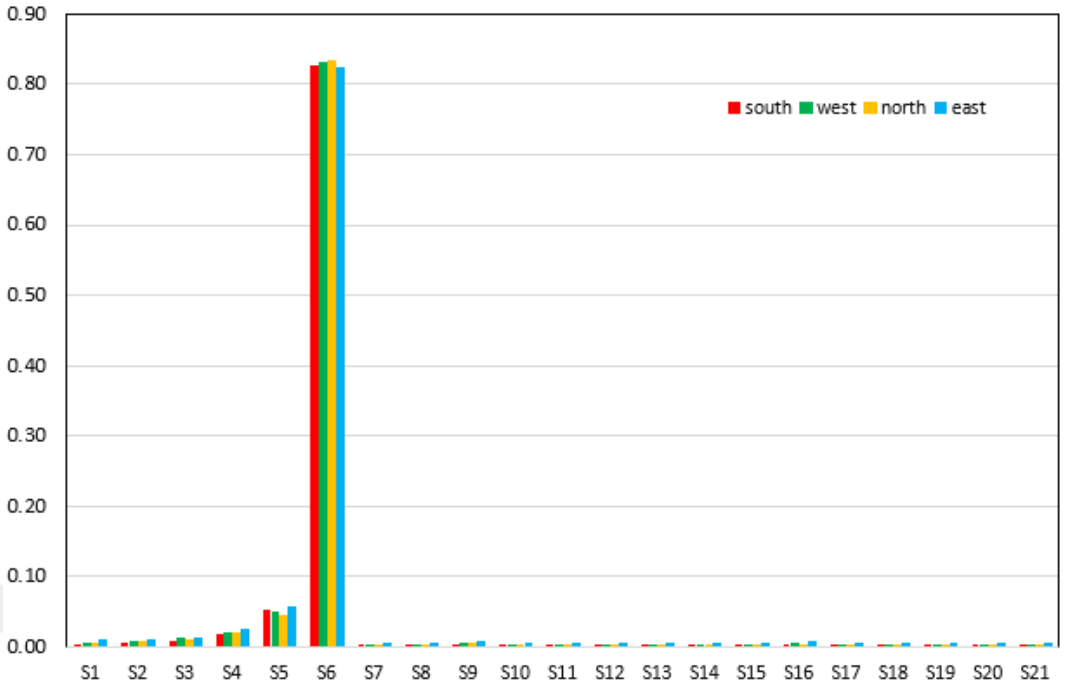

Figure 6.5: Sensitivity indices of 21 parameters for winter for four wall orientation.

crystalline phases. The presentation typically includes detailing peak positions, intensities, and profiles refined to extract quantitative data for FGDG and commercial plaster. Results of XRD measurement for FGDG and commercial plaster before hydration are presented in Figure 6.6. Figure 6.7 shows the XRD measurement results of commercial plaster and FGDG after 7 days of hydration.

The percentages of individual stages are accurately determined using established methodologies such as the Rietveld improvement method. Results of Rietveld analysis are presented in Table 6.2 for FGDG and commercial plaster before hydration and Table 6.3for FGDG and commercial plaster after 7 days of hydration.

6.5 Specific Weight

Figure 6.8 presents the specific weight of all samples. As seen in Figure 6.8, the specific weight of FGDG samples is higher than that of commercial plaster samples. The chemical composition of raw FGDG and commercial plaster is similar, as seen in XRF Table 5.2. Also, the crystal structure of the hydrated form of FGDG and

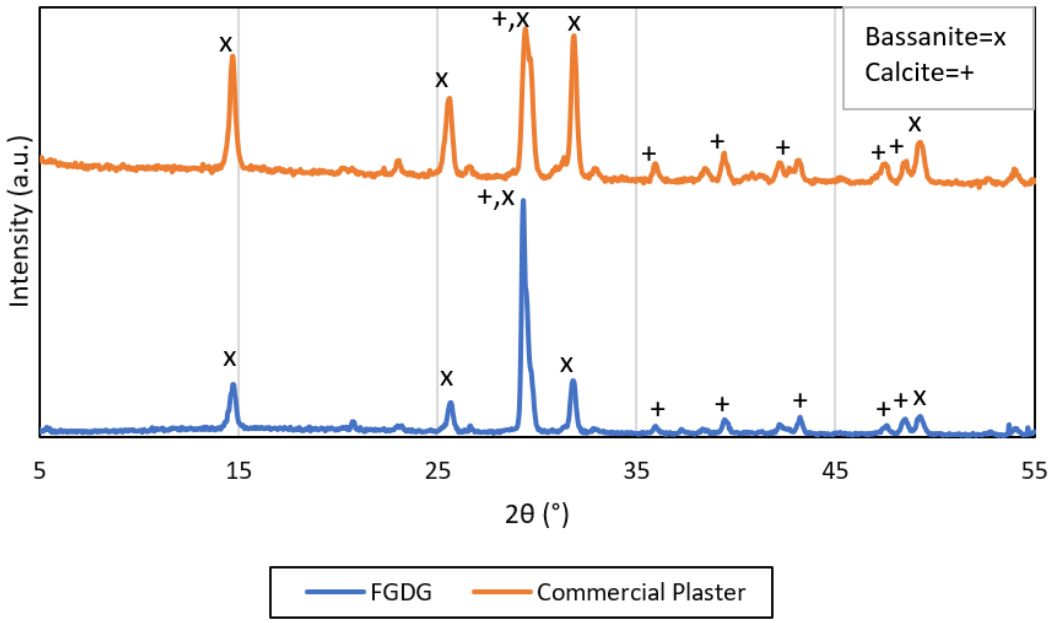

Figure 6.6: XRD result of FGDG and Commercial Plaster results before hydration.

Table 6.2: Mineral Ratio of FGDG and Commercial Plaster results before hydration.

Mineral	**FGDG after Hydration (%)**	**Commercial Plaster after Hydration (%)**
Bassanite	47.4	55.8
Gypsum	1.6	8.1
Anhydrate	0.0	14.1
Calcite	49.8	21.2
Quartz	1.2	1.0

commercial plaster are similar, as seen in Figure 6.7. As seen in Table 6.3, FGDG contains more calcite compared to commercial plaster. There are two main reasons for specific weight differences. Firstly, calcite has a higher specific weight compared to commercial plaster, and since FGDG contains more calcite, it is expected to have a higher specific weight. Secondly, the difference in specific weight can be attributed to the porosity caused by the air-entraining agent in the commercial plaster samples. The air-entraining agent in commercial plaster creates a whipped cream consistency caused by tiny air bubbles entraining during the mixing process. As expected, the

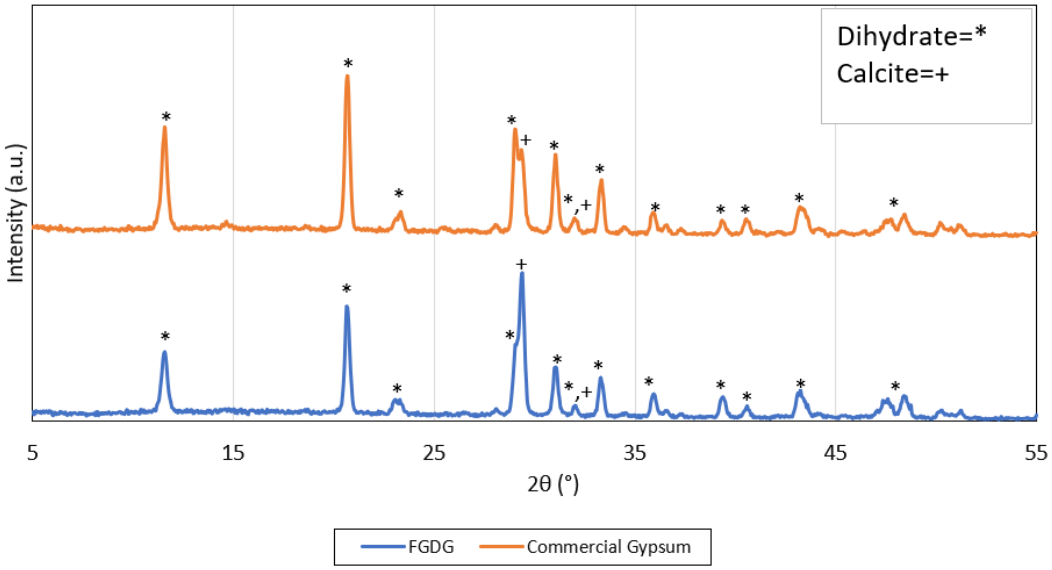

Figure 6.7: XRD result of hydrated FGDG and Commercial Plaster results after 7 days.

Table 6.3: Mineral Ratio of FGDG and Commercial Plaster after 7 days.

Mineral	**FGDG after Hydration (%)**	**Commercial Plaster after Hydration (%)**
Bassanite	0.5	1.7
Gypsum	55.4	76.8
Anhydrate	0.0	0.4
Calcite	43.5	22.6
Quartz	0.6	0.6

specific weight of FGDG samples decreases with increasing PCM content. The unit weight of plaster does not have a monotonic relation with increasing mPCM content. The reason for this situation is the filling effect. MPCMs fill air bubbles in plaster samples.

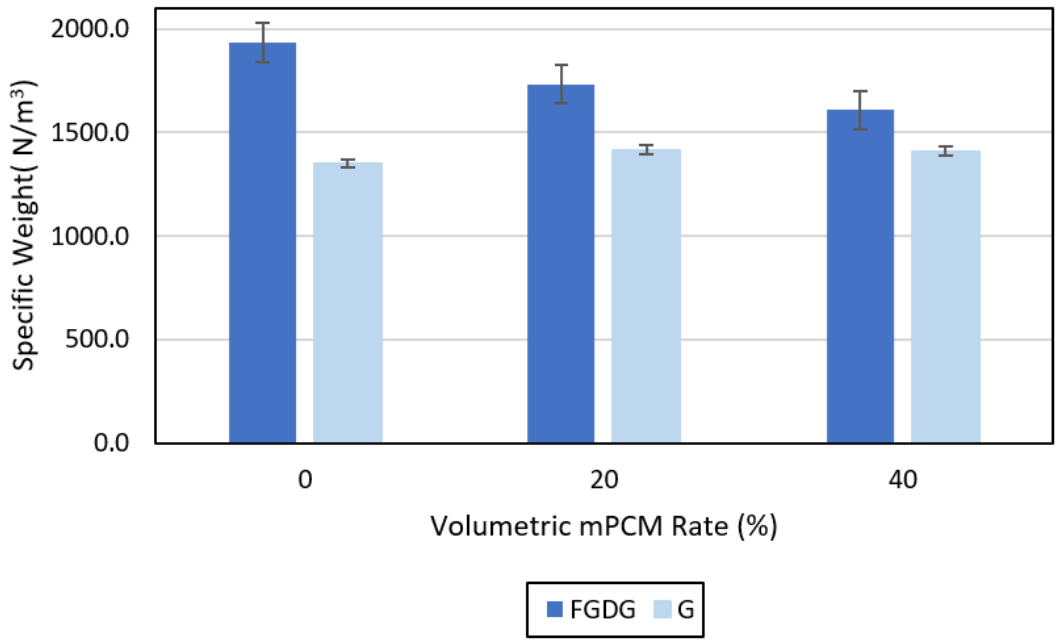

Figure 6.8: Specific weight of FGDG and Commercial Plaster samples with different MPCM inclusion rates.

6.6 Flexural and Compressive Strength

Results of experiments conducted using the methodology in 5.3.2 are shown in Figure 6.9 and Figure 6.10. Flexural and compressive strength results of FGDG composites are given in Figure 6.9, and flexural and compressive strength results of commercial plaster composites are shown in Figure 6.10. In FGDG samples, compressive strength tends to decrease with increasing MPCM content, while flexural strength tends to increase slightly. Notably, the decrease in compressive strength outweighs the gain in flexural strength. The reason for the compressive strength decrease in FGDG samples can be explained with MPCM content. Since MPCM has a lower breakage point, its content weakens the composite regarding compressive strength.

In commercial plaster, flexural and compressive strength do not have a monotonic relation with increasing MPCM content. The flexural and compressive strengths for G-PCM20 slightly increased compared to G-PCM0 (control sample) by 7% and 10%, respectively. In contrast, both flexural and compressive strength for G-PCM40 samples decrease by 7% and 36%, respectively, compared to the control sample G-PCM0.

On average, both the flexural and compressive strength of FGDG samples are slightly higher than the commercial plaster samples.

The overall strength performance of FGDG is higher than commercial plaster composites. It can be explained with a specific weight of samples. There is a tendency such way: The denser the composite, the higher the compressive strength.

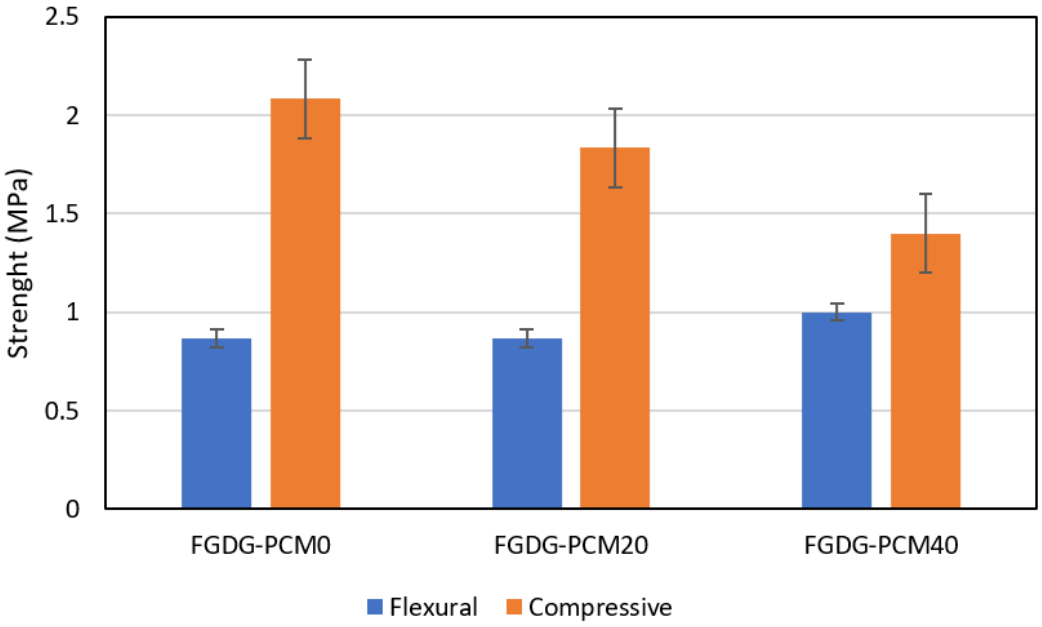

Figure 6.9: Flexural and compression strength of FGDG samples.

6.7 Thermal Conductivity

The results of the experiments presented in 5.3.3.1 are shown in Figure 6.11 and Figure 6.12. The 14 days thermal conductivity of FGDG-PCM20 decreased by 38% compared to FGDG-PCM0, while the thermal conductivity of the FGDG-PCM40 sample decreased by 41% compared to FGDG-PCM0. The reduction in thermal conductivity is more significant for FGDG-PCM20 compared to FGDG-PCM40; i.e., a 20 vol% MPCM inclusion causes a 38% decrease, and an additional 20 vol% MPCM inclusion causes a further 3% reduction of thermal conductivity.

The thermal conductivity of commercial plaster samples at 14 days has no monotonic relation with increasing MPCM content. The thermal conductivity of G-PCM20 in-

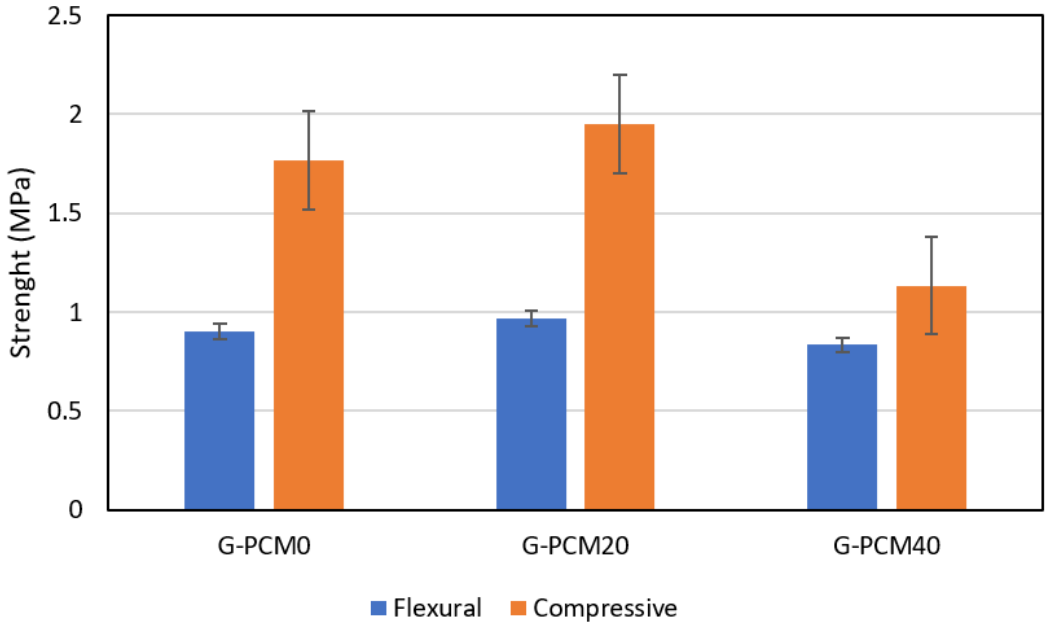

Figure 6.10: Flexural and compression strength of commercial plaster samples.

creased by 4% compared to G-PCM0, and the thermal conductivity of G-PCM40 decreased by 7%.

The thermal conductivity of commercial plaster samples is less affected by the inclusion of MPCM; the reason for that might be that the thermal conductivity of commercial plaster is lower than FGDG and closer to the thermal conductivity of MPCM. The average thermal conductivity of FGDG samples is 60% compared to the average thermal conductivity of the commercial plaster samples.

Note that the thermal conductivity of samples does not change with time, i.e. there is no meaningful change between the thermal conductivity of 14-day-old and 56-day-old samples.

The thermal conductivity of commercial plaster samples is lower compared to FGDG samples. The density of commercial plaster and FGDG samples can explain that phenomenon. The specific weight of FGDG samples is higher than commercial plaster samples, as detailed in Section 6.5. That means commercial plaster samples contain more pores compared to FGDG composites. Since these pores have air and the thermal conductivity of air is 0.0263 W/m K at room temperature [98], the thermal

conduction of commercial plaster samples is lower than FGDG samples.

Even though the chemical composition of raw FGDG and commercial plaster is very similar, as seen in XRF Table 5.2, FGDG contains more calcite compared to commercial plaster, as seen in Table 6.3. This leads to one of the reasons why the thermal conductivity of FGDG is higher: calcite has higher thermal conductivity than gypsum, 2.721 W/m K and 2.316 W/m K, respectively [129]. The other reason behind the difference in thermal conductivity is bubble formation in commercial plaster samples. The specific weight of commercial plaster mixes is lower compared to FGDG, and the reason for this might be higher bubble formation, as explained in section 6.5. These air bubbles cause more porous structures, and this leads to lower thermal conduction in commercial plaster samples.

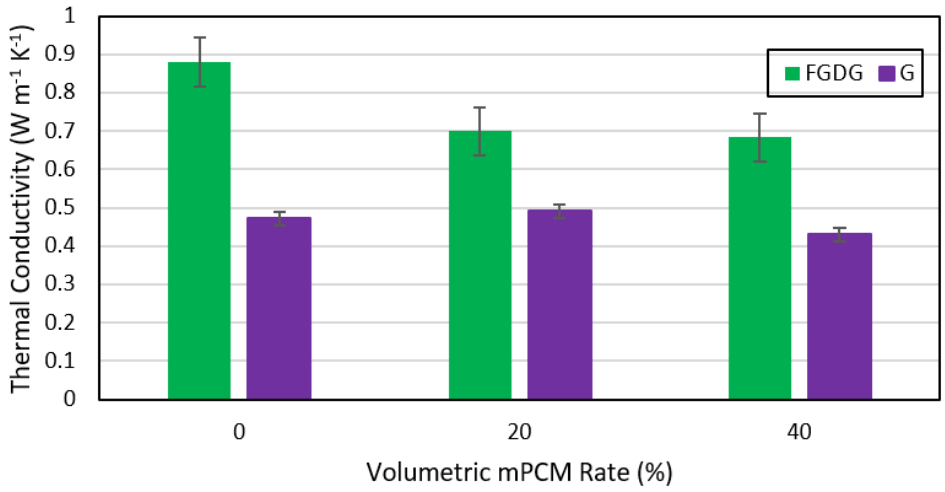

Figure 6.11: Thermal conductivity of FGDG and commercial plaster samples at 14 days.

6.8 Latent and Specific Heat

Differential Scanning Calorimetry (DSC) results for six composites and pure MPCM is given in Table 6.4. The latent heat of samples is derived by integrating the area under the phase change curves. As presented in Table 6.4, phase change range as well as phase change peak for all composites and MPCM are similar.

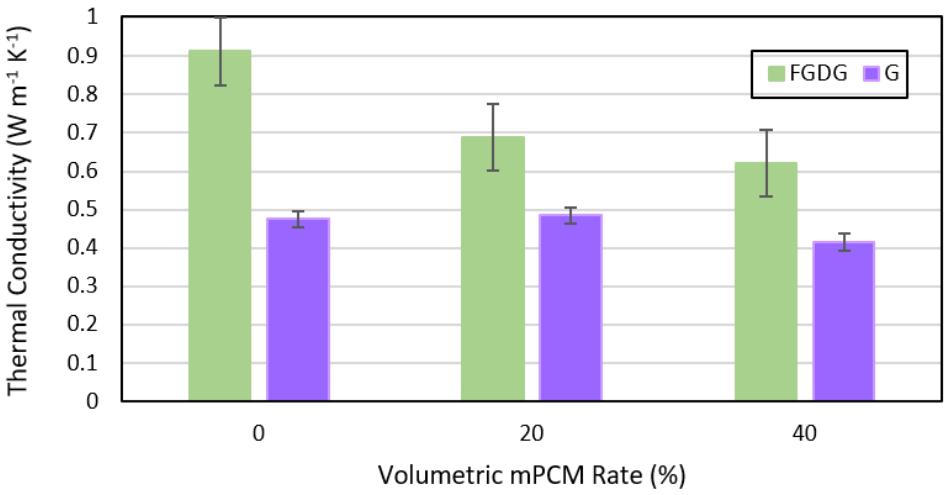

Figure 6.12: Thermal conductivity of FGDG and commercial plaster samples at 56 days.

As seen from Table 6.4, there are two different c_p columns. The reason of that heat flux data of DSC measurement were not considered meaningful.

First obtained specific heat capacity (c_p) is numerically calculated by using DSC curves. Simple method [130] is used for obtaining the specific heat capacity of MPCM and composite samples. The simple method is fundamentally integrating the area under the heat flow curve and dividing it into temperature ranges. Since heat flux at the sensible region of DSC measurement is not meaningful. Even though latent heat measurements are reasonable, it is assumed that there is a measurement error at the sensible heat flux measurement region, and sensible specific heat calculation is performed by known volumetric percentage of mixtures and found values for minerals and paraffin from literature.

Second calculated and assumed to be the correct specific heat capacity (c_p*) numerically calculated by obtained values from [131] for gypsum, calcite, and quartz sand; values from [132] for MPCM.

Table 6.4: Melting/Solidification Enthalpy, Peak Melting/Solidification Temperature and Specific Heat of MPCM and PCM incorporated composites. c_p is obtained by DSC values and c_p* is obtained by volumetric calculation.

Mixture	Melting		Solidification			
	T_p (C)	ΔH_m (J/g)	T_p (C)	ΔH_c (J/g)	C_p (J/g K)	C_p* (J/g K)
Micronal 24D	25.2	75.74	18.36	71.32	26.91	2.50
FGDG-PCM0	-	-	-	-	0.87	0.89
FGDG-PCM20	24.39	1.24	19.84	1.40	1.40	0.97
FGDG-PCM40	24.53	4.09	19.56	4.33	0.63	1.04
G-PCM0	-	-	-	-	0.850	0.91
G-PCM20	24.26	1.44	20.35	1.43	0.68	0.99
G-PCM40	24.40	3.29	19.96	3.21	0.97	1.07

6.9 Microstructure

As seen in the SEM images of the crystal structures of commercial plaster and FGDG in Figure 6.13 and Figure 6.14, the crystal structure of commercial plaster and FGDG are different. While FDGD has a needle-like crystal structure, commercial plaster has more prismatic structures. The aggregate particles in the G-PCM0 and FGDG-PCM0 mixtures are presented in Figure 6.15. The void formation is relatively low in these samples. The microstructures of G-PCM20 and FGDG-PCM20 are shown in Figure 6.16a and Figure 6.16b, respectively. Aggregate particles, MPCM, and voids caused by aggregates and MPCM can be seen in Figure 6.16. The microstructures of G-PCM40 and FGDG-PCM40 can be seen in Figure 6.17a and Figure 6.17b. Similar to the microstructures of G-PCM20 and FGDG-PCM20, aggregate particles, MPCM, and voids caused by aggregates and MPCM can be seen.

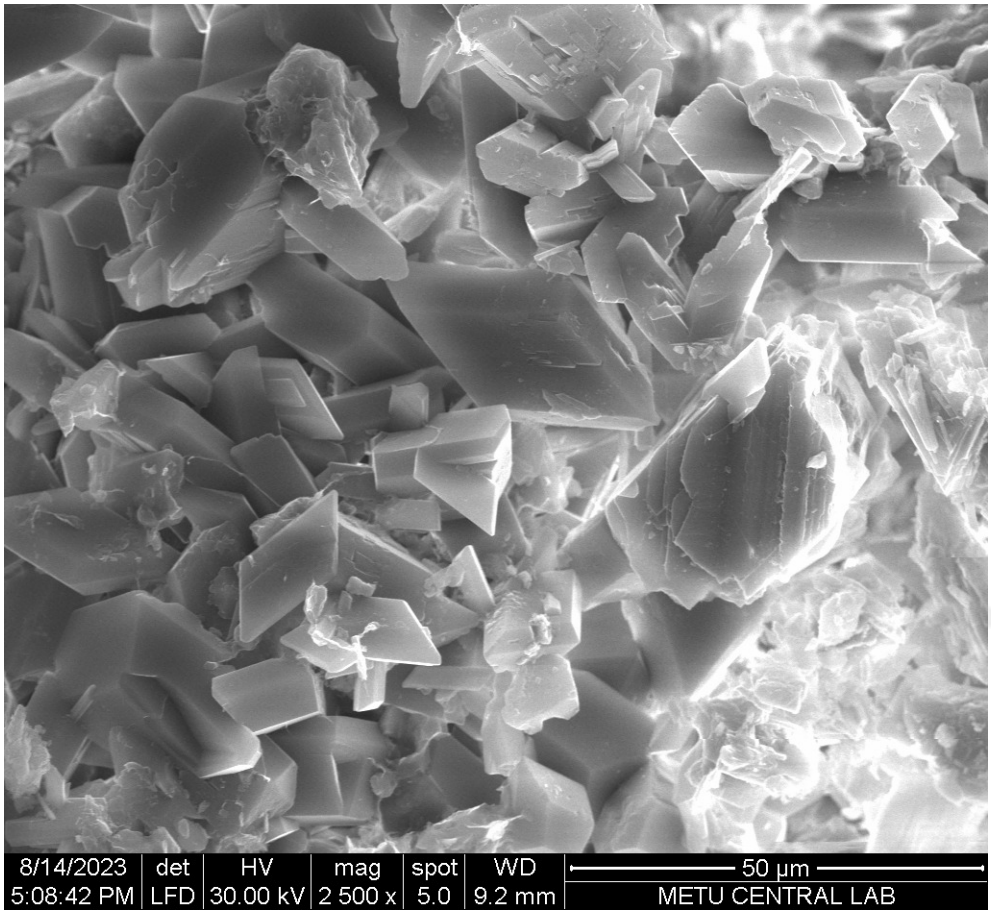

Figure 6.13: SEM image of the crystal structure of commercial plaster 21 days after pouring.

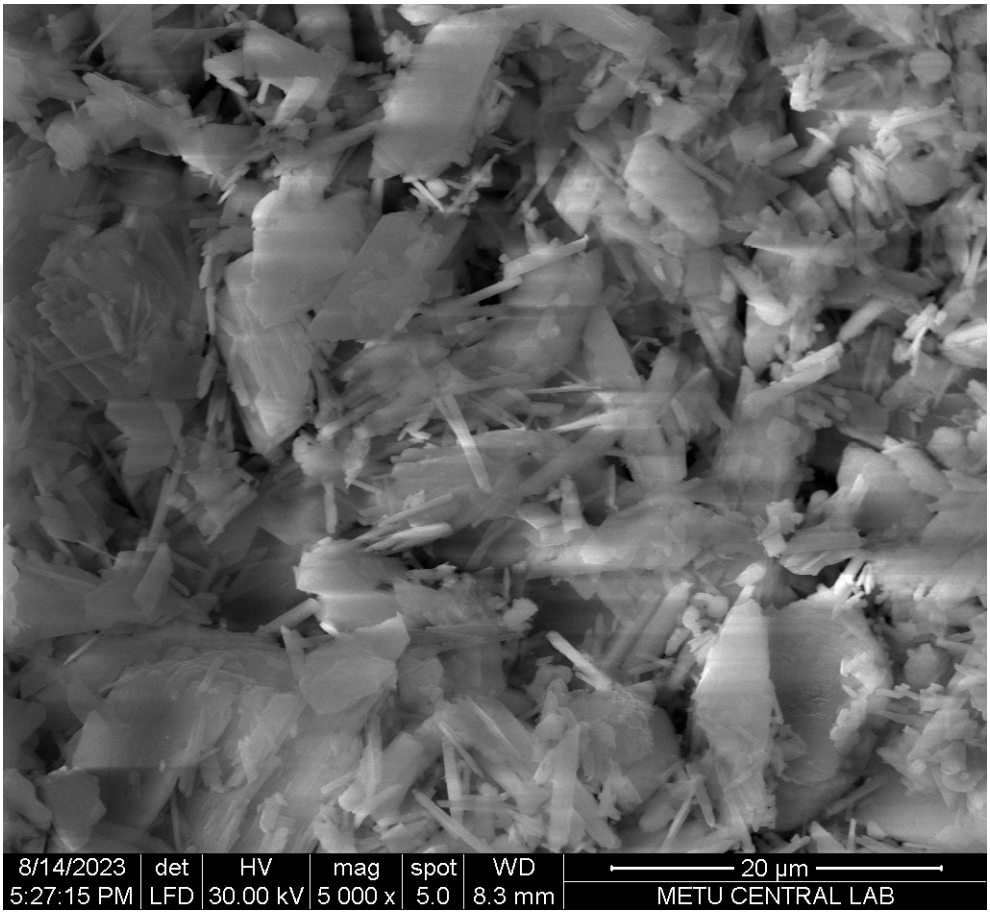

Figure 6.14: SEM image of the crystal structure of FGDG 21 days after pouring.

(a) G-PCM0

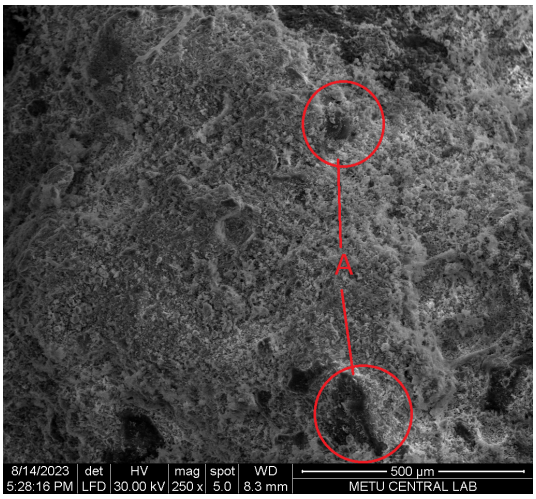

(b) FGDG-PCM0

Figure 6.15: SEM images of samples without MPCM 21 days after pouring. Note that: A=aggregate.

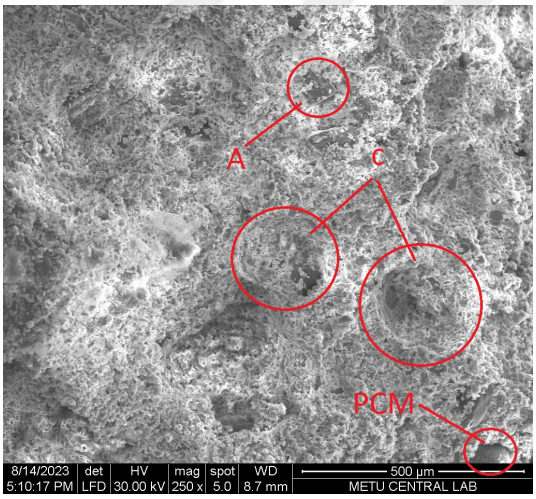

(a) G-PCM20

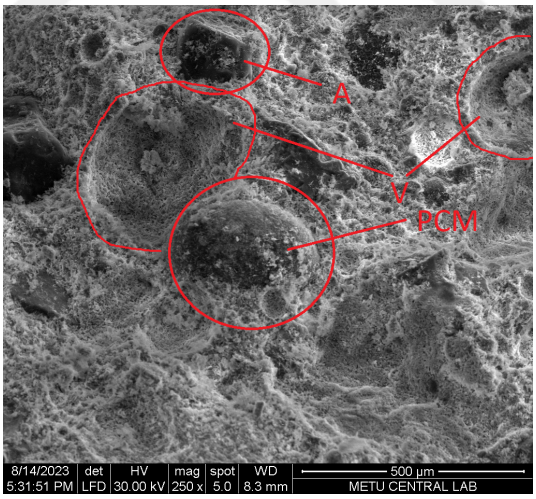

(b) FGDG-PCM20

Figure 6.16: SEM images of samples containing 20 vol% MPCM 21 days after pouring. Note that: A=aggregate, V=Void, PCM= MPCM.

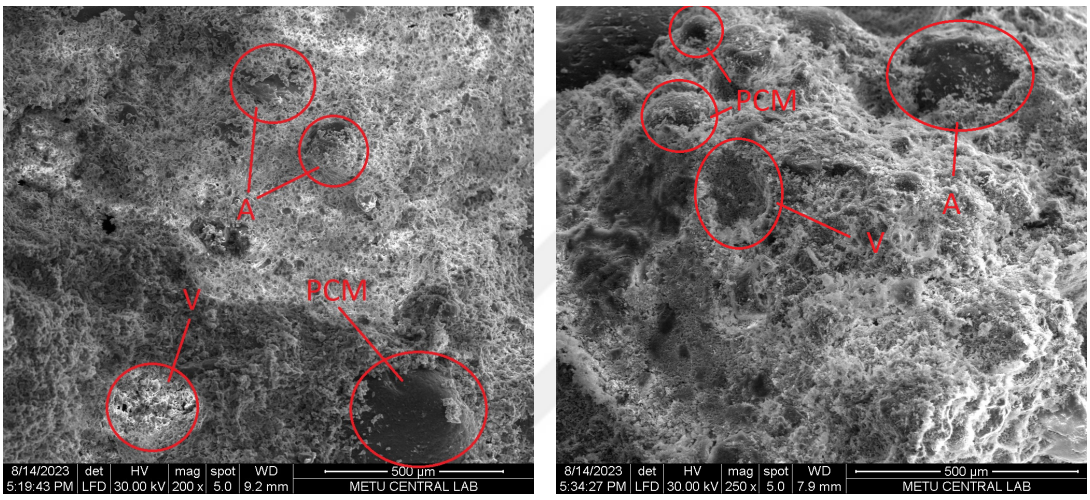

(a) G-PCM40

(b) FGDG-PCM40

Figure 6.17: SEM images of samples containing 40 vol% MPCM 21 days after pouring. Note that: A=aggregate, V=Void, PCM= MPCM.

CHAPTER 7

CONCLUSION

FDM and GSA models for walls are developed in this study. Although FDM is widely used in the literature, GSA applications for wall models were not encountered in the literature review. The sensitivity analysis identified key parameters affecting energy demand within the specified parameter range for walls oriented in various directions in Ankara, Türkiye.

In addition, a unique MPCM-incorporated FGDG composite is developed in this study for usage in passive building applications to lower the heating and cooling energy demand of buildings.

Based on the numerical and experimental results, the following conclusion can be drawn:

- Temperature profiles for summer and winter season are investigated for different wall configurations. Temperature profiles changed depend on materials at the outermost and innermost layers. The inclusion of PCM resulted in variations in the temperature profile depending on whether the innermost node was in the phase change or not.
- T_m is the most sensitive parameters for the four wall orientations for both summer and winter seasons. It should be noted that it is extremely important to decide on the application location, melting temperature and amount of MPCM, considering the specific characteristics of the wall to be applied, in terms of energy savings. Otherwise, improper use of PCMs in walls can worsen energy efficiency rather than improve it.
- Mechanical properties, thermal conductivity and microstructure of FGDG and

commercial plaster composites are investigated.

- 7-day flexural and compressive strength for FGDG composite without MPCM with different water ratios are investigated. As the water ratio increases, both flexural and compressive strength decrease.

- 14-day flexural and compressive strength for final FGDG composites are investigated. With an increase in MPCM, compressive strength tends to decrease.

- 7-day FGDG composites and 14-day FGDG composites with the same water content and no PCM have different compressive strengths and the same flexural strength. The compressive strength of the 7-day FGDG composite is approximately three times that of the 14-day composite. While determining the possible causes of this situation, it was thought that the most likely factor could be close to 10 °C difference in ambient and material temperatures between the two castings.

- Specific weight of FGDG samples is higher than commercial plaster samples due to the following reasons. First, FGDG contains more calcite, which has a higher density than gypsum, compared to commercial plaster. Second, commercial plaster contains an air-entreating agent, which causes more bubble formation.

- It is observed that there is no monotonic relationship between strength and MPCM amount for commercial plaster composites. Commercial plaster composite containing 20 vol% has the highest flexural and compressive strengths among other gypsum composites. On the other hand, commercial plaster composite containing 40 vol% has the lowest flexural and compressive strengths.

- Thermal conductivity of all FGDG composites is higher than commercial plaster composites due to two situations. First, calcite has higher thermal conductivity than gypsum since FGDG contains more calcite than commercial plaster, which contributes to its higher thermal conductivity. Second, commercial plaster samples have lower specific weight and more air bubble formation.

- The thermal conductivity of FGDG composites decreases with an increase in the MPCM ratio. There is no monotonic relationship between thermal conduc-

tivity and MPCM quantity for commercial plaster composites due to the filler effect. A 20 vol% gypsum composite offers the highest thermal conductivity among various gypsum composites. However, gypsum composite with 40 vol% gypsum has the lowest thermal conductivity.

- The microstructure of all composites is investigated, and aggregates, MPCM, and voids are seen. Also, it is seen that the crystal structures of FGDG and gypsum are different.

7.1 Possible Future Works

To understand composite behaviours and sensitivity analysis model better:

- Thermal cycling can be applied to composites to understand the effect of thermal ageing.
- After thermal ageing, mechanical and thermal properties should be measured.
- Rheological characterisation of both FGDG and commercial plaster can be performed.
- Since acoustic characteristic is essential for mortars/plasters, acoustic properties should be measured.
- Fire resistance is a frequently studied and essential parameter for gypsum-based composites. Therefore, a fire resistance test can be very beneficial.
- Second-order sensitivity analysis can be performed in order to observe interactions between parameters.

REFERENCES

[1] N. Soares, J. Costa, A. Gaspar, and P. Santos, "Review of passive pcm latent heat thermal energy storage systems towards buildings' energy efficiency," *Energy and Buildings*, vol. 59, pp. 82–103, 2013.

[2] S. Memon, "Phase change materials integrated in building walls: A state of the art review," *Renewable and Sustainable Energy Reviews*, vol. 31, pp. 870–906, 03 2014.

[3] D. Zhou, C. Zhao, and Y. Tian, "Review on thermal energy storage with phase change materials (pcms) in building applications," *Applied Energy - APPL ENERG*, vol. 92, 04 2012.

[4] A. Sharma, V. Tyagi, C. Chen, and D. Buddhi, "Review on thermal energy storage with phase change materials and applications," *Renewable and Sustainable Energy Reviews*, vol. 13, pp. 318–345, 02 2009.

[5] F. Incropera, D. DeWitt, T. Bergman, and A. Lavine, *Fundamentals of Heat and Mass Transfer*. 01 2007.

[6] S. E. KalnÃ¦s and B. P. Jelle, "Phase change materials and products for building applications: A state-of-the-art review and future research opportunities," *Energy and Buildings*, vol. 94, pp. 150–176, 2015.

[7] M. Hawlader, M. Uddin, and H. Zhu, "Encapsulated phase change materials for thermal energy storage: Experiments and simulation," *International Journal of Energy Research*, vol. 26, pp. 159 – 171, 02 2002.

[8] F. Pianosi, K. Beven, J. Freer, J. W. Hall, J. Rougier, D. B. Stephenson, and T. Wagener, "Sensitivity analysis of environmental models: A systematic review with practical workflow," *Environmental Modelling Software*, vol. 79, pp. 214–232, 2016.

[9] S. Burhenne, D. Jacob, and G. Henze, "Sampling based on sobol' sequences for monte carlo techniques applied to building simulations," pp. 1816–1823, 01 2011.

[10] T. Tolga, "Thermal performance enhancement of microencapsulated phase change material/geopolymer composites through graphite platelets and nano-additives for building energy storage applications," Master's thesis, Middle East Technical University, 2023.

[11] M. Parry and W. II, *Climate change 2007: impacts, adaptation and vulnerability : contribution of Working Group II to the fourth assessment report of the Intergovernmental Panel on Climate Change*. 01 2007.

[12] J. Laustsen, "Energy efficiency requirements in building codes, energy effic policies new build (iea information paper)," *IEA*, 2008.

[13] U. N. E. Programme, "Buildings and climate change: Summary for decision makers," 2009.

[14] I. E. Agency, *Transition to Sustainable Buildings*. 2013.

[15] "Energy consumption and use by households." `https://ec.europa.eu/eurostat/web/products-eurostat-news/-/ddn-20190620-1`. Accessed: 2021-09-30.

[16] E. Asadi, M. Gameiro da Silva, C. Antunes, and L. Dias, "Multi-objective optimization for building retrofit strategies: A model and an application," *Lancet*, vol. 44, 01 2012.

[17] C. Diakaki, E. Grigoroudis, and D. Kolokotsa, "Towards a multi-objective optimization approach for improving energy efficiency in buildings," *Energy and Buildings*, vol. 40, pp. 1747–1754, 12 2008.

[18] L. Pérez-Lombard, J. Ortiz, and C. Pout, "A review on buildings energy consumption information," *Energy and Buildings*, vol. 40, pp. 394–398, 01 2008.

[19] A. Abhat, "Low temperature latent heat thermal energy storage: Heat storage materials," *Solar Energy*, vol. 30, no. 4, pp. 313–332, 1983.

[20] A. Palacios, L. Cong, M. Navarro, Y. Ding, and C. Barreneche, "Thermal conductivity measurement techniques for characterizing thermal energy storage materials – a review," *Renewable and Sustainable Energy Reviews*, vol. 108, pp. 32–52, 2019.

[21] P. Marin, M. Saffari, A. de Gracia, X. Zhu, M. M. Farid, L. F. Cabeza, and S. Ushak, "Energy savings due to the use of pcm for relocatable lightweight buildings passive heating and cooling in different weather conditions," *Energy and Buildings*, vol. 129, pp. 274–283, 2016.

[22] B. James and P. Delaney, "Phase change materials: Are they part of our energy efficient future?," *ACEEE summer study on energy efficiency in buildings*, 2012.

[23] X. Sun, Q. Zhang, M. Medina, and K. O. Lee, "Experimental observations on the heat transfer enhancement caused by natural convection during melting of solid–liquid phase change materials (pcms)," *Applied Energy*, vol. 162, 04 2015.

[24] T. Qian, J. Li, Y. Deng, W. Guan, and L. Ning, "Diatomite: A promising natural candidate as carrier material for low, middle and high temperature phase change material," *Energy Conversion and Management*, vol. 98, 07 2015.

[25] R. Baetens, B. Jelle, and A. Gustavsen, "Phase change materials for building applications: A state-of-the-art review," *Energy and Buildings*, vol. 42, pp. 1361–1368, 09 2010.

[26] V. Tyagi and D. Buddhi, "Pcm thermal storage in buildings: A state of art," *Renewable and Sustainable Energy Reviews*, vol. 11, pp. 1146–1166, 08 2007.

[27] H. Akeiber, P. Nejat, M. Z. A. Majid, M. A. Wahid, F. Jomehzadeh, I. Zeynali Famileh, J. K. Calautit, B. R. Hughes, and S. A. Zaki, "A review on phase change material (pcm) for sustainable passive cooling in building envelopes," *Renewable and Sustainable Energy Reviews*, vol. 60, pp. 1470–1497, 2016.

[28] L. F. Cabeza, G. Zsembinszki, and M. Martín, "Evaluation of volume change in phase change materials during their phase transition," *The Journal of Energy Storage*, vol. 28, 01 2020.

[29] F. Kuznik, D. David, and K. Johannes, "A review on phase change materials integrated in building walls," *Renew Sustain Energy Rev*, vol. 8, pp. 1–13, 01 2010.

[30] Y. Zhang, G. Zhou, K. Lin, Q. Zhang, and H. Di, "Application of latent heat thermal energy storage in buildings: State-of-the-art and outlook," *Building and Environment*, vol. 42, pp. 2197–2209, 06 2007.

[31] F. Alphonse, S. Solanki, and J. Saini, "Heat transfer characteristics of thermal energy storage system using pcm capsules: A review," *Renewable and Sustainable Energy Reviews*, vol. 12, pp. 2438–2458, 12 2008.

[32] M. Hawlader, M. Uddin, and M. Khin, "Microencapsulated pcm thermal-energy storage system," *Applied Energy*, vol. 74, pp. 195–202, 02 2003.

[33] V. Tyagi, s. Kaushik, S. Tyagi, and T. Akiyama, "Development of phase change materials based microencapsulated technology for buildings: A review," *Energy Reviews*, vol. 15, pp. 1373–1391, 02 2011.

[34] L. F. Cabeza, A. Castell, C. Barreneche, A. de Gracia, and A. Fernández, "Materials used as pcm in thermal energy storage in buildings: A review," *Renewable and Sustainable Energy Reviews*, vol. 15, pp. 1675–1695, 04 2011.

[35] A. Waqas and Z. Din, "Phase change material (pcm) storage for free cooling of buildings—a review," *Renewable and Sustainable Energy Reviews*, vol. 18, p. 607–625, 02 2013.

[36] P. Schossig, H. Henning, S. Gschwander, and T. Haussmann, "Micro-encapsulated phase-change materials integrated into construction materials," *Solar Energy Materials and Solar Cells*, vol. 89, pp. 297–306, 11 2005.

[37] H. Inaba and P. Tu, "Evaluation of thermophysical characteristics on shape-stabilized paraffin as a solid-liquid phase change material," *Heat and Mass Transfer*, vol. 32, pp. 307–312, Apr 1997.

[38] A. Sari, "Form-stable paraffin/high density polyethylene composites as solid–liquid phase change material for thermal energy storage: Preparation and thermal properties," *Energy Conversion and Management*, vol. 45, pp. 2033–2042, 08 2004.

[39] Y. Zhang, K. Lin, R. Yang, H. Di, and Y. Jiang, "Preparation, thermal performance and application of shape-stabilized pcm in energy efficient buildings," *Energy and Buildings*, vol. 38, no. 10, pp. 1262–1269, 2006.

[40] T. Parfait, N. Pierres, and L. Luo, "A review of potential materials for thermal energy storage in building applications," *Renewable and Sustainable Energy Reviews*, vol. 18, pp. 327–349, 02 2013.

[41] Z. Zhou, Z. Zhang, J. Zuo, K. Huang, and L. Zhang, "Phase change materials for solar thermal energy storage in residential buildings in cold climate," *Renewable and Sustainable Energy Reviews*, vol. 48, pp. 692–703, 08 2015.

[42] B. Diaconu and M. Cruceru, "Novel concept of composite phase change material wall system for year-round thermal energy savings," *Energy and Buildings - ENERG BLDG*, vol. 42, pp. 1759–1772, 10 2010.

[43] M. Iten, S. Liu, and A. Shukla, "A review on the air-pcm-tes application for free cooling and heating in the buildings," *Renewable and Sustainable Energy Reviews*, vol. 61, pp. 175–186, 08 2016.

[44] G. Gholami and M. Farid, "Application of an active pcm storage system into a building for heating/cooling load reduction," *Energy*, vol. 210, p. 118572, 08 2020.

[45] P. Liu and G. Chen, "Chapter ten - characterization methods: Physical properties," in *Porous Materials* (P. Liu and G. Chen, eds.), pp. 493–532, Boston: Butterworth-Heinemann, 2014.

[46] Z. Uykun, "Investigation of mechanical and thermal properties of sintered bauxite and sand particles as heat transfer and storage media," Master's thesis, Middle East Technical University, 2021.

[47] S. Al-Ajlan, "Measurements of thermal properties of insulation materials by using transient plane source technique," *Applied Thermal Engineering*, vol. 26, pp. 2184–2191, 12 2006.

[48] A. Fopah Lele, K. N'Tsoukpoe, T. Osterland, F. Kuznik, and W. Ruck, "Thermal conductivity measurement of thermochemical storage materials," *Applied Thermal Engineering*, vol. 89, pp. 916–926, 10 2015.

[49] S. Dubois and F. Lebeau, "Design, construction and validation of a guarded hot plate apparatus for thermal conductivity measurement of high thickness crop-based specimens," *Materials and Structures*, vol. 48, 01 2013.

[50] J. Xamán, L. Lira-Cortés, and J. Arce, "Analysis of the temperature distribution in a guarded hot plate apparatus for measuring thermal conductivity," *Applied Thermal Engineering - APPL THERM ENG*, vol. 29, pp. 617–623, 03 2009.

[51] D. Zhao, X. Qian, X. Gu, S. Jajja, and R. Yang, "Measurement techniques for thermal conductivity and interfacial thermal conductance of bulk and thin film materials," *Journal of Electronic Packaging*, vol. 138, 12 2016.

[52] H. Czichos, T. Saito, and L. Smith, *Springer Handbook of Materials Measurement Methods*, vol. 153-158. 01 2006.

[53] "Standard Test Method for Measurement of Thermal Effusivity of Fabrics Using a Modified Transient Plane Source (MTPS) Instrument," standard, ASTM International, West Conshohocken, PA, June 2016.

[54] S. Min, J. Blumm, and A. Lindemann, "A new laser flash system for measurement of thermophysical properties," *Thermochimica Acta*, vol. 455, p. 46–49, 04 2007.

[55] N. Yüksel, "The review of some commonly used methods and techniques to measure the thermal conductivity of insulation materials," in *Insulation Materials in Context of Sustainability* (A. Almusaed and A. Almssad, eds.), ch. 6, Rijeka: IntechOpen, 2016.

[56] D. Cahill, "Thermal conductivity measurement from 30 to 750 k: the 3omega method," *Review of Scientific Instruments*, vol. 61, pp. 802 – 808, 03 1990.

[57] S. Memon, T. Lo, and H. Cui, "Utilization of waste glass powder for latent heat storage application in buildings," *Energy and Buildings*, vol. 66, pp. 405–414, 11 2013.

[58] H. Mehling and L. F. Cabeza, *Heat and Cold Storage with PCM: An Up to Date Introduction Into Basics and Applications*. 01 2008.

[59] S.-D. Clas, C. R. Dalton, and B. C. Hancock, "Differential scanning calorimetry: applications in drug development," *Pharmaceutical Science Technology Today*, vol. 2, no. 8, pp. 311–320, 1999.

[60] T. Whiffen and S. Riffat, "A review of PCM technology for thermal energy storage in the built environment: Part I," *International Journal of Low-Carbon Technologies*, vol. 8, pp. 147–158, 05 2012.

[61] P. Haines, M. Reading, and F. Wilburn, "Chapter 5 - differential thermal analysis and differential scanning calorimetry," in *Principles and Practice* (M. E. Brown, ed.), vol. 1 of *Handbook of Thermal Analysis and Calorimetry*, pp. 279–361, Elsevier Science B.V., 1998.

[62] J. Y. Choi, B. Y. Yun, Y. U. Kim, Y. Kang, S. C. Lee, and S. Kim, "Evaluation of thermal/acoustic performance to confirm the possibility of coffee waste in building materials in using bio-based microencapsulated pcm," *Environmental Pollution*, vol. 294, p. 118616, 2022.

[63] L. O. Afolabi, A. M. Elfaghi, T. Alomayri, A. I. Arogundade, S. Mahzan, N. M. Isa, C. L. Saw, and T. A. Otitoju, "Thermal energy storage phase change material cement mortar incorporated with clinical waste composites," *International Journal of Energy Research*, vol. 45, p. 13575–13590, Apr 2021.

[64] S. Cunha, P. Leite, and J. L. Aguiar, "Characterization of innovative mortars with direct incorporation of phase change materials," *Journal of Energy Storage*, vol. 30, p. 101439, 08 2020.

[65] L. Afolabi, Z. Ariff, P. Sri, M. Megat-Yusoff, H. Al-Kayiem, A. Arogundade, and O. Afolabi-owolabi, "Red-mud geopolymer composite encapsulated phase change material for thermal comfort in built-sector," *Solar Energy*, vol. 181, pp. 464–474, 02 2019.

[66] S. Pilehvar, V. D. Cao, A. M. Szczotok, L. Valentini, D. Salvioni, M. Magistri, R. Pamies, and A.-L. Kjøniksen, "Mechanical properties and microscale changes of geopolymer concrete and portland cement concrete containing micro-encapsulated phase change materials," *Cement and Concrete Research*, vol. 100, pp. 341–349, 2017.

[67] V. D. Cao, S. Pilehvar, C. Salas-Bringas, A. Szczotok, T. Bui, M. Carmona, J. Rodríguez, and A.-L. Kjøniksen, "Thermal analysis of geopolymer concrete walls containing microencapsulated phase change materials for building applications," *Solar Energy*, vol. 178, pp. 295–307, 12 2018.

[68] V. D. Cao, S. Pilehvar, C. Salas-Bringas, A. Szczotok, J. Rodríguez, M. Carmona, N. Al-Manasir, and A.-L. Kjøniksen, "Microencapsulated phase change materials for enhancing the thermal performance of portland cement concrete and geopolymer concrete for passive building applications," *Energy Conversion and Management*, vol. 133, pp. 56–66, 02 2017.

[69] S. Pilehvar, L. Valentini, R. Pamies, S. G. Sanfélix, and M. Lanzón, "Effect of temperature on geopolymer and portland cement composites modified with micro-encapsulated phase change materials," *Construction and Building Materials*, vol. 252, 04 2020.

[70] V. D. Cao, S. Pilehvar, C. Salas-Bringas, A. Szczotok, L. Valentini, M. Carmona, J. Rodríguez, and A.-L. Kjøniksen, "Influence of microcapsule size and shell polarity on thermal and mechanical properties of thermoregulating geopolymer concrete for passive building applications," *Energy Conversion and Management*, vol. 164, pp. 198–209, 05 2018.

[71] C. Mankel, A. Caggiano, and E. Koenders, "Thermal energy storage characterization of cementitious composites made with recycled brick aggregates containing pcm," *Energy and Buildings*, vol. 202, 08 2019.

[72] C. Rubino, S. Liuzzi, F. Martellotta, P. Stefanizzi, and P. Straziota, "Nonwoven textile waste added with pcm for building applications," *Applied Sciences*, vol. 11, p. 1262, 01 2021.

[73] M. Frigione, M. Lettieri, A. Sarcinella, and J. L. Aguiar, *Mortars with Phase Change Materials (PCM) and Stone Waste to Improve Energy Efficiency in Buildings*, pp. 195–201. 04 2018.

[74] B. Dębska, L. Lichołai, and J. Szyszka, "Innovative composite on the basis of an aerogel mat with an epoxy resin modified with pet waste and pcm," *E3S Web of Conferences*, vol. 44, p. 00031, 01 2018.

[75] Z. Wang, H. Su, S. Zhao, and N. Zhao, "Influence of phase change material on mechanical and thermal properties of clay geopolymer mortar," *Construction and Building Materials*, vol. 120, pp. 329–334, 09 2016.

[76] L. Liu, G. Lu, G. Qiu, C. Yue, M. Guo, R. Ji, and M. Zhang, "Characterization of novel shape-stabilized phase change material mortar: Portland cement containing nao and fly ash for energy-efficient building," *International Journal of Energy Research*, vol. 43, pp. 5812–5823, June 2019.

[77] A. Moshtaghi Jafarabad, M. Madhkhan, and N. Pourakbar Sharifi, "Thermal and mechanical properties of pcm-incorporated normal and lightweight concretes containing silica fume," *Canadian Journal of Civil Engineering*, vol. 46, 01 2019.

[78] S. Ramakrishnan, K. Pasupathy, and J. Sanjayan, "Synthesis and properties of thermally enhanced aerated geopolymer concrete using form-stable phase change composite," *Journal of Building Engineering*, vol. 40, p. 102756, 2021.

[79] A. Sari, G. Hekimoglu, Y. Karabayır, R. Sharma, H. Arslanoglu, O. Gencel, and V. Tyagi, "Capric-stearic acid mixture impregnated carbonized waste sugar beet pulp as leak-resistive composite phase change material with effective thermal conductivity and thermal energy storage performance," *Energy*, vol. 247, p. 123501, 02 2022.

[80] Y. Luo, C. Li, F. Zhang, and Z. Li, "Novel industrial waste-based shape-stabilized composite phase change materials with high heat storage performance from calcium carbide furnace dust," *Solar Energy Materials and Solar Cells*, vol. 242, p. 111745, 08 2022.

[81] R. Novais, G. Ascensão, M. Seabra, and J. Labrincha, "Lightweight dense/-porous pcm-ceramic tiles for indoor temperature control," *Energy and Buildings*, 09 2015.

[82] W. Liu, L. Teng, S. Rohani, Z. Qin, B. Zhao, C. C. Xu, S. Ren, Q. Liu, and B. Liang, "Co2 mineral carbonation using industrial solid wastes: A review of recent developments," *Chemical Engineering Journal*, vol. 416, p. 129093, 2021.

[83] H. Tayibi, C. Mohamed, F. López, F. Alguacil, and A. López-Delgado, "Environmental impact and management of phosphogypsum," *Journal of environmental management*, vol. 90, pp. 2377–86, 05 2009.

[84] N. H. Koralegedara, P. X. Pinto, D. D. Dionysiou, and S. R. Al-Abed, "Recent advances in flue gas desulfurization gypsum processes and applications – a review," *Journal of Environmental Management*, vol. 251, p. 109572, 2019.

[85] Aakriti, S. Maiti, N. Jain, and J. Malik, "A comprehensive review of flue gas desulphurized gypsum: Production, properties, and applications," *Construction and Building Materials*, vol. 393, p. 131918, 2023.

[86] G. Shafabakhsh, M. Faramarzi, and M. Sadeghnejad, "Use of surface free energy method to evaluate the moisture susceptibility of sulfur extended asphalts modified with antistripping agents," *Construction and Building Materials*, vol. 98, pp. 456–464, 2015.

[87] S. Liu, W. Liu, F. Jiao, W. Qin, and C. Yang, "Production and resource utilization of flue gas desulfurized gypsum in china - a review," *Environmental Pollution*, vol. 288, p. 117799, 2021.

[88] H. Zhang, Q. Xu, Z. Zhao, J. Zhang, Y. Sun, L. Sun, F. Xu, and Y. Sawada, "Preparation and thermal performance of gypsum boards incorporated with microencapsulated phase change materials for thermal regulation," *Solar Energy Materials and Solar Cells*, vol. 102, pp. 93–102, 2012. Organic, Dye sensitized and Innovative approaches for Photovoltaic Applications.

[89] D. Feldman, D. Banu, D. Hawes, and E. Ghanbari, "Obtaining an energy storing building material by direct incorporation of an organic phase change material in gypsum wallboard," *Solar Energy Materials*, vol. 22, no. 2, pp. 231–242, 1991.

[90] B. Srinivasaraonaik, L. Singh, S. Sinha, I. Tyagi, and A. Rawat, "Studies on the mechanical properties and thermal behavior of microencapsulated eutectic mixture in gypsum composite board for thermal regulation in the buildings," *Journal of Building Engineering*, vol. 31, p. 101400, 2020.

[91] J. H. Park, Y. Kang, J. Lee, S. Wi, J. D. Chang, and S. Kim, "Analysis of walls of functional gypsum board added with porous material and phase change material to improve hygrothermal performance," *Energy and Buildings*, vol. 183, pp. 803–816, 2019.

[92] T. Toppi and L. Mazzarella, "Gypsum based composite materials with micro-encapsulated pcm: Experimental correlations for thermal properties estimation on the basis of the composition," *Energy and Buildings*, vol. 57, p. 227–236, 02 2013.

[93] C. ming Lai, R. Chen, and C.-Y. Lin, "Heat transfer and thermal storage behaviour of gypsum boards incorporating micro-encapsulated pcm," *Energy and Buildings*, vol. 42, no. 8, pp. 1259–1266, 2010.

[94] A. M. Borreguero, I. Garrido, J. L. Valverde, J. F. Rodríguez, and M. Carmona, "Development of smart gypsum composites by incorporating thermoregulating microcapsules," *Energy and Buildings*, vol. 76, pp. 631–639, 2014.

[95] J. Zhang, X. Guan, X. Song, H. Hou, Z. Yang, and J. Zhu, "Preparation and properties of gypsum based energy storage materials with capric acid–palmitic acid/expanded perlite composite pcm," *Energy and Buildings*, vol. 92, pp. 155–160, 2015.

[96] B. Zhang, Y. Tian, X. Jin, T. Y. Lo, and H. Cui, "Thermal and mechanical properties of expanded graphite/paraffin gypsum-based composite material reinforced by carbon fiber," *Materials*, vol. 11, no. 11, 2018.

[97] M. Özişik, H. Orlande, M. Colaco, and R. Cotta, "Finite difference methods in heat transfer: Second edition," *Taylor Francis Group.*, pp. 1–578, 01 2017.

[98] F. Incropera, D. DeWitt, T. Bergman, and A. Lavine, *Fundamentals of Heat and Mass Transfer*. 01 2007.

[99] H. Bashirpour-Bonab, "Investigation and optimization of pcm melting with nanoparticle in a multi-tube thermal energy storage system," *Case Studies in Thermal Engineering*, vol. 28, p. 101643, 11 2021.

[100] X. Jin, M. A. Medina, and X. Zhang, "Numerical analysis for the optimal location of a thin pcm layer in frame walls," *Applied Thermal Engineering*, vol. 103, pp. 1057–1063, 2016.

[101] R. A. Kishore, M. V. Bianchi, C. Booten, J. Vidal, and R. Jackson, "Optimizing pcm-integrated walls for potential energy savings in u.s. buildings," *Energy and Buildings*, vol. 226, p. 110355, 2020.

[102] X. Jin, S. Zhang, X. Xu, and X. Zhang, "Effects of pcm state on its phase change performance and the thermal performance of building walls," *Building and Environment*, vol. 81, pp. 334–339, 2014.

[103] E. Tunçbilek, M. Arıcı, M. Krajčík, S. Nižetić, and H. Karabay, "Thermal performance based optimization of an office wall containing pcm under intermittent cooling operation," *Applied Thermal Engineering*, vol. 179, p. 115750, 2020.

[104] M. Arıcı, F. Bilgin, S. Nižetić, and H. Karabay, "Pcm integrated to external building walls: An optimization study on maximum activation of latent heat," *Applied Thermal Engineering*, vol. 165, p. 114560, 2020.

[105] J. Duffie and W. Beckman, *Solar Engineering of Thermal Processes*. Elsevier Science B.V., 2013.

[106] "ASHRAE standard thermal environmental conditions for human occupancy," standard, American Society of Heating, Refrigerating and Engineers, Air-Conditioning, Atlanta, USA, 1992.

[107] V. D. Cao, S. Pilehvar, C. Salas-Bringas, A. M. Szczotok, T. Q. Bui, M. Carmona, J. F. Rodriguez, and A.-L. Kjøniksen, "Thermal analysis of geopolymer concrete walls containing microencapsulated phase change materials for building applications," *Solar Energy*, vol. 178, pp. 295–307, 2019.

[108] A. Saltelli, S. Tarantola, F. Campolongo, M. Ratto, *et al.*, *Sensitivity analysis in practice: a guide to assessing scientific models*, vol. 1. Wiley Online Library, 2004.

[109] D. Harenberg, S. Marelli, B. Sudret, and V. Winschel, "Uncertainty quantification and global sensitivity analysis for economic models," *Quantitative Economics*, vol. 10, no. 1, pp. 1–41, 2019.

[110] S. Marino, I. B. Hogue, C. J. Ray, and D. E. Kirschner, "A methodology for performing global uncertainty and sensitivity analysis in systems biology," *Journal of Theoretical Biology*, vol. 254, no. 1, pp. 178–196, 2008.

[111] B. Iooss and P. Lemaître, "A review on global sensitivity analysis methods," *Operations Research/ Computer Science Interfaces Series*, vol. 59, 04 2014.

[112] A. Saltelli, M. Ratto, T. Andres, F. Campolongo, J. Cariboni, D. Gatelli, M. Saisana, and S. Tarantola, *Global Sensitivity Analysis. The Primer*, vol. 304. 01 2008.

[113] A. Saltelli, P. Annoni, I. Azzini, F. Campolongo, M. Ratto, and S. Tarantola, "Variance based sensitivity analysis of model output. design and estimator for the total sensitivity index," *Computer Physics Communications*, vol. 181, no. 2, pp. 259–270, 2010.

[114] X. Zhang, M. Trame, L. Lesko, and S. Schmidt, "Sobol sensitivity analysis: A tool to guide the development and evaluation of systems pharmacology models," *CPT: Pharmacometrics Systems Pharmacology*, vol. 4, 02 2015.

[115] M. Tosin, A. Cortes, and A. Cunha Jr, *A Tutorial on Sobol' Global Sensitivity Analysis Applied to Biological Models*, pp. 93–118. 10 2020.

[116] I. Sobol, "Theorem and examples on high-dimensional model representation," *Reliability Engineering System Safety*, vol. 79, p. 187–193, 02 2003.

[117] F. Cannavò, "Sensitivity analysis for volcanic source modeling quality assessment and model selection," *Computers Geosciences*, vol. 44, pp. 52–59, 07 2012.

[118] Y. Gan, Q. Duan, W. Gong, C. Tong, Y. Sun, W. Chu, A. Ye, C. Miao, and Z. Di, "A comprehensive evaluation of various sensitivity analysis methods: A case study with a hydrological model," *Environmental Modelling Software*, vol. 51, pp. 269–285, 2014.

[119] K. Menberg, Y. Heo, and R. Choudhary, "Sensitivity analysis methods for building energy models: Comparing computational costs and extractable information," *Energy and Buildings*, vol. 133, pp. 433–445, 2016.

[120] H. Johra, *Thermal properties of building materials - Review and database*. No. 289 in DCE Technical Reports, Department of the Built Environment, Aalborg University, 2021.

[121] J. TORRESOLA, "Solidification properties of certain waxes and paraffins," Master's thesis, Massachusetts Institute of Technology, 1998.

[122] M. K. Rathod and J. Banerjee, "Thermal stability of phase change materials used in latent heat energy storage systems: A review," *Renewable and Sustainable Energy Reviews*, vol. 18, pp. 246–258, 2013.

[123] A. Kilic and Kilic, "The phase transition in natural gypsum," *Asian Journal of Chemistry*, vol. 19, pp. 3157–3168, 07 2007.

[124] Z. Thoeny, "The effect of particle size distribution on some properties of gypsum," vol. 31, pp. 741–751, 09 2020.

[125] "Standard Test Method for Flexural Strength of Hydraulic-Cement Mortars," standard, Norma ASTM Int, PA, USA, 2018.

[126] "Standard test method for compressive strength of hydraulic-cement mortars (Using portions of prisms broken in flexure)," standard, ASTM Int, PA, USA, 2002.

[127] R. Shadnia, L. Zhang, and P. Li, "Experimental study of geopolymer mortar with incorporated pcm," *Construction and Building Materials*, vol. 84, pp. 95–102, 2015.

[128] "Plastics — Determination of thermal conductivity and thermal diffusivity — Part 2: Transient plane heat source (hot disc) method," standard, International Organization for Standardization, Geneva, CH, June 2022.

[129] K. iti Horai and G. Simmons, "Thermal conductivity of rock-forming minerals," *Earth and Planetary Science Letters*, vol. 6, no. 5, pp. 359–368, 1969.

[130] M. Pomianowski, P. Heiselberg, and Y. Zhang, "Review of thermal energy storage technologies based on pcm application in buildings," *Energy and Buildings*, vol. 67, pp. 56–69, 2013.

[131] D. W. Waples and J. S. Waples, "A review and evaluation of specific heat capacities of rocks, minerals, and subsurface fluids. part 1: Minerals and nonporous rocks," *Natural Resources Research*, vol. 13, pp. 97–122, Jun 2004.

[132] A. Thiele, Z. Wei, G. Falzone, B. Young, N. Neithalath, G. Sant, and L. Pilon, "Figure of merit for the thermal performance of cementitious composites containing phase change materials," *Cement and Concrete Composites*, vol. 65, 11 2015.